UCLouvain

École polytechnique de Louvain

Development of 3D-printable porous biodegradable polymer materials for biological applications

Author: **Lise Evrard**
Supervisors: **Sophie Demoustier, Alain Jonas**
Readers: **Quentin Papeloer, Evelyne Van Ruymbeke**
Academic year 2022–2023
Master [120] in Biomedical Engineering

Abstract

Tissue engineering is a rapidly growing field dedicated to the development of functional tissue substitutes for the regeneration of damaged tissues. Porous scaffolds play a crucial role in providing structural support for cell growth, differentiation and tissue regeneration. The porosity of scaffolds is a key parameter that influences their biocompatibility, vascularization and ability to promote cell migration. On the one hand, micropores, with a size of 50 to 200 µm, allow the circulation of the cells required for the growth of new tissue. On the other hand, macropores, 300 to 500 µm in size, facilitate vascularization by providing the oxygen and nutrients essential for cell survival.
This study focused on the development of a 3D-printed polymer that exhibits both porosity and biodegradability, thereby meeting the requirements of biological applications. To induce microporosity in the scaffolds, an innovative solvent-free method was developed. This method involves mixing polylactic acid (PLA) and polyethylene glycol (PEG). Based on a previous study, the composition of the mixture was set at 70% PLA and 30% PEG, but three different molar masses of PEG were investigated: PEG3K, PEO100K and PEO1M with a molar mass of 3,350 g/mol, 100,000 g/mol and 1,000,000 g/mol respectively.
Firstly, filaments were made by extruding the PLA/PEG polymer blend. These filaments were then used in a 3D printer to produce 3D objects. Macroporosity was induced by the 3D printing design itself, while microporosity was successfully obtained by dissolving PEG in water, which allowed the PEG to be extracted from the structures.
In principle, the lower the molecular weight of PEG, the lower its rigidity and mechanical strength. This was reflected in the prints after PEG removal as the amount of PEG remaining varied between 7 and 10%. Although the structure with PEG100K was very slightly stiffer than that with PEG1M. Molecular weight also had an effect on porosity. With PEG3K, the pores were few and medium-sized (<100 µm) and the macropores were 800 µm in size. With PEG100K, the micropores were very numerous and highly variable in size (between 15 and over 200 µm) and the macropores were 650 µm in size. Finally, PEG1M had a large number of small pores (<30 µm) and macropores 950 µm in size. The results showed that the PLA/PEO100K blend had the best combination of micropores and macropores, as well as acceptable mechanical properties.
This study proposes a new approach to developing porous structures as scaffolds for tissue regeneration applications. However, further improvements are still needed, in particular the optimization of 3D printing parameters.

Aknowledgements

Firstly, I would like to express my deep gratitude to my supervisors, Professor Sophie Demoustier and Professor Alain Jonas, for their guidance and advices throughout this year. Their expertise was of great help in interpreting the results and finding solutions when I encountered difficulties.

I would particularly mention Quentin Papeloer for his availability and his reactivity. He was a day-to-day support and spent a considerable amount of time answering my questions from the beginning to the end of this project. His precise and clear explanations greatly contributed to the achievement of this project.

I would also like to thank the members of the BSMA laboratory, and in particular Pascal van Velthem, who willingly shared his knowledge of the functioning of the different equipment, including the DMA and the extruder. His help in the comprehension of the results was extremely precious. I would like to thank Delphine Magnin for her contribution and the time she devoted to SEM imaging. I would also like to thank Naïma Sallem for her assistance with the tensile tests.

Last but not the least, I would like to thank my family and friends who have been a real source of support during these years of study, motivating me in challenging moments.

Contents

Abbreviations

3D Three-dimensional

3DP Three-dimensional printing

CAD Computer-aided design

DMA Dynamic Mechanical Analysis

DSC Differential Scanning Calorimetry

E Young's modulus

E' Storage modulus

E" Loss modulus

FDA Food and Drug Administration

FDM Fused Deposition Modeling

LA Lactic acid

M_n Number-average molar mass

M_w Weight-average molar mass

NMR Nuclear Magnetic Resonance

PDLA Poly-D-lactic acid

PDLLA Poly-D,L-lactic acid

PEG Polyethylene glycol

PEO Polyethylene oxide

PLA Polylactic acid

PLLA Poly-L-lactic acid

SEM Scanning Electron Microscope

SLA Stereolithography

SLS Selective Laser Sintering

$\boldsymbol{T_{cc}}$ Cold crystallization temperature

$\boldsymbol{T_g}$ Glass transition temperature

$\boldsymbol{T_m}$ Melting temperature

TE Tissue Engineering

$\boldsymbol{X_c}$ Degree of crystallinity

Chapter 1

Introduction

Currently, in France, more than 11,000,000 people suffer from heart disease, almost 4,000,000 from bone disease and nearly 300,000 from peripheral nerve damage. [1, 2, 3].

One of the first solutions to overcome these diseases was to replace the defective tissue with new healthy tissue from donors. There exist three different types of transplants. Firstly, autograft is a transplant where the donor and recipient are the same person. The second type is allograft, which is characterized by the implantation of a graft from human to human. And finally, xenograft is defined as the transplantation of different species. This transplantation procedure is most commonly seen between a pig and a human. Unfortunately, this technique has many weaknesses. First at all, the number of donors is much lower than the number of recipients. This is due to the ageing population, which increases the waiting lists for organ donation over time, but with a stable number of donors. Moreover, even if the donor and the recipient are compatible, the graft may be rejected due to an immune reaction of the recipient's organism which considers the graft as foreign. Transplant surgeries are complicated and burdensome for the patient. After a transplant, the patient is hospitalised for more than ten days if all goes well, but in view of the complexity of this type of operation, it can happen that the patient has to be re-operated or that the disease recurs. Finally, the patient must be monitored regularly for the next few years. Although these operations remain the gold standard of treatment, they are not optimal [4].

Orthopaedic implants are also an important advance in replacing a defective bone or joint in the event of a traumatic fracture. They are made of biocompatible materials such as stainless steel, titanium or ceramic. In addition, they have a high strength and a high fracture resistance. However, the Young's modulus is usually too high, resulting in stress shielding and bone deterioration. This technology is not very flexible and as the bone continues to remodel over time, regardless of the patient's age, the implant must be removed to re-implant another one better adapted to his skeleton. This makes it even less feasible to place an implant in children, who show the greatest bone growth [5].

Since the 1980s, a new technology appeared in order to solve the issues mentioned previously : tissue engineering (TE). TE is defined by its creators Langer and Vacanti as "an interdisciplinary field which applies the principles of engineering and life sciences

toward the development of biological substitutes that restore, maintain, or improve tissue function". It consists of three poles: the cells that provide a functional tissue, the scaffold made of biomaterials that supports the transplantation and the cells, and the biophysical and chemical signals (cytokines and growth factors) that induce tissue formation. This method has the advantage of being highly tunable thanks to the numerous choices of biomaterials and manufacturing techniques. Therefore, it is possible to create biological tissues specifically adapted to patient's needs. Nevertheless, the material must meet certain constraints such as biocompatibility, porosity, biodegradability and mechanical requirements specific to the application [6, 7].

The porosity of scaffolds is crucial for stimulating new tissue growth. The pores of the scaffold allow the exchange of essential substances, such as nutrients, oxygen and waste products, with the surrounding environment. In addition, growth factors and cytokines pass through the pores to influence cell behaviour, including attachment, migration, proliferation and differentiation. Therefore, the creation and control of scaffold porosity is essential to achieve the appropriate physical and biological properties required for successful tissue regeneration. However, a scaffold that is too porous does not provide sufficiently strong mechanical support for tissue growth, while a scaffold with low porosity does not provide sufficient space for cells to migrate and proliferate. A balance between mechanical properties and porosity must therefore be reached to ensure the successful regeneration of a functional tissue. In conclusion, scaffold porosity is a critical element of tissue engineering, and optimization of its design and control is essential for successful tissue regeneration applications.

After the scaffold is implanted in the body, spontaneous vascularization of the tissue occurs. Vascularization refers to the process of forming new blood vessels within the engineered tissue to supply the cells with nutrients and oxygen and to remove waste products. Without adequate vascularization, the cells at the centre of the tissue will not receive the necessary resources, resulting in necrosis. However, this spontaneous vascularization is regrettably not very rapid and therefore strategies to induce vascularization are needed. One possibility is to prevascularize the implant using, for example, pre-formed vessels or endothelial cells seeded onto the scaffold to form capillary networks. A second approach is to incorporate angiogenic growth factors into the implant that will induce blood vessel formation. Despite these advances, achieving functional vascularization remains a challenge, especially when dealing with more complex structures [8].

Polylactic acid (PLA) is one of the most widely used biopolymers for tissue engineering due to its numerous successes as a scaffold in different applications such as bone, nerve and skin regeneration. PLA has been shown to have excellent biocompatibility, controlled mechanical properties, degradability, processability, and thermal stability. One of its main shortcoming is its brittle nature.
As far as the technology of manufacturing a scaffold, the most promising and one of the most recent methods is three-dimensional (3D) printing. It offers the possibility to create a wide range of designs and to insert all kinds of materials in powder, solid and liquid form. Any type of design can be created with great precision and is easily reproducible. This can range from micro-architectures to simple shapes. This allows for patient-specific

scaffolds, which is the most important feature in scaffold design. Finally, this technology has already been used to recreate both soft tissue such as tendons and liver and hard tissue like bone. Therefore, there are no restrictions on its use and it can be used for any type of biomedical application.
To improve the properties of a material, it is common to combine it with another polymer with better mechanical properties. To improve the strength of PLA, it turns out that polyethylene glycol (PEG) is a good candidate. Moreover, the blend formed from PLA and PEG not only provides better mechanical properties, but also physical characteristics such as degradation and chemical properties such as hydrophobicity. Numerous research studies have focused on the manufacture of PLA and PEG scaffolds, which have proven to be effective implants. The results have often been compared with scaffolds made only of PLA. The addition of PEG was found to have an impact not only on the mechanical properties of the biopolymer composite, but also on other properties. The flexibility and strength of the scaffold increase considerably, leading to a reduction in Young's modulus and yield strength but an increase in elongation at fracture. Surface roughness and wettability are also properties that are increased by the addition of PEG [9].

This thesis is therefore dedicated to the 3D printing of a porous and biodegradable scaffold based on a PLA/PEG mixture. However, PEG will no longer be used as an additive to PLA as it has been in previous studies [7, 10]. Instead, it will serve as a sacrificial agent that will be removed at the end of the process, resulting in additional porosity of the scaffold. It is therefore on this new point that the thesis will focus. This research is a continuation of the work done by Q.Papeloer.

Chapter 2

State of the art

2.1 PLA

Polylactic acid (PLA) is a biodegradable aliphatic polyester that belongs to the family of thermoplastic polymers. Its chemical formula is shown in Figure 2.1.

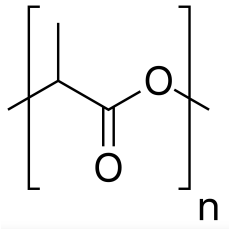

Figure 2.1: Chemical formula of PLA

PLA consists of a two-stage process. Firstly, lactic acid (LA), the basic unit of PLA, is obtained by fermenting the dextrose contained in certain natural resources such as corn, for example. LA, is a chiral molecule and two enantiomers exist: L- and D-lactic acid represented in Figure 2.2. Secondly, this LA is polymerized either by ring opening to give a high molecular weight PLA or by polycondensation or by enzymatic polymerization or by azeotropic dehydration [11].

Ring-opening polymerization is a reaction in which a polymer chain with a reactive centre at its terminal end reacts with another cyclic monomer (in this case, LA), opening its ring system to form a longer polymer chain. This reaction usually requires catalysis [13].
Polycondensation is a step-growth polymerization reaction in which monomers react with each other to form larger units while discarding smaller molecules as a by-product, such as water or methanol. In this case, it will be an esterification of the carboxyl function present in the LA [13].
Enzymatic polymerization is defined as the chemical synthesis of polymers in vitro by non-biosynthetic pathways catalyzed by an isolated enzyme [14].
Azeotropic dehydration requires that the LA is first distilled under vacuum to remove most of the water of condensation. Then, a heated azeotropic solvent under reflux and a catalyst are added [15].

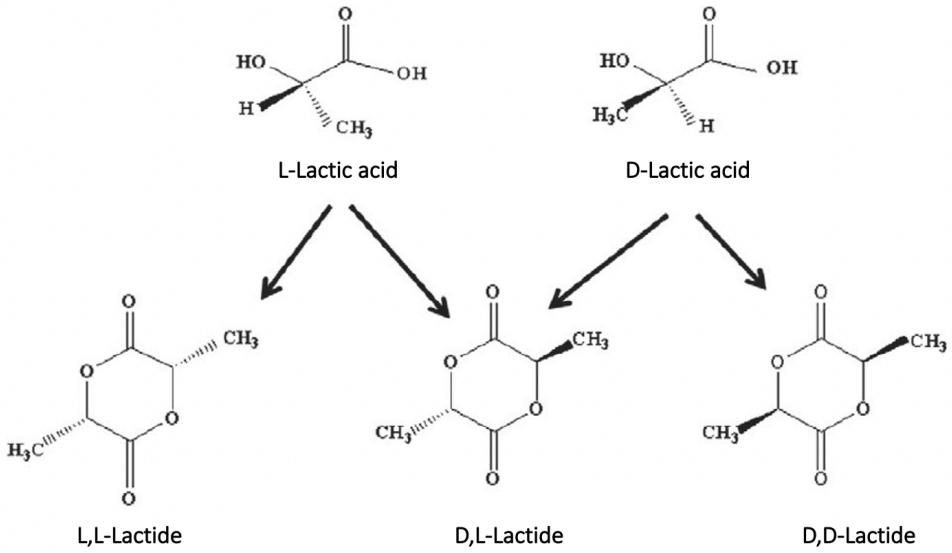

Figure 2.2: Enantiomers of LA on the first line and stereoisomers of PLA on the second line [12]

Consequently, due to the nature of LA, three stereoisomers of PLA are possible: poly-L-lactic acid (PLLA), poly-D-lactic acid (PDLA) and poly-D,L-lactic acid (PDLLA). PLLA and PDLA are known to be semicrystalline, which is not the case with PDLLA which is amorphous due to the random arrangement of the L and D-lactic acid units. L-LA is a molecule produced by the human body and therefore PLLA can be inserted into the human body without any risk of toxicity and without quantity limitations. This is why PLLA has been approved by the FDA. This study will use PLLA material exclusively but for the sake of simplicity, the term PLA will be used as a reference for PLLA in the following discussion [12, 16, 17].

2.1.1 Properties

In order to create a suitable tissue engineering scaffold, it is mandatory that the properties of the scaffold are compatible with those of the tissue to be regenerated. Since the final product will be (almost) exclusively made of PLA, it is important to review all of its properties.

Physical properties

PLA is a semi-crystalline thermoplastic. Semi-crystalline thermoplastic polymers are a class of polymers that soften on heating and harden on cooling. During these temperature changes, no chemical reaction is observed, only a change in structure. The reason is that semi-crystalline thermoplastics are made up of long chains of molecules that move relative to each other and are quite mobile when heated, allowing the material to be moulded into different shapes. As the material cools, the chains fold back on themselves, reducing their

significant mobility and forming crystals. This process is known as crystallization.

The crystallinity of a thermoplastic is important for TE as it governs its mechanical properties. The thermal properties of thermoplastics including their glass temperature (T_g) and melting temperature (T_m), are essential considerations for designing scaffolds and determining their stability and degradation rate when implanted in the body. T_g refers to the transition from the glassy state to the rubbery state of the material and T_m describes the transformation of the solid material to a liquid state. Namely, the glass temperature of a thermoplastic has an impact on its structural stability and degradation rate when implanted in the body. The melting temperature of a thermoplastic defines its ability to be shaped into a desired form when designing scaffolds. Finally, the wettability of a material is responsible for the behaviour of the material on its surface that will be in contact with the cells. Understanding and controlling the physical properties of thermoplastics is therefore important for their successful use in tissue engineering applications.

Crystallinity
PLA exists in two forms, either semi-crystalline (PLLA or PDLA) or amorphous (PDLLA). The content of each phase depends on many factors such as stereoisomers, thermal history, chain length, etc. When the polymer is cooled below its melting point, the regions start to order and the crystals start to grow, leading to the formation of the spherulitic structure. This is the beginning of nucleation, which means the formation of a small ordered group of atoms or molecules, which serves as the building block for the growth of a larger crystal. The size and morphology of the spherulites is influenced by the cooling rate. If the rate is slow enough, the crystallites can grow radially, forming the characteristic spherulite structure. On the other hand, if the cooling rate is too fast, the nucleation and growth of crystallites can be more random, resulting in a less ordered structure. The length of the polymer chain also affects the crystallinity. The longer the chains, the more likely they are to fold back on themselves and form more crystalline regions. In addition, having longer chains reduces the effect of terminations which act as defects in the crystal phase. The structure of a spherulite is shown in Figure 2.3.

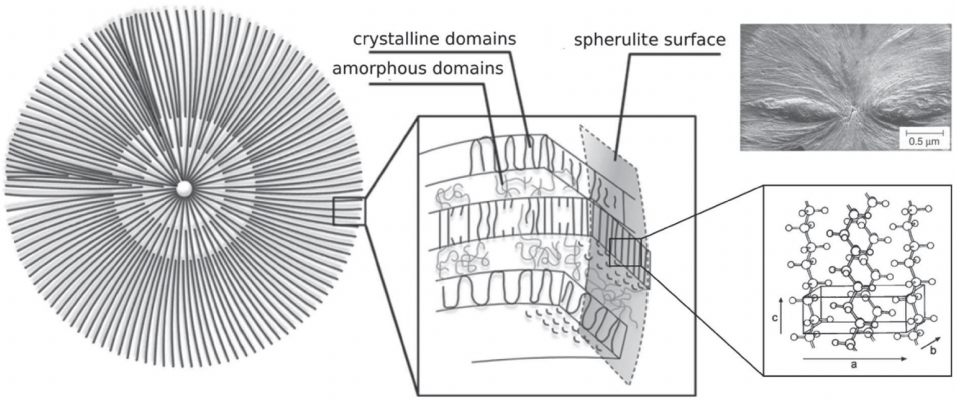

Figure 2.3: Schematic structure of a spherulite [18]

It can be seen that the crystalline phase consists of lamellae that fold back on themselves in an orderly fashion and that the amorphous part is composed of long irregular chains. In a semi-crystalline polymer, there is an alternation of lamellae and amorphous phases.

The degree of crystallinity (X_c) of a polymer is given by :

$$X_c = \frac{\Delta H_m}{\Delta H_m^o} * 100 \tag{2.1}$$

where H_m is the enthalpy of crystals and ΔH_m^o is the enthalpy of fusion of a perfectly crystalline material and is 93.1 J/g for PLA [19].
For an amorphous polymer, degree of crystallinity is equal to 0% and for a highly crystalline polymer, it is higher than 40% [20].

Thermal properties
PLA, being a semi-crystalline thermoplastic, is characterized by two temperatures specific to the material: glass temperature (T_g) and melting temperature (T_m). The values of these temperatures for PLLA (semi-crystalline) and PDLLA (amorphous) is summarized in Table 2.1.

Table 2.1: Characteristic temperatures of PLLA and PDLLA [21]

Temperature	**PLLA**	**PDLLA**
Glass temperature (T_g)	55-65°C	50-60°C
Melting temperature (T_m)	170-200°C	no T_m

By definition, a semi-crystalline consists of amorphous and crystalline phases. Below T_g, the material is in a glassy state and the chains can not move. Above T_g, the amorphous regions of the thermoplastic become more mobile and can be considered as a liquid. In contrast, crystalline phases that remain solid up to T_m.

In addition, the molecular weight of the material has an impact on its thermal properties, including T_g and T_m. As the molecular weight of a material increases, its T_g and T_m tend to increase as well. The increase in T_g is due to the longer and more entangled chains, resulting in a decrease in free volume, making it more difficult for the material to transition from glassy to rubbery and therefore a higher T_g is required. For T_m, as larger molecules have stronger intermolecular forces, more energy is needed to form the melt and so T_m increases. Furthermore, as mentioned in the previous section, longer chains fold more easily and form more crystals. But the effect of end chains acting as defects in the crystal phases is also reduced. The crystallinity is higher and the T_m increases.
However, the relationship between molecular weight and T_g and T_m is limited. When the molecular weight reaches a certain point, M_n*, T_g and T_m stop increasing with molecular weight, as shown in Figure 2.4. This is because at this point the intermolecular forces are at their maximum and the free volume is at its minimum [22, 23].

Finally, the thermal history of a material influences its T_g and T_m. When a polymer is cooled slowly, the polymer chains have more time to arrange themselves in a more ordered and crystalline structure, resulting in a higher degree of crystallinity and a higher T_m. In contrast, if the polymer is cooled rapidly, the polymer chains do not have enough time to arrange themselves in a highly ordered structure, resulting in a lower degree of crystallinity and a lower T_m [19].

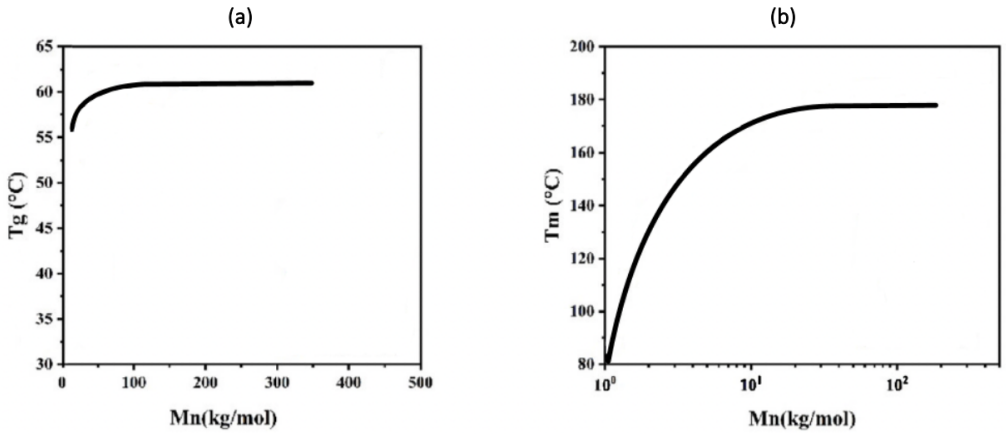

Figure 2.4: T_g (a) and T_m (b) in function of the molecular weight of the PLA [23]

Two important heat treatment processes exist: annealing and quenching. Annealing consists of heating the material to a temperature between T_g and T_m for a certain period of time. At this temperature, the chains are mobile. The material is then slowly cooled to allow time for the chains to arrange themselves in the most orderly way resulting in a recrystallization with a higher degree of crystallinity. Quenching consists of a rapid cooling of the polymer to allow no time for the chains to arrange themselves, resulting in an amorphous polymer or to freeze the material in a metastable state for analysis.

Wettability

The wetting angle defines the hydrophilic or hydrophobic behaviour of the surface of a material. If the angle is greater than 90°, the surface is said to be hydrophobic and if it is not, the surface is hydrophilic. The behaviour of the surface is important for tissue engineering because it is directly related to cell adhesion. In other words, cells are more likely to attach and proliferate on surfaces that are compatible with their own behaviour. However, depending on the biomedical application, the cells will be different. It is therefore not possible to define an optimal contact angle. In some cases, a hydrophilic surface may be preferred to promote cell attachment and growth, while in other cases a hydrophobic surface may be desirable to promote the growth of other specific cell types. It is important to carefully examine the surface properties of materials used in tissue engineering to ensure that they generate the desired biological response. On the other hand, neglecting these factors can lead to the implementation of a material with the wrong surface characteristics, for example using a hydrophilic material when a hydrophobic surface is required. This can have a negative impact on biocompatibility and make the implant unviable [24].

Nevertheless, it is feasible to modify the surface of a material by making it more hydrophilic or more hydrophobic when the surface properties do not initially match. To achieve such a result, two basic techniques are used : surface coating and surface roughness.

Surface coating consists of depositing a thin layer of various materials, which can be biopolymers, proteins, hydrogels or inorganic materials. By choosing the appropriate coating material, it is possible to completely change the character of the surface, making

it hydrophilic or hydrophobic depending on the biological application [24].

Roughness accentuates the surface behaviour of the material. A hydrophobic rough surface will be even more hydrophobic (larger wetting angle) and a hydrophilic rough surface will be even more hydrophilic (smaller wetting angle). If a hydrophilic surface is made rough, there will be more anchor points for water molecules, facilitating its attachment. This increased adhesion of water molecules will result in a surface that is even more hydrophilic than before. Conversely, if the hydrophobic surface is rough, it is even more difficult for water to penetrate these holes, resulting in a much more hydrophobic surface.

Several techniques exist to add roughness to the surface of a polymer. The best known are plasma treatment, crystallization and porosity.
Plasma etching is carried out under low-pressure conditions, where the material is exposed to plasma, a partially ionized gas. The process enables chemical reactions to occur, resulting in the removal of material from the surface. In additional to being applicable for metals and polymers, this method is done at low temperatures and can therefore treat heat sensitive materials [25].
During *crystallization*, the molecular chains of the material rearrange themselves into ordered crystal structures, which induce the formation of crystals in specific crystallographic planes. These planes can create a roughness on the surface of the material.
Porosity creates a rough surface texture by introducing a three-dimensional network of voids or pores on the surface.

Due to its chemical structure, PLA is hydrophobic. The repeating unit of PLA, which is lactic acid (LA), is non-polar and lacks polar bonds. As a result, when LA molecules polymerize to form PLA, the resulting polymer retains its non-polarity and hydrophobic nature [21].

Mechanical properties

Mechanical properties play an important role in tissue engineering as they determine whether a biomaterial is suitable for use in a particular application. It is therefore crucial that the mechanical properties match those of the damaged tissue, otherwise there is a risk of rejection, inflammation and destruction of the biomaterial. Mechanical properties also have an impact on the cells seeded on the scaffold. For example, if the material is too rigid, the cells are unable to adhere and proliferate as expected and are not able to survive. Obviously, without cells no tissue can be regenerated. It is therefore crucial to select the right material for the application based on its mechanical properties.

With regard to the mechanical properties, PLA is characterized as a stiff and brittle material. Its stiffness (E), tensile strength (σ_y), elongation at break (ϵ) and mechanical strength (σ_{max}) can be quantified thanks to a tensile test, as represented in Figure 2.5.

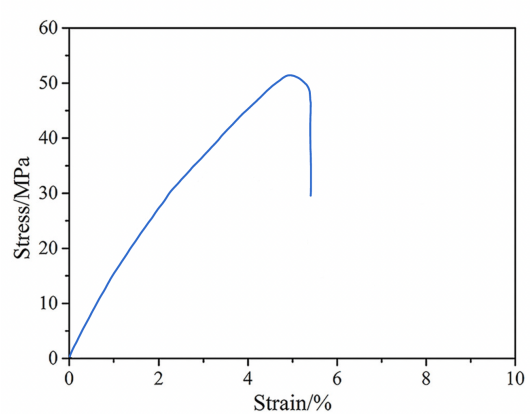

Figure 2.5: Tensile stress-strain curve of PLA [26]

However, these values are strongly dependent on the crystallinity and molecular weight. The higher the molecular weight, the higher the modulus of elasticity and strength and the lower the strain. This is due to the fact that higher molecular weight chains are longer, facilitating stress transfer. This makes the material stiffer and stronger but less flexible. By analogy, a higher degree of crystallinity also corresponds to a stiffer and stronger but more brittle material.

The crystallinity of a material is related to T_g and T_m. Below T_g, the material is glass and has its best rigidity because the chains can not move. Above T_g, the amorphous regions are considered as a liquid. As a result, the amorphous regions lose the mechanical strength they had at lower temperatures but are able to deform more easily. In contrast, the crystalline regions of the thermoplastic retain their mechanical strength up to their melting temperature (T_m) because they are held together by strong intermolecular forces. Therefore, a highly crystalline thermoplastic generally has better mechanical properties at higher temperatures, because the crystalline regions will remain intact even if the amorphous regions become more mobile. This is illustrated by Figure 2.6. In conclusion, a highly crystalline polymer is characterized by high stiffness and low strength, a high T_m , while an amorphous polymer is rather soft and flexible and has no T_m.

It is therefore relevant to compare the mechanical property values between a semicrystalline material (PLA) and an amorphous material (quenched PLA). One study looked at the difference between the mechanical properties of PLA and PLA subjected to a temperature of 60°C for 20 minutes and then immersed in ice water [28]. The values are shown in Table 2.2.

Table 2.2: Mechanical properties of PLA and quenched PLA

Properties	**PLA**	**Quenched PLA**
Elastic modulus (E)	4.2-4.4 GPa	2.3-3.7 GPa
Yield strength (σ_y)	57.9-58.9 MPa	52.8-54 MPa
Elongation at break (ϵ)	13-21%	372-472%

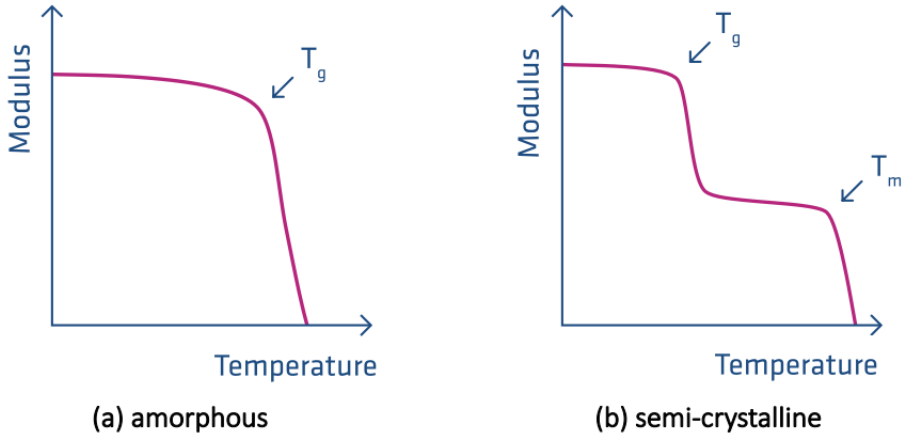

Figure 2.6: Young's modulus in function of temperature for an amorphous and semi-crystalline polymer [27]

Biological properties

From a biological point of view, two main characteristics are important for any type of TE application: biocompatibility and biodegradability. Biocompatibility is the ability of a material to co-exist in a living system without harming it and causing immunological rejection. Any material inserted into the body generates a foreign body response. However, this response must be safe for humans. A biodegradable material is one that is able to decompose after interacting with biological elements. This feature allows, once the tissue begins to regenerate, the scaffold to be gradually and safely removed from its implant site so that the tissue can continue to grow. A second advantage of biodegradability is that it prevents the patient from needing a second operation to remove the implant.

Biocompatibility

Numerous studies have proven that PLLA is a biocompatible material. The immune response generated by PLLA implantation is usually minimal. Furthermore, PLLA is favourable to cellular integration, a key point in tissue revascularization, conferring in addition to biocompatibility an angiogenic character [29].

Biodegradability

A second reason for the FDA approval of PLLA is the products obtained after its biodegradation. PLLA degrades to L-lactic acid by hydrolysis, a molecule that is completely non-toxic to the human body. Actually, L-LA is already known to the body as it is produced by the body in large quantities and present in many tissues and fluids of the body, such as muscle tissue and blood. When PLLA is degraded in the body, the resulting lactic acid is metabolised by the liver and other organs into water and carbon dioxide, which are then excreted from the body through the urine [16].

The rate of degradation of a scaffold is essential for successful tissue regeneration. If the implant degrades too quickly, the cells do not have time to insert themselves into the scaffold. If the degradation is too slow, the scaffold is incorporated into the regeneration and then degrades, creating a hole in the new tissue. Ideally, the scaffold should degrade as fast as the patient's tissue grows. The rate of degradation should therefore be equal to the rate of deposition of the extracellular matrix (ECM) of the specific tissue to be regenerated [30, 31].
Furthermore, as the scaffold degrades, its mechanical properties are reduced. In order to be used in a biomedical application, it must be able to retain its mechanical properties for a sufficiently long time.

The degradation kinetics of PLLA depends on multiple factors such as crystallinity, deformation, microstructure, specific application, implantation site and the physiology of the patient (temperature, pH, pulsation...). In a high crystallinity polymer, the molecular chains are tighter, making it more difficult for water molecules or enzymes to penetrate and degrade the material. Conversely, a low crystallinity polymer has more disordered and loose chains, making it easier for water and enzymes to penetrate and degrade. Similarly, when a material is subjected to greater deformation, it undergoes more deformation and mechanical stress, which can lead to the breakdown of molecular bonds and chains within the material. This can increase the accessibility of water and enzymes to the degraded sites, accelerating the degradation process. In conclusion, lower crystallinity and higher strain result in a faster degradation rate.
For the PLLA, the degradation time has been studied in vitro and in vivo, and it was found that about 40 weeks and 20 weeks respectively are needed to degrade PLLA [32, 33].

2.1.2 Biomedical applications

To show the properties discussed, a study focused on a biomedical application that used a 3D printed porous PLA scaffold. The scaffold was used for bone tissue replacement and was created using a 3D printing. The researchers varied the printing parameters such as layer thickness, fill density and printing speed to achieve the desired scaffold architecture. The porosity of the scaffold was controlled by adjusting the fill density and reached a range of 45-60%.

The porosity of the scaffold was only 30%, which is lower than the recommended porosity of about 90% for bone tissue replacement. However, the study showed that high porosity is not always necessary for bone tissue regeneration. The scaffold with a pore size of 0.7 mm allowed sufficient cell proliferation and contained more material in its structure, which provides better mechanical durability. The toxicity of this material and its effect on cell viability, proliferation and differentiation were evaluated using osteosarcoma cells. The results indicated that the scaffold promoted cell proliferation and showed good osteoconductivity, indicating its potential for bone tissue regeneration.
Figure 2.7 shows that the scaffold has high cell viability, with the majority of cells stained green representing live cells compared to the small number of cells stained red, dead cells, after seeding the cells on the scaffold.

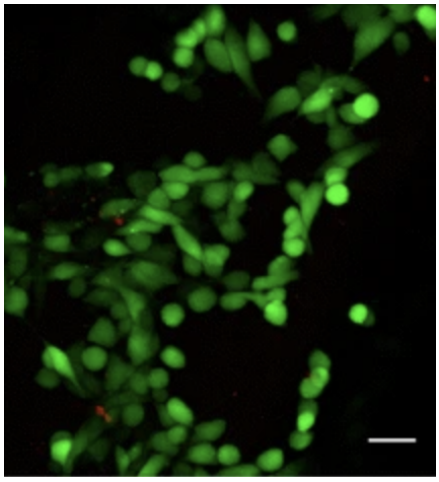

Figure 2.7: Green staining of live cells and red staining of osteosarcoma dead cells seeded on the scaffold after a 4-day culture [34]

Overall, this study demonstrated the successful fabrication of a scaffold for bone tissue regeneration using 3D printing and commercially available PLA. The findings indicate that it is possible to optimize the porosity and pore size of the scaffold to improve mechanical properties and cell proliferation, while simplifying the printing process [34].

Another study explored 3D printing technology to fabricate a scaffold using a combination of polylactic acid (PLA) and nano-hydroxyapatite (nHAp). Several steps were required for the fabrication of this scaffold. Firstly, the PLA and nHAp were mixed at a ratio of 90% and 10%, respectively, and then melt extruded to obtain a filament of 1.75 mm diameter. This filament was then used by the 3D printer to create the scaffold layer by layer. After a series of material characterizations, it was found that the scaffold had comparable mechanical strength to human trabecular bone. Furthermore, the porosity was also evaluated, and it revealed that the structure was porous and highly interconnected, which is suitable for bone tissue regeneration. The biocompatibility of the scaffold was also assessed by cytotoxicity tests, which gave favourable results. In addition, in vivo tests on rats for 4, 8 and 12 weeks showed bone progression in terms of osteogenesis and osteoconductivity. Figure 2.8 illustrates bone reformation after scaffold implantation in rats. After 4 weeks, the first signs of bone formation are observed. After 8 weeks, there is a significant increase in the progression of bone formation compared to 4 weeks. Finally, after 12 weeks, the bone is almost completely regenerated [35].

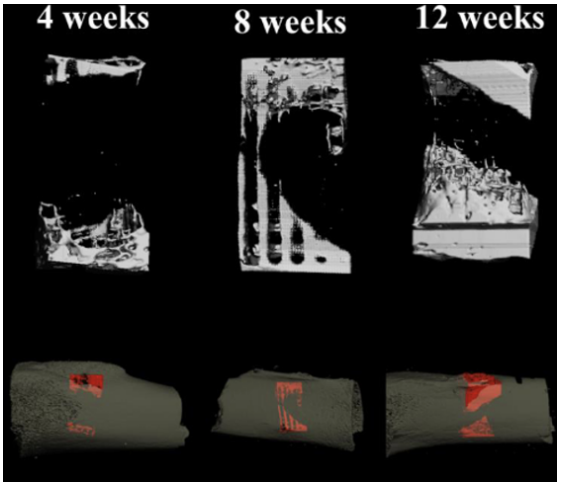

Figure 2.8: Micro-CT 3D images of bone formation after 4, 8, and 12 weeks of scaffold implantation in rats [35]

2.2 Blend PLA/PEG

Polymer blending is a widely adopted technique for improving the properties of materials to best meet specific application requirements. PEG and PLA offers interesting properties for biomedical applications.

2.2.1 PEG

Polyethylene glycol (PEG) or polyethylene oxide (PEO) is a linear polyether with a wide range of molecular weights. Its chemical formula is represented in Figure 2.9. In fact, PEG and PEO both refer to the same polymer, except that the term PEG is used for a polymer with a molecular weight of less than 20,000 g/mol and PEO is employed if the molecular weight is above 20,000 g/mol. For simplicity, the term PEG will be used to refer to the polymer in general, without reference to molecular weight. However, if the molecular weight is of any importance, the distinction between PEG and PEO will be made.

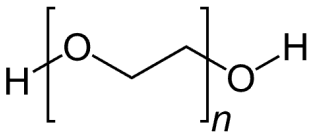

Figure 2.9: Chemical formula of PEG

PEG is an FDA-approved polymer that has already been used in medical applications, as in pharmaceuticals and cosmetics. Therefore, PEG is considered as a safe material for biomedical applications, which explains its large use in tissue engineering research. Using PEG as a hydrogel or scaffolding material, researchers are relying on its biocompatibility and other properties to create effective materials for tissue regeneration and growth.

Properties

An understanding of the physical and mechanical properties of the PLA/PEG blend is crucial to the results interpretation of the mixture analysis. This knowledge will help to explain the results of the analyses and provide relevant information on the behaviour of the mixture.

Physical properties

As mentioned earlier, the physical properties of a material are strongly dependent on its thermal history, molecular weight and degree of crystallization.

The T_g of PEG is between -67°C and -22°C and the T_m is between 20°C and 70°C. It is found that the T_m increases with increasing molecular weight until a certain M_n*. The same behaviour is observed for T_g. For example, for a heating of 5°C/min, the T_m of the PEG of different molecular weights evolves as indicated in Figure 2.10 [36, 37].

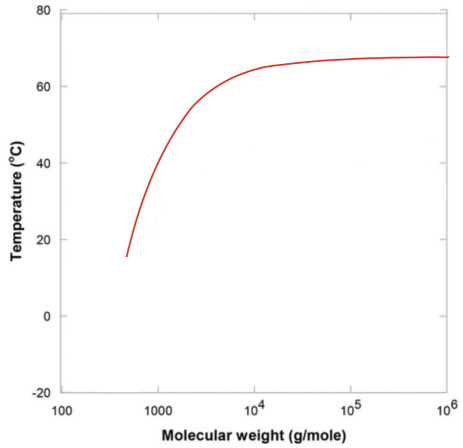

Figure 2.10: T_m in function of the molecular weight of PEG [36]

This finding is related to crystallization. In fact, for the same heating cycle, if the T_m increases, it means that the chains are more ordered and consequently the degree of crystallization is more important.

Moreover, PEG is a naturally hydrophilic and water-soluble polymer. Its high solubility in water is due to its chemical structure consisting of many oxygen atoms, which allows it to easily form hydrogen bonds with water molecules. This hydrophilic nature makes PEG an attractive choice for applications where water solubility is desired, such as in many pharmaceutical formulations. However, as with PLA, it is always possible to modify the surface behaviour of a material by adding a coating.

Mechanical properties

The mechanical properties of PEG have not been clearly defined in previous research. Only one study has investigated the Young's modulus of PEG alone and the data is shown in Figure 2.3[38]. Other research has focused solely on PEG as a hydrogel coupled with another component but in no case were the mechanical properties studied alone. However, research by Ruilong Li et al has shown that increasing the molecular weight of PEG leads

to an increase in elongation at break, which means that the material will be more resistant to deformation and flexible. For example, for a M_w of 2,000 g/mol, the Young's modulus is 31 MPa and for a M_w of 2,000,000 g/mol, the Young's modulus is 633 MPa [39].

Table 2.3: Mechanical property of PEG [38]

Properties	**PEG**
Elastic modulus (E)	31-633 MPa

2.2.2 Interest of PEG

First and foremost, PEG is used as a plasticizer for PLA to improve its flexibility and processability. When PEG is added to PLA, it modifies the arrangement of the polymer chains, which increases their mobility and leads to a reduction in T_g and T_m values. As a result, PLA becomes more thermoplastic and can be processed at lower temperatures. In addition, the increased thermoplasticity of PLA leads to a reduction in its mechanical properties, resulting in a softer material. This makes PLA easier to shape into the desired form, which allows for a wider range of applications [40].
On the basis of a DSC (differential scanning calorimetry) performed as part of a study, the decrease of the characteristic temperatures is well observed as the amount of PEG in the blend increases. For pure PLA, the T_g is about 70°C and that for a blend with 15% PEG the T_g is close to 60°C. Another observation is that when the PEG content of the mixture is higher than 30 wt%, a significant increase in the endothermic peak at 50°C is observed, indicating that PEG melts at this temperature, together with the T_g of PLA. The DSC can be seen in Figure 2.11, PEG0 represents a mixture with 0% PEG while PEG5 is a mixture with 5% PEG and 95% PLA. Therefore, from 30% PEG onwards, the PEG melting is significant and the phase separation is more noticeable. This is due to the difference in solubility between PLA and PEG, which causes them to separate into distinct phases as the PEG concentration increases [41].

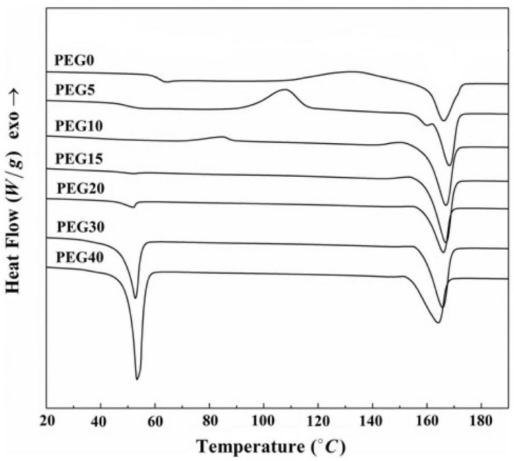

Figure 2.11: DSC thermograms of PLA/PEG blends [41]

Consequently, adding PEG to PLA for 3D printing reduces extrusion temperatures, which in turn makes the material easier to extrude. The viscosity of the polymer is decreased which leads to an increase in flow. By keeping the same printing parameters (print speed and feed speed), the polymer is therefore extruded in greater quantities and the layers are obviously thicker. As a result, the pore size imposed by the 3D printer's design model is reduced. Furthermore, this change in structure has also an impact on the quality of the print. Lower extrusion temperatures and thicker layers can lead to a reduction in printing accuracy, resulting in a rougher structure. As the amount of PEG increases, the pore structure becomes rougher and the pore diameter decreases. In Figure 2.12, the mixture of chopped PLA filament (M_w=182,000 g/mol) and PEG pellets (M_w= 6,000 g/mol) were dissolved in chloroform with a stirrer. Then, the chloroform was removed from the mixture by placing the mixture in an oven at 40°C for 24 hours. Several blends were prepared depending on the amount of PEG present in the blend, for example PEG5 represents a blend with 5% PEG. The prints were all extruded at 210°C and at a speed of 10 mm/s with a feed rate of 100%. It is clear that the pure PLA print is uniform and the macropores are square. As the amount of PEG increases, the structure becomes less regular and the pores become more and more rounded.
But this effect can be counteracted by changing the print and feed speeds so that the filament exits the nozzle smoother. It is therefore essential to find a balance between the amount of PEG and the 3D printing parameters, in order to closely approximate the desired properties the specific properties of the biological application [9, 42].

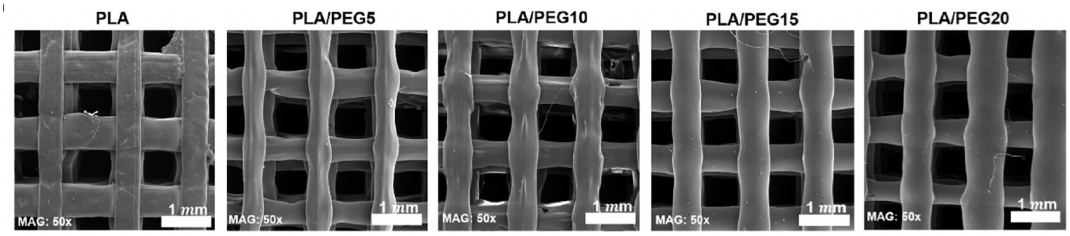

Figure 2.12: SEM images of 3D printed scaffolds of PLA/PEG blends [42]

In a tensile test on different PLA/PEG blends, it was evident that the addition of PEG decreases the Young's modulus but increases its flexibility. To give an idea of values, for pure PLA, the Young's modulus is 3.1 GPa and the elongation at break is about 3%. If, on the other hand, the mixture is made up of 20% PEG, the Young's modulus is reduced to 1.3 GPa but its breaking point is increased to 34%.

During the mixing of PEG and PLA, hydrophilic PEG chains are added to a hydrophobic material. This creates an amphiphilic blend with both hydrophilic and hydrophobic regions. Figure 2.13 shows that the contact angle decreases as the amount of PEG in the mixture increases. This means that the surface becomes less hydrophobic and more hydrophilic as the PEG concentration increases. The addition of PEG has also an impact on the degradation rate of the polymer. The material now has more hydrophilic content. Therefore, when these regions are exposed to molecules of water, they dissolve due to the water solubility of PEG, creating holes in the polymer. There are now more sites through which water can penetrate and degrade the material. This is why degradation will be accelerated.

Figure 2.13: Water contact angle graph of PLA/PEG blends [42]

In conclusion, PEG has interesting properties for biomedical applications, such as biocompatibility, high water solubility and its ability to reduce polymer stiffness. By blending PEG with PLA, it is possible to create a material with lower stiffness, higher flexibility and lower characteristic temperatures. At the same time, it is crucial to find a balance between printing parameters and 3D printing accuracy to ensure that the addition of PEG does not compromise the overall porosity defined by the object design.

2.2.3 Biomedical applications

A first study investigated the development of porous 3D PLA/PEG scaffolds by solvent casting and leaching of porogens. It was found that PEG increased the pore size without impacting the total porosity. The study also examined the effect of PEG incorporation on cell proliferation and bone matrix formation by culturing cells on the scaffolds. Initial cell attachment was not affected by the addition of PEG, but the PEG-containing scaffolds promoted cell growth over time. SEM images 2.14 highlights this enhanced cell migration within the scaffold [43].

This study suggests that PLA/PEG scaffolds may have major applications in bone tissue engineering, and that PEG can be incorporated to enhance osteogenic behaviour.

Another study was conducted to investigate the suitability of electrospun PLA/PEG nanofibres as a delivery system for antimicrobial peptides. The PLA/PEG combination appears to be a good choice of materials as it offers a balance between hydrophobic and hydrophilic properties, which allows for controlled release of peptides. In addition, the biodegradability makes the materials easier to process into fibre. Several proportions of PLA/PEG were studied, but the most effective for drug delivery was 50/50 because it had the lowest mass loss over time. The SEM images 2.15 from this study confirm that the 50/50 mixture loses the least mass over time. The study also showed that electrospinning was suitable for the application. More specifically, the high surface-to-volume ratio of the electrospun nanofibres favours the contact time with the infected surface, enhancing the effectiveness of the antimicrobial peptides [44].

In conclusion, this study demonstrates that the addition of PEG to PLA can modify the properties of the material to meet the requirements of biological applications, such as drug delivery in the case of this study.

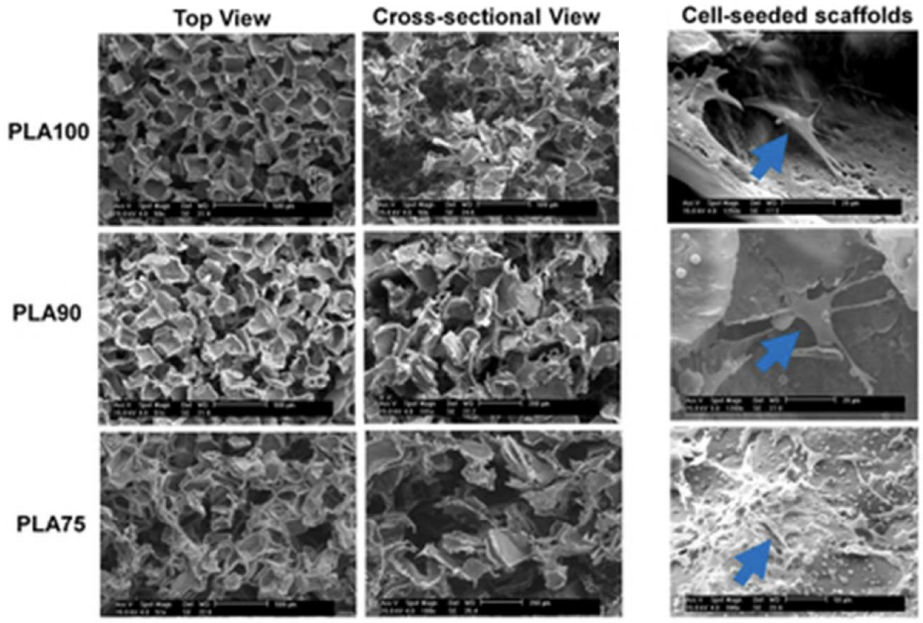

Figure 2.14: SEM images display the scaffold surface for each composition in both top view and cross-sectional view, without cells, based on their respective orientation. Meanwhile, SEM images with seeded cells demonstrate cell attachment and appearance, which are indicated by a blue arrow [43]

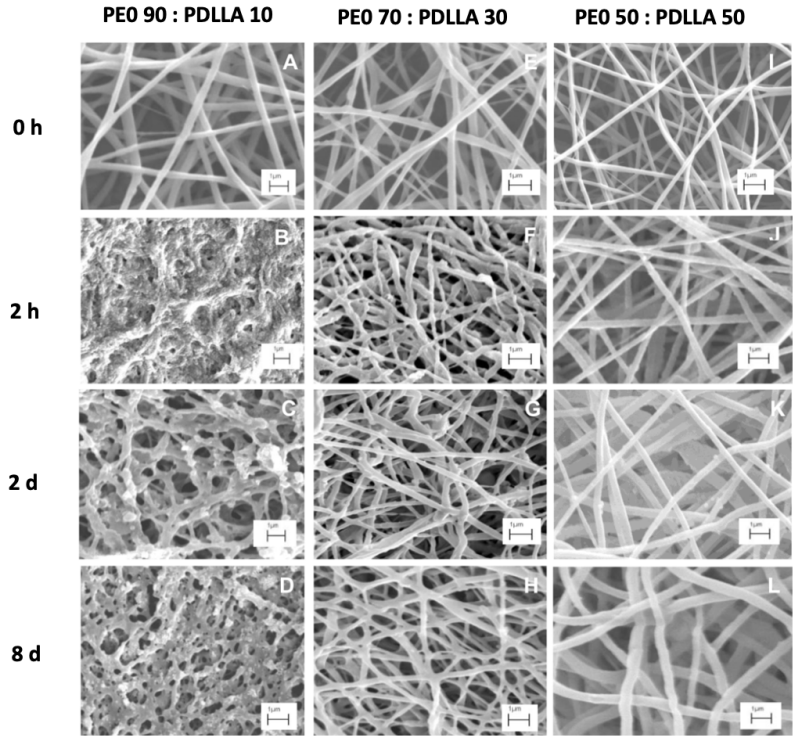

Figure 2.15: SEM images of PEO/PDLLA blend fibers after 0h, 2h, 2 days and 8 days [44]

2.3 Porosity

Porosity is a critical parameter in tissue engineering that can significantly impact the functionality of an implant. The use of porous scaffolds can facilitate cell adhesion, proliferation, and migration, as well as the diffusion of nutrients, oxygen, and waste. The structure of the pore network can influence tissue formation and promote new tissue growth. A porous surface can also promote mechanical interlocking between the surrounding tissue and the scaffold. Effectively, the porosity allows both the new tissue to penetrate and surround the scaffold, making the connection between the scaffold and the tissue. However, it is important to be careful with the mechanical properties of a scaffold, as high porosity reduces its stiffness and strength, making it more vulnerable to failure.

2.3.1 Types of porosity

There are several types of porosity, classified according to pore size. Three categories exist: microporosity, mesoporosity and macroporosity. Microporosity, as the name suggests, is made up of relatively small pores with diameters lower than 100 µm. Macroporosity, on the other hand, refers to large pores with a diameter greater than 300 µm. Finally, mesoporous materials belong to the intermediate class between microporosity and macroporosity, characterized by a pore size between 100 an 300 µm.

These categories are further subdivided into two sub-categories based on the connectivity between the pores. When the pores are connected to each other, the porosity is said to be open. Otherwise, the porosity is called closed [45]. This is illustrated in Figure 2.16.

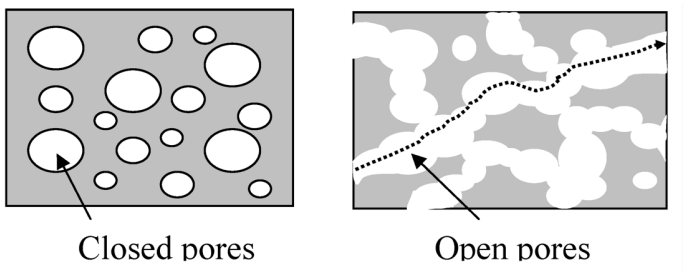

Figure 2.16: Closed and open porosity

For successful tissue engineering, a single pore size is not universally suitable but it depends on the type of application in which the scaffold will be used. For example, macropores are advantageous for blood vessel revascularization and bone tissue growth, while micropores play a critical role in the capillary levels of bone tissue. On the other hand, the porosity must absolutely be open, otherwise it would block the exchange of nutrients, oxygen and waste products, which are vital for the proper functioning and growth of cells. Without open porosity, the cells would be isolated from the environment and unable to receive the necessary substances, thus compromising their survival. Therefore, although pore size is important, open porosity is mandatory in tissue engineering for successful

tissue regeneration [46, 47].

2.3.2 Methods for creating a porous structure

The methods of making a porous scaffold fall into two categories: conventional and rapid prototyping. While conventional techniques refer to methods of creating a scaffold that were established a long time ago and have proven effective in the past, rapid prototyping includes recent techniques that model a structure from three-dimensional computer-aided design (CAD) data. At present, conventional techniques are much less used as they do not allow good control of the porosity architecture, often use toxic solvents that can lead to cell death and provide mechanical properties that are far inferior to those of all hard and most soft tissues. The main conventional techniques are porogen leaching, freeze drying, gas foaming and electrospinning. In contrast, prototype methods offer better control of the architecture at both micro and macroscopic levels and the mechanical properties are more suitable for tissue engineering. This approach also provides a good repeatability in design. However, the number of biomaterials that can be used by these techniques remains limited. The major prototyping technique is 3D printing [48, 49, 50, 51].

Porogen leaching involves dissolving a polymer in a volatile solvent and uniformly distributing a porogen within the solution. The most known porogen is salt. When the solvent is evaporated and the polymer cures, the porogen is trapped inside the polymer. The biomaterial is then immersed in a suitable porogen solvent, which leaches out the porogen and creates pores with a diameter between 50 and 300 µm within the matrix. This is illustrated in Figure 2.17 A).

This method is distinguished by its wide choice of polymers supporting this technology. It also allows for the control of pore size by adjusting the size of the porogen used. However, this technique is very time consuming and results in scaffolds with low interconnectivity between pores and getting a complex structure is almost impossible.

Freeze drying or lyophilization starts with a step to prepare the polymer as a solution. This polymer solution is then frozen. Thirdly, the polymer is sublimated to remove the ice crystals and fourthly, the remaining ice crystals are removed during secondary drying. The sublimation process creates pore sizes 40-300 µm where the ice crystals used to be. This is summarized by Figure 2.17 B).

Freeze-drying is a process with several advantages, including the efficiency with which water is removed from the biomaterial and the variation in pore size via temperature or rate of drying. Notwithstanding, as with porogen leaching, this method is time consuming, especially for the drying steps. In addition, as freezing is difficult to control, it results in heterogeneous scaffolds that prevent a homogeneous pore structure from being obtained.

Gas foaming uses an effervescent salt, such as ammonium bicarbonate, as a foaming agent to create a porous microstructure in a polymer gel. When immersed in hot water or under pressure, the ammonium bicarbonate particles produce ammonia and carbon dioxide, which escape and create pores in the polymer matrix. The use of gaseous porogens induces the escape of gas during polymerization, which leads to the formation of bubbles

and thus to pores of size 20-500 µm. This is shown in Figure 2.17 C).

This method offers a key advantage by eliminating the use of organic solvents, which eliminates potential health hazards. The resulting scaffold can be highly porous, but one drawback is that the pores often lack interconnectivity, which can limit their usefulness. Additionally, controlling the porosity of the scaffold can be challenging.

Electrospinning is a process that employs an electrical field to create fine fibers from a polymer solution. The device consists of a syringe connected to a high voltage power source. The syringe containing the polymer solution is subjected to a pressure that ejects the solution from the syringe. Subsequently, the applied electric field causes a jet of charged material to be formed. The charged jet is then drawn towards a grounded collection vessel. This ensures that the fibres emerge continuously and not as droplets. Once the fibres are collected, the solvent evaporates and the fibres solidify to form a porous material of size between 0.01 and 45 µm. Figure 2.17 D) highlights this process.

Electrospinning is the most widely used conventional technique due to its simplicity and cost. In addition, it allows the creation of scaffolds with a high surface-to-volume ratio, which is very useful for TE. Fibres produced by electrospinning can have very small diameters of the order of ten nanometres. And it appears that the extracellular matrix of many tissues in the body has fibres of similar size. Therefore, electrospinning can create structures that strongly resemble the extracellular matrix, which is beneficial for successful tissue regeneration. However, the results are different from one method to the other because electrospinning depends on many parameters such as humidity, temperature and flow rate. Reproducibility is therefore low.

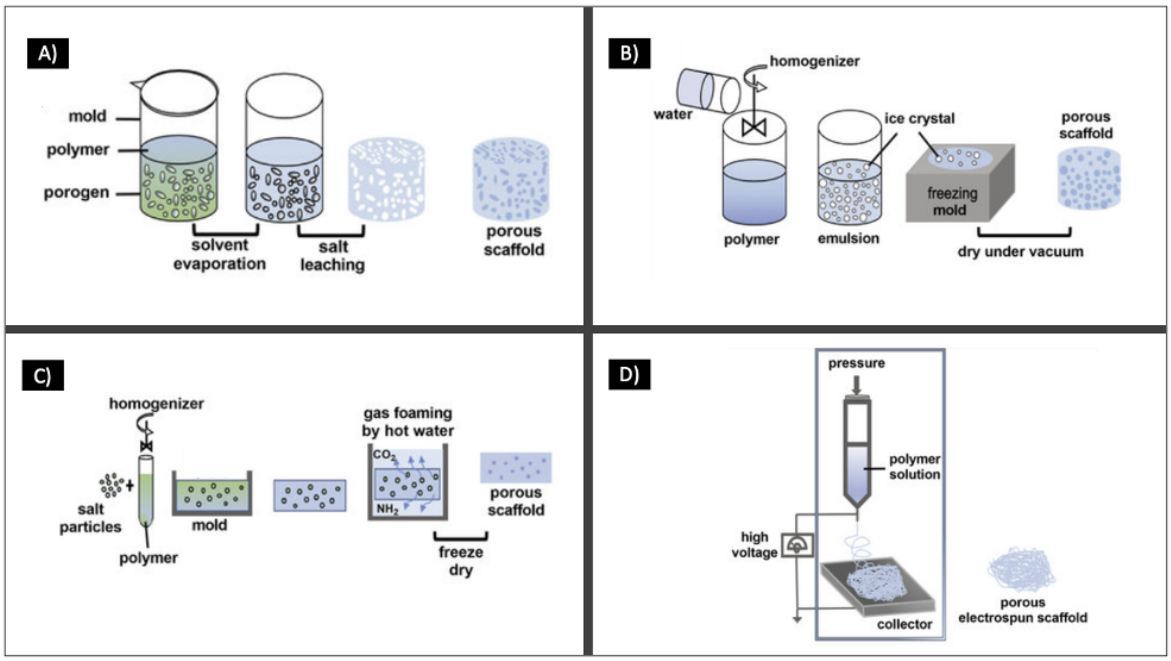

Figure 2.17: Conventional techniques for creating a porous scffold. A) Porogen leaching, B) Freeze drying, C) Gas foaming and D) Electrospinning [46]

3D printing (3DP) is a technology that creates three-dimensional objects from a digital model. The principle of 3D printing is to deposit material layer by layer to create a physical object. With this technique, the porosity is induced directly by the design. The choice of pore size is left to the user, who can select a size to suit the specific needs and requirements of his application. But variations in pore size are observed due to machine inaccuracies. Processing parameters such as printing speed, temperature, material flow and raw material quality influence the accuracy of the machine. In addition, the pore size also depends on the position of the layer, the density of the material and the roughness of the surface. Figure 2.18 illustrates the 3D printing mechanism.
3D printing has promising features and advantages, such as cost effectiveness and speed.

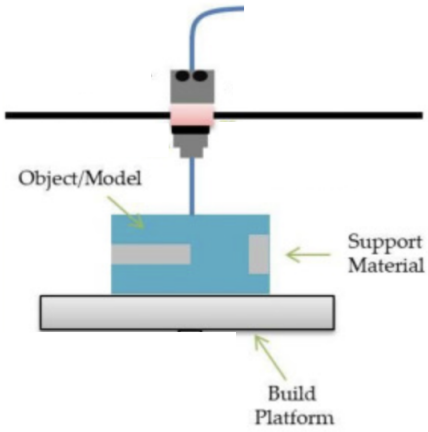

Figure 2.18: 3D printing [52]

This technology allows the production of complex 3D structures. The level of porosity of 3D printed structures can be precisely controlled by the user's choice of design and processing parameters. However, the availability of polymers suitable for the 3DP technique is currently limited, and relatively negligible design imperfections can occur. Despite these limitations, 3DP technology remains very versatile and adaptable. More details on 3D printing will be given in the next section 2.4.

2.4 Benefits of 3D printing

When designing a scaffold, the ability to create a structure adapted to the patient's needs is crucial, which requires the integration of the patient's specific characteristics in the design of the implant as well as its shape. The functionality of the implant also depends on its porosity, which must be appropriate for the biomedical application in which it will be used. To transform PLA pellets into a suitable scaffold, a range of technologies can be used.

The methods discussed earlier (see 2.3.2), including freeze-drying, gas foaming, and porogen leaching, could be suitable but these only allow the creation of simple structures. And implants are rarely such simple structures. On the other hand, electrospinning allows the creation of complex 3D structures. However, its poor reproducibility makes it unsuitable for scaffolds. Since repeated tests are required to validate a scaffold, any

variation in the structure from one test to the next would lead to significant discrepancies in the results, which would hamper validation. Therefore, all such conventional techniques should be excluded.

With this in mind, there are two main competing techniques for manufacturing objects: injection moulding and 3D printing.
Injection moulding involves uniformly melting the polymer and injecting it at high pressure into a mould of the desired shape. The material then cools and solidifies inside the mould, resulting in the final object. This technique has various advantages, such as a high production rate, precision and the ability to create complex shapes. However, there are limitations, as the mould must be customised for each object, making the process expensive and time consuming. Additionally, it can be difficult to generate porosity using injection moulding, as the high pressure used to inject the polymer into the mould compresses the material, minimising the creation of pores.
3D printing therefore seems the most suitable, as the change of design does not necessitate the creation of a new mold; rather, it only requires editing the structure that has been saved in the CAD file and subsequently programmed into the printer.

Four main categories of 3D printing can be used for tissue engineering: fused deposition modeling, bioprinting, selective laser sintering and stereolithography [52].

Fused deposition modeling (FDM) involves the layer-by-layer deposition of molten thermoplastic material to create a 3D object. The model to be reproduced is drawn using CAD software and then translated so that the FDM printer reproduces the defined model. The FDM printer contains a coil of thermoplastic material that is fed into a heated nozzle. As the material passes through the nozzle, it is melted and extruded onto a build platform in a specific pattern based on the CAD design. The nozzle moves either in the x-y plane and the build platform moves in the z-axis, allowing the final object to be built layer by layer, as shown in Figure 2.19. Once the first layer is deposited, the material cools and solidifies quickly, allowing the finished product to be easily removed from the printer platform.

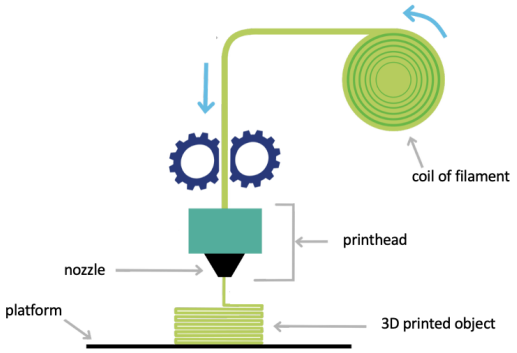

Figure 2.19: Schematic of a fused deposition modeling 3D printer [53]

FDM is a widely used 3D printing technology. One of its advantages is that many non-cytotoxic materials can be shaped using FDM, making it safer for biomedical applications. In addition, FDM is a relatively inexpensive 3D printing method. On the other hand, the use of FDM has some limitations. One of the main limitations is that FDM can only work with thermoplastic materials, which limits the types of materials that can be printed. The resolution of FDM is slightly lower than other 3D printing technologies, which can result in less accurate prints.

In order to use FDM, it is essential that the polymer material is in the form of a filament. An additional process is therefore required to convert the raw polymer material into the desired filament form, and this process is known as extrusion. The extrusion process involves heating the raw polymer material to its melting point, allowing it to become a viscous liquid. Once the material has reached its melting point, it is transported by means of a rotating screw to a die with an opening shaped to match the filament. The filament is then cooled and solidified [19, 54].

Bioprinting follows the same principle as fused deposition modeling but with the use of a bioink instead of a filament. The bioink is a special material containing all the necessary elements for tissue engineering, namely living cells suspended in a biomaterial matrix, together with growth factors. The bioprinter then deposits the bioink in a precise pattern, layer by layer, to create the desired three-dimensional structure. This is depicted in Figure 2.20.

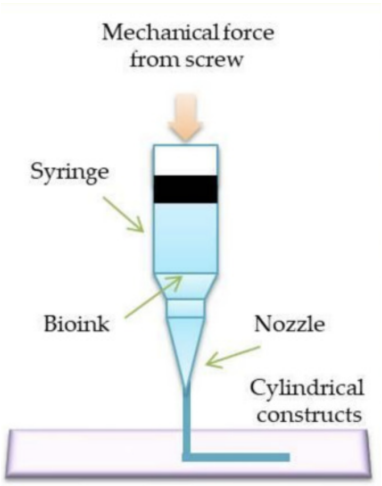

Figure 2.20: Schematic of a 3D bioprinter [52]

Bioprinting is an innovative technology whose main advantage is the printing of viable cells for soft tissue applications, such as muscle tissue or cartilage. This type of biological tissue manufacturing method is generally considered as an alternative for patients waiting for organ transplants, as 3D printed tissues can be produced quickly and customised to the needs of each patient. However, this technique also has its drawbacks. Firstly, support structures are often required to maintain the shape of the 3D printed tissue. In addition, the size of the printing nozzles limits the resolution of the details that can be printed,

which can make the reproduction of more complex structures difficult. Finally, during the printing process it is essential that the materials used do not become cytotoxic, in order to preserve the viability of the printed cells.

Selective laser sintering (SLS) is a technolgy that uses a laser to selectively melt and fuse small particles of a powder material to create a three-dimensional object defined by CAD. The powdered material is spread out on a build platform and the laser is directed onto the surface of the powder, melting and fusing the particles according to a pre-defined pattern by the computer. Once the first layer is complete, the platform is lowered and a new layer of powder material is spread over the previous layer. The laser then fuses the particles of the new layer to the previous layer. The process is repeated layer by layer until the final object is formed. The porosity of the object is generated voluntarily via the computer-defined model. This is shown in Figure 2.21.

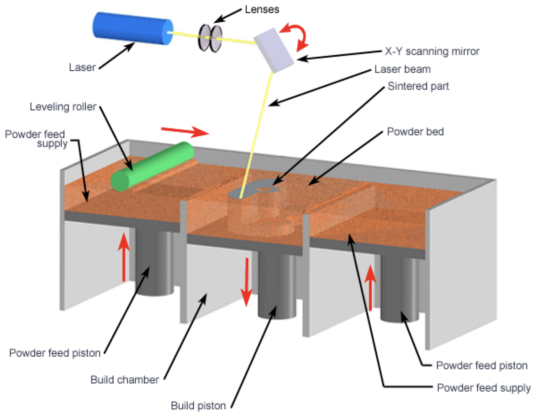

Figure 2.21: Schematic of a selective laser sintering 3D printer [55]

This technology offers the benefits of precise control of porosity by design, achieved quickly and inexpensively. However, there is a potential risk of material degradation due to the high temperatures required to sinter the powders. In addition, SLS printing requires a large amount of material, which is not suitable for small-scale printing. In SLS printing, a large bin filled with powder is used to selectively sinter the material into the desired shape. When the printing process is complete, there may be a significant amount of unused powder left over, which can be recycled for subsequent print runs. However, the unused powder represents an additional cost.

Stereolithography (SLA) is a method that involves the use of a liquid resin that solidifies when exposed to a beam of UV light, as illustrated in Figure 2.22. The process begins by depositing and solidifying the resin on a platform that lowers as each layer is completed, according to the CAD model. This is repeated until the desired prototype is obtained. Once printing is complete, any uncured resin is washed off and the prototype is subjected to further UV exposure to ensure that it is fully cured and ready for use.

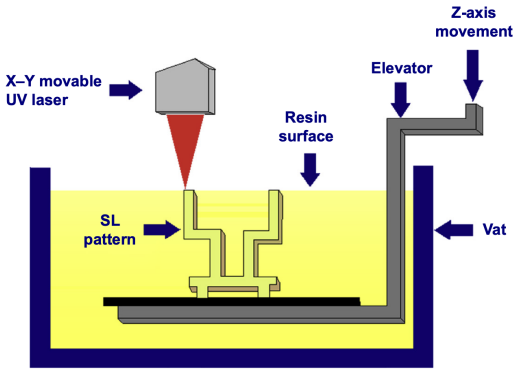

Figure 2.22: Schematic of a stereolithography 3D printer [56]

Despite the fact that this technology is very accurate, the longer the processing time, the more accurate it is. In addition, only a few photo-sensitive polymers can also be used for tissue engineering. Finally, although SLA printing does not require as much material as SLS printing, it does require liquid resin. The utilization of this liquid resin may be necessary in large quantities and its cost may also be high, especially for high performance materials.

In conclusion, the choice of technology for scaffold fabrication in tissue engineering is essential to achieve correct results. Although there are several 3D printing methods, FDM is the most suitable for printing a mixture of PLA/PEG materials. Bioprinting with PLA is not possible due to its high rigidity, and SLA is not suitable due to the use of UV. Although SLS is an option, it is the least suitable compared to FDM in terms of cost and simplicity. Therefore, FDM is the preferred option for creating scaffolds based on a blend of thermoplastics as it offers a combination of ease of use and affordability.

Chapter 3

Objectives, strategy and methodology

3.1 Objectives and strategy

The overall objective of this thesis is to develop a non-toxic and environmentally friendly process to create two levels of porosity (macroporosity and microporosity) in a 3D printed polylactic acid (PLA) scaffold. In the future, this implant could be used for tissue engineering. By developing an efficient process for creating PLA scaffolds with controlled levels of porosity, this research will help improve tissue engineering techniques.

PLA is a widely used material in tissue engineering due to its biocompatibility, FDA approval and numerous successes as a scaffold. One of the main requirements of tissue engineering is the ability to adapt the scaffold to the patient. The most promising method at present for the patient-specific is 3D printing [34, 35].

Furthermore, to promote tissue regeneration, it is crucial to induce porosity in the scaffold, which allows for cell infiltration and the exchange of nutrients and waste products. 3D printing allows the creation of macroporosity through the design imposed by the model, but not microporosity. It is possible to create pores with a minimum size of 300 µm for the most efficient printers. However, the optimal pore size for biomedical applications is between 150 and 350 µm to allow, in addition to cell infiltration, the incorporation of new blood vessels into the scaffold, which facilitates vascularization and cell survival. Pores smaller than this range are also interesting because they allow the transport of cells and nutrients, which is the most important characteristic of porosity. In terms of size, the porosity generated by 3D printing is therefore not optimal because it is too large. The scaffold must retain a certain mechanical strength for the biological application in which it will be used, and the more porous the material, the lower its mechanical properties. Therefore, although 3D printing can create porous scaffolds, 3D printing is more useful for implant customisation than for generating microporosity [57, 58].

To generate micropores in the 3D structure, it is essential to develop an additional technique that can be used in combination with 3D printing to produce smaller pores. This technique should not use solvents that could affect the biocompatibility of PLA. The process involves mixing PLA with polyethylene glycol (PEG), which is also an FDA approved polymer. Previous studies have focused on PLA/PEG blending and it has been

found that PEG is a good additive for PLA in 3D printing, improving printability. In addition, PEG is water soluble, which is an added benefit for creating microporosity in the scaffold by simply extracting PEG in water.

Once the porosity has been generated in the scaffold, it is essential to verify that porous PLA still presents appropriate properties for application in tissue engineering. This involves an assessment of the physical properties (T_g, T_m and X_c) after all these processing and material design steps, the viscoelastic properties and the mechanical properties. Through a detailed analysis, the following research questions will be answered: How do the physical, viscoelastic and mechanical properties of porous PLA/PEG scaffolds compare with those of pure PLA scaffolds ? And are these properties considered acceptable for tissue engineering ?

This study focuses on the elaboration of porous scaffold by proposing a solvent-free and toxic substance-free method to induce suitable porosity for tissue engineering in 3D printed scaffolds from a PLA/PEG mixture.

3.2 Methodology

To reach the goal, different tasks have to be achieved. Firstly, filaments made of PLA/PEG blends, with the right diameter for 3D printing, should be created by extrusion. This step is described in section 4.2. These filaments will then be used to print the desired structures presenting macroporosity. In a third step, PEG uses as porogen polymer will be removed by dissolution in water to create microporosity in the 3D printed structures.

Preliminary results obtained on 90/10, 70/30 and 50/50 PLA/PEG films showed that the most interesting composition was 70/30 as it offered the best 3D pre-printing properties. The 90/10 composition did not have enough porosity and the 50/50 composition was very porous but more fragile and brittle when the PEG was removed. Therefore, from now on, only the 70/30 composition will be studied [59].

It is known that there is a strong relationship between porosity and mechanical properties. Therefore, it is important to study the mechanical properties of the material. It turns out that the mechanical properties of the scaffold depend strongly on several scaffold parameters: molar mass of PEG, geometry of the printed object and crystallinity. The 3D printing parameters have an indirect effect on the mechanical properties as they influence the crystallinity which, in turn, has an impact on the mechanical properties. It is therefore important to quantify the effect of these parameters on the mechanical properties after 3D printing. To this end, each parameter will be studied individually and its impact on the mechanical properties will be analyzed using a tensile test and a dynamic mechanical analysis (DMA). DMA gives the Young's modulus as a function of a certain temperature whereas the tensile test gives, in addition to the Young's modulus, yield strength and elongation at break.

The parameters influencing the mechanical properties to be evaluated are :

- Porosity

  The porosity of the implant is essential for the incorporation of the cells, nutrients and hormones for the differentiation and function of these substances. Porosity is also very important for the revascularization of the defective tissue. More specifically, the size and interconnectivity of the pores characterize porosity. If the pore size is large (in the range of 200 to 300 µm), then this allows the infiltration of new blood vessels into the scaffold facilitating vascularization and cell survival. However, the larger the pore size, the more fragile the material. Finally, a large interconnection between the pores improves the permeability of the scaffold. Improved permeability is a critical characteristic for a scaffold to facilitate the diffusion of nutrients, gases, and waste products within the tissue engineering construct. A higher level of interconnectivity between the pores ensures that cells receive sufficient oxygen and nutrients while waste products are efficiently removed. This process is vital for the maintenance of tissue health and viability [58].
  The PLA/PEG blend can have a double porosity. The first porosity can be created thanks to 3D printing and the second one is elaborated by the removal of PEG in the scaffold. Therefore, the pore size should ideally be between 50 and 200 µm for the PEG removal porosity and between 300 µm and 500 µm for the 3D printing porosity. The overall porosity should be of the open porosity type, as this would reflect pore interconnectivity, which is one of the desired aspects in creating a scaffold.
  In this work, the porosity was studied by Scanning Electron Microscopy (SEM).

- Molar mass of PEG

  The molar mass of PLA chains is 100,000 g/mol (100K), while the molar masses of PEG can vary: 3,350 g/mol (PEG3K), 100,000 g/mol (PEO100K) and 1,000,000 g/mol (PEO1M). The three PEG molar masses were chosen so that one is much lower than the molar mass of PLA, the next is equal and the last is much higher. The aim of studying this parameter is to observe the changes in properties according to the molar mass of the PEG.

- Crystallinity

  Crystallinity is related to mechanical properties. A higher crystallinity results in a higher Young's modulus and therefore greater rigidity. However, the material is more brittle and less resistant to deformation. On the other hand, a lower crystallinity results in a lower Young's modulus but a higher toughness, allowing the material to better resist deformation without fracturing. Thus, the ideal crystallinity for a tissue engineering scaffold must strike a balance between stiffness and brittleness.
  Differential Scanning Calorimetry (DSC) is a commonly used technique to analyze the crystallinity of materials. By analysing the DSC data, the influence of crystallinity on the mechanical properties of the material was established.

In summary, filaments will be created by extrusion using a 70/30 PLA/PEG blend. By varying the molar mass of the PEG in the blend, three different types of filaments will be created: PLA/PEG3K, PLA/PEO100K and PLA/PEO1M. To ensure the quality of the filaments, they will be characterized using different techniques. Differential scanning calorimetry (DSC) will be used to assess the impact of extrusion on the filament, while nuclear magnetic resonance (NMR) will be used to confirm the composition of the blend. During handling, there was a loss of material, which makes it uncertain whether the blend contains 70% PLA and 30% PEG. The filament will be used to print 3D structures. These printed objects will be analyzed by DSC to study the effect of the second extrusion generated by the 3D printer and their mechanical properties will be tested by DMA and tensile tests. Finally, the prints will be immersed in water to remove the PEG. The PEG removal method will be analyzed by NMR to verify that the PEG has been completely removed. Pore size will be determined using SEM, while DSC will be used to determine if there has been a change in crystallinity upon PEG removal. Finally, the mechanical properties of the porous structures will be assessed using DMA and tensile tests and compared to the print values from the previous step. This will help to understand the effect of porosity on 3D printing. The procedure followed is summarized in the scheme presented in Figure 3.1.

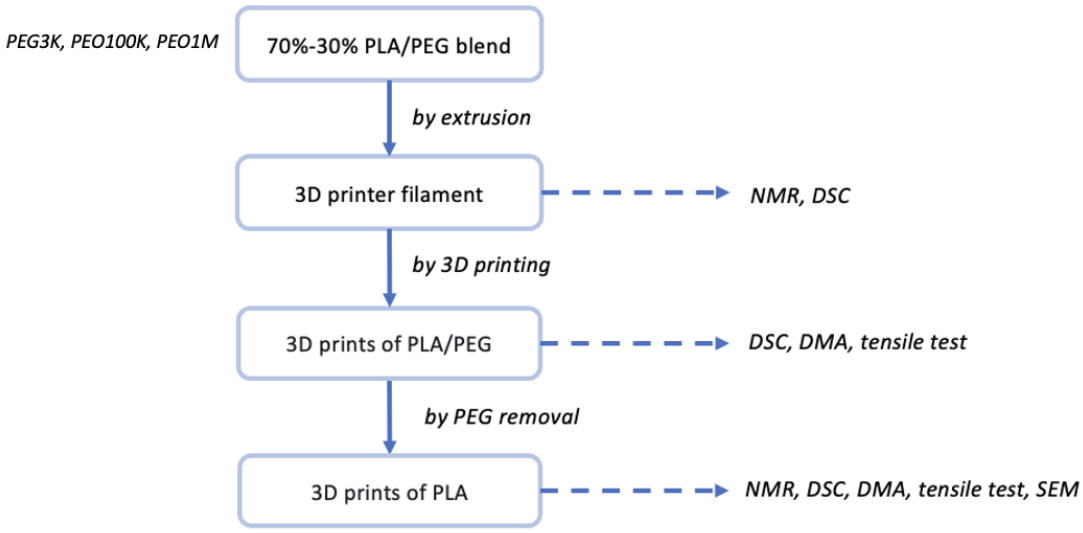

Figure 3.1: Main steps of the methodology

Chapter 4

Experimental section

4.1 Materials

The raw materials used in this thesis are PLA, PEG3K, PEO100K and PEO1M. The PLA of weight average molecular weight (M_w) of 100,000 g/mol comes from NatureWorks and is an Ingeo biopolymer 2500HP in pellet form. PEG3K, PEO100K and PEO1M are all supplied by Sigma-Aldrich in a powder form with a M_w of 3,350 g/mol, 100,000 g/mol and 1,000,000 g/mol respectively.

4.2 Preparation of 3D printer filaments

First of all, PLA pellets and PEG powder of three different molar masses (PEG3K, PEO100K and PEO1M) were mixed to achieve a PLA/PEG ratio 70/30 (expressed by mass) and dried under vacuum at 50°C for 24 hours before use. This step is crucial to remove moisture present in the samples.

The manufacturing process of 3D printing filaments consists of three steps and is summarized in Figure 4.1. The first stage, which is carried out using a double screw extruder, enables an irregular filament to be obtained in terms of diameter. The aim is for the mixture to be homogeneous and in the same solid form. Then, a pelletizer is used to cut the irregular filament into pellets. Finally, these pellets are fed into the second single screw extruder which produces a regular filament of 1.75 mm diameter, the standard diameter for 3D printer filaments.

4.2.1 First extrusion (double screw)

The twin screw extruder used is the DSM Micro 15 Compounder. The device consists of two long rotating screws and requires the encoding of several parameters: three temperatures on each side of the two screws (T_{rear} and T_{front}) at three different screw heights (T_1 being the highest, followed by T_2 and T_3), a melt temperature (T_{melt}) and a screw rotation speed. For the blend of 70% PLA and 30% PEG (either 3K, 100K or 1M), the optimal parameters are shown in Table 4.1. Thanks to a loop, the molten polymers can be circulated through the extruder and passed between the screws several times to ensure a homogeneous mixture of PLA and PEG. With a 70/30 composition, three minutes was

sufficient. Once the sample is out of the extrusion head, it is cooled by the ambient air. This process is illustrated by the first step of Figure 4.1.

The machine is capable of handling samples of up to 15 g. Therefore, the experiment was repeated several times before 100 grams were obtained for each molar mass.

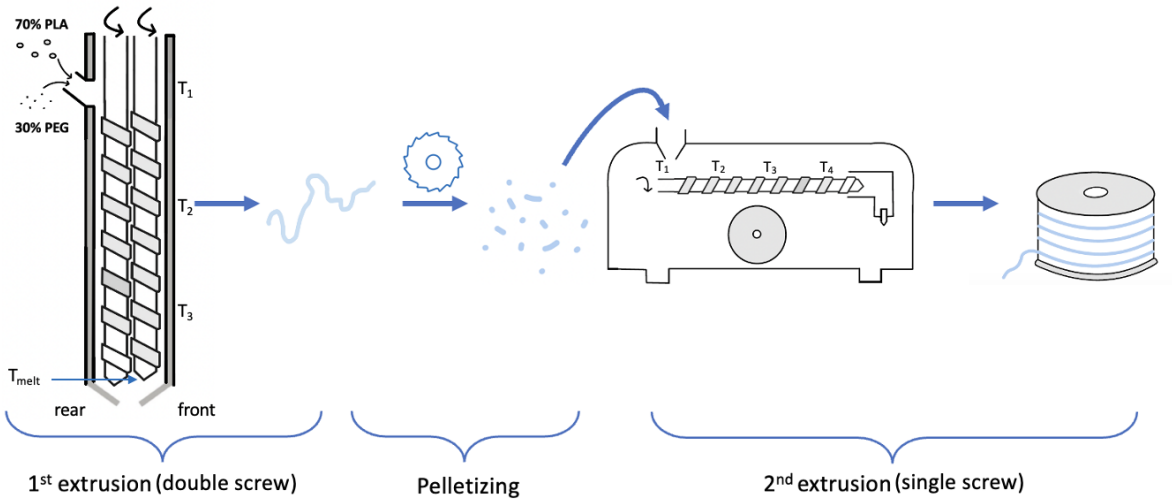

Figure 4.1: Simplified diagram of the 3D printing filament manufacturing process. In the initial stage of the process, the first extrusion step results in a homogeneous mixture between PLA and PEG. The second step, pelletizing, transforms the homogeneous mixture into pellets, an optimal shape for the final step. The second extrusion process produces a regular 1.75 mm diameter filament that is ideal for 3D printing.

Table 4.1: Selection of the extruder parameters

Parameters	**Value**	**Parameters**	**Value**
T_{rear} 1	180°C	T_{front} 1	180°C
T_{rear} 2	190°C	T_{front} 2	190°C
T_{rear} 3	180°C	T_{front} 3	180°C
T_{melt}	170°C	Speed	20 rpm

4.2.2 Pelletizing

With the pelletizer from Thermoscientific, the different filaments were cut into pellets, as represented by the second step in Figure 4.1. The purpose of making pellets is to facilitate the second extrusion and to control the quality of the filament.

4.2.3 Second extrusion (single screw)

The 3devo Composer Filament Maker is equipped with a diameter control system, which makes it possible to obtain very precise and regular filaments, as shown in the third step of Figure 4.1. To configure the machine, the following settings must be entered: four temperatures along the screw (T_1 being the closest to the feed hopper, T_2, T_3 and T_4 the furthest away) and the speed of rotation. For the PLA/PEG blend, the temperatures are 170°C, 190°C, 180°C and 175°C at a speed of 3 rpm. For pure PLA, the four temperatures are 180°C, 200°C, 195°C and 180°C at a speed of 3.5 rpm. The pellets produced in section 4.2.2 are then inserted into the extruder tank to create the 3D printing filament with a diameter of 1,75 mm.

4.3 3D-printing

The 3D printer used is the Creator 3 Pro from FlashForge. Before printing, all filaments were dried in an oven at 50°C during 24 hours. Then, the Flashprint program was used to slice the file containing the desired structure for 3D printing. During this process, various parameters were optimized, including platform temperature, nozzle temperature, print speed, number of shells and fill rate. These parameters play an essential role in producing a high quality print, and their optimal values depend on the specific characteristics of the material used.

The platform temperature is the temperature of the print bed on which the object is printed. This temperature must be set at a level that allows the first layer of the object to adhere to the print bed and retain its shape.
The nozzle temperature is the temperature at which the filament is melted by the printer's extruder. It is important to adjust the nozzle temperature at an appropriate level that allows the filament to melt enough to exit the nozzle and flow onto the platform.
Print speed is the speed at which the printer's extruder moves along the X and Y axes to deposit the filament. A slower print speed results in a more accurate and detailed print, while a higher print speed results in a shorter print time. However, a higher print speed can also reduce the accuracy and detail of the print and result in a rougher surface finish.
The number of shells is the number of perimeter walls that surround the object to be printed. A higher number of shells may result in a stronger, more durable print, while a lower number of shells may result in a less durable print.
The filling density is the percentage of the object's interior that is filled with printed material.

The summary tables 4.2, 4.3 and 4.4 show the optimum values for these parameters for the different PLA/PEG blends and for PLA alone.

Some characterization techniques, described in the section 4.5, require a particular structure. For example, for the tensile test, the specimen is a dogbone structure according to the measurements established by the ISO-527-2-5A standard (see Appendix A). For the DMA, the specimen is a parallelepiped of 20x4x1 mm.

Table 4.2: Main 3D printing parameters for PLA/PEO100K and 1M

Parameters	Values
T_{nozzle}	210°C
$T_{platform}$	50°C
Printing speed	45 mm/s
Number of shells	3
Filling density	100%

Table 4.3: Main 3D printing parameters for PLA/PEG3K

Parameters	Values
T_{nozzle}	165°C
$T_{platform}$	50°C
Printing speed	15 mm/s
Number of shells	3
Filling density	100%

Table 4.4: Main 3D printing parameters for PLA

Parameters	Values
T_{nozzle}	220°C
$T_{platform}$	55°C
Printing speed	45 mm/s
Number of shells	3
Filling density	100%

4.4 PEG removal

The process of removing PEG was conducted in two stages. Firstly, the 3D prints were placed in containers filled with distilled water at room temperature on a turntable. To prevent PEG saturation, the water was changed periodically during the first three hours, after which the prints remained immersed in water for 24 hours. In the second step, the same procedure was repeated, but this time the water was heated to 50°C during one day.

4.5 Characterization methods

4.5.1 Dynamic Mechanical Analysis

Dynamic Mechanical Analysis (DMA) was carried out on a Mettler Toledo DMA/SDTA1+ equipment. The aim of DMA is to obtain the mechanical properties of viscoelastic materials, i.e. the storage modulus (E'), the loss modulus (E") and the damping factor (Tan $\delta = \frac{E''}{E'}$).

In order to ensure that the material deforms exclusively in the plastic domain, a preliminary test was carried out. This test aimed to identify the optimum parameters, which were determined to be a maximum force of 3N and a displacement of 10 µm. In addition, an offset of 3N was applied to ensure that the material would only undergo sinusoidal deformation in the positive range, avoiding any negative values so that the material would only undergo tension and not compression. The tests were then carried out in a temperature range of -100°C to 150°C. These tests were carried out at two different vibration frequencies, namely 1Hz and 100Hz.

4.5.2 Differential Scanning Calorimetry

Differential Scanning Calorimetry (DSC) analysis was carried out on Mettler Toledo DSC 1 equipment.

In order to calculate the crystallinity, the enthalpy of melting (ΔH_m) and enthalpy of cold crystallization (ΔH_{cc}) values were computed from DSC measurements. This value was subsequently divided by the ΔH_m^o (=93.1 J/g) of the 100% crystalline PLA based on its weight fraction in each blend. The formula is described here under :

$$X_c = \frac{\Delta H_m - \Delta H_{cc}}{93,1 * \%_{PLA}} * 100 \tag{4.1}$$

The enthalpy of cold crystallization is subtracted from the enthalpy of melting of PLA as it represents the formation of new crystal structures from the amorphous state during heating. However, in the context of characterizing the crystallinity of the process, the main focus is on the amount of crystalline material formed during the process itself. Therefore, the contribution of crystals formed by heating is removed.

The DSC method had a heating rate of 10°C/min over a temperature range of -90°C to 200°C. DSC tests were performed under a nitrogen flow of 50 ml/min, an inert atmosphere to prevent oxidative degradation of the sample.

4.5.3 Nuclear magnetic resonance

Nuclear magnetic resonance (NMR) is a powerful analytical technique used to determine the structure and composition of molecules. This technique was used to determine the amount of PEG removed by water extraction in the different PLA/PEG blends.

Thanks to the intensities of the different peaks obtained, it is possible to quantify the number of moles of PEG (n_{PEG}) present in the mixture. Once this value is obtained, the proportion of PEG present in the mixture can be determined using the following formula:

$$w_{PEG} = \frac{1}{1 + \frac{M_{PLA}}{M_{PEG}} * (\frac{1}{n_{PEG}} - 1)} * 100 \tag{4.2}$$

where $M_{PLA} = 72$ g/mol and $M_{PEG} = 44$ g/mol are the molar mass of PLA and PEG respectively.

Given the chemical formulae of PLA and PEG, the use of the $^1H - NMR$ technique was sufficient to characterize these molecules. As the machine required samples in liquid form, the samples were dissolved in deuterated chloroform at a concentration of 40 mg/ml for analysis.

4.5.4 Scanning electron microscope

The scanning electron microscope (SEM) imaging process starts with the preparation of the sample. First of all, the sample must be metallised by depositing a thin layer of

metal on the surface of the sample, which is intended to improve the electrical conductivity of the sample surface, a necessary step for the sample to be correctly imaged by SEM.

For the analysis, the samples were coated with a 12 nm gold layer using a sputter coating device (Ted Pella, Cressington208HR High Vacuum Turbo Sputter Coater). Then, they were placed in the JEOL 7600F SEM where they were subjected to an acceleration voltage of 5 kV. The samples were observed at a working distance of 8 mm.

4.5.5 Tensile test

A tensile test is a mechanical test used to determine the mechanical properties of a material. In this test, a sample of the material is subjected to a progressively increasing tensile force in a tensile tester until it breaks.

In accordance with ISO SO-527-2-5A, the test required the manufacture of a specific 3D structure, which was produced by 3D printing. The detailed dimensions of this object are shown in Appendix A. The tests were performed by the Instron 6800 series machine at room temperature with an elongation rate of 25 mm/min. In order to ensure statistical reliability, the tests were carried out in triplicate, which meets the requirements for statistical acceptability.

Chapter 5

Results and discussion

The experimental investigations carried out in this study have provided valuable information about the material studied in term of composition, thermal properties, mechanical properties and porosity of the material. In order to analyze the impact of each of these properties on the material, a step-by-step approach was adopted. The first analyses focused on a single property at a time.
As a reminder, here is a summary of the experiments done and their objectives. NMR spectroscopy was used to check the proportion of PLA and PEG in the 3D prints. Secondly, DSC measurements were conducted at various stages of the manufacturing process, including the filaments, 3D prints before and after PEG removal for PLA-only compositions and blends (PLA/PEG3K, PLA/PEO100K and PLA/PEO1M) to analyze the effect of these steps on the thermal properties of these structures. Microporosity and macroporosity were observed using SEM on the 3D prints of the blends after PEG removal. DMA was also performed on the 3D prints before and after PEG removal to characterize the viscoelastic properties of the blends and pure PLA. Finally, tensile tests were carried out on the 3D prints before and after PEG removal to determine the mechanical properties of the blends and PLA alone.
Once each property has been examined separately, it will be possible to link this information together to gain a more complete understanding of the material as a whole.

5.1 Checking the compositions of PLA/PEG blends before and after PEG removal

NMR was used at two stages in the process. Firstly, to check that the blended filaments (PLA/PEG3K, PLA/PEO100K and PLA/PEO1M) were composed of 30% PEG and 70% PLA. This step was necessary because material losses were observed during the extrusion process for manufacturing the filaments. With the volatilization of the PEG powder and the adhesion of the blend to the upper part of the twin screws, the composition of the initial blends was perhaps modified. And in a second step, to identify the quantity of PEG remaining in the 3D prints of the blends (with and without macropores) after the PEG extraction method.

To this end, a reference spectrum of the 70/30 PLA/PEG mixture had to be established. The reference sample was prepared using a proportion of 70% by weight PLA granules and 30% by weight PEG powder. This sample was then run through NMR and its spectrum is shown in the following Figure 5.2 A). This sample allowed the identification of the characteristic peaks of the 70/30 PLA/PEG blend. The signals corresponding to the 3H of PLA ($3H_{PLA}$) were observed at 1.56 ppm, shown in blue in Figure 5.1. In addition, a 1H signal from PLA ($1H_{PLA}$) was detected at 5.14 ppm, shown in red in Figure 5.1. The two 2H signals of PEG ($4H_{PEG}$) were also observed at 3.6 ppm, shown in green in Figure 5.1.

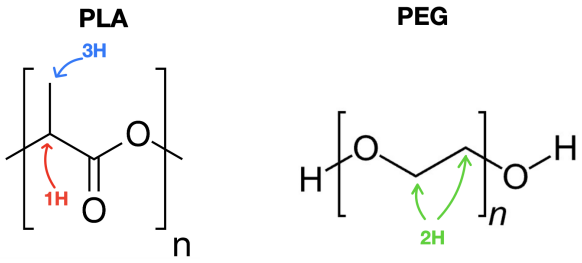

Figure 5.1: Identification of proton (H) nuclear magnetic resonance (NMR) signals in the chemical formulae of PLA and PEG

The number of moles of PEG (n_{PEG}) is :

$$n_{PEG} = \frac{4H_{PEG}/4}{1H_{PLA} + 4H_{PEG}/4} \tag{5.1}$$

where $4H_{PEG}$ and $1H_{PLA}$ are the peak intensities at 3.6 ppm and 5.14 ppm respectively. And using equation 4.2, the amount of PEG in the PLA/PEG filaments could be determined quantitatively and the relative proportion of the two components could be assessed. For example, Figure 5.2 B) shows the spectrum of the PLA/PEO1M filament, revealing that its composition is 72% PLA and 28% PEO1M. This result indicates that the desired proportions have been preserved, despite potential losses during the handling process.

In order to evaluate assess the efficacy of the PEG extraction method in the mixtures, NMR was also performed on the samples after extraction. Although several treatments were carried out to remove the PEG in the blend, unfortunately not all of the PEG could be removed from the 3D prints of the different blends.

PEG was eliminated in two types of 3D printed structures: one with full fill density and one with intentionally imposed macropores less than 1 mm in length. The spectrum of the PLA/PEO1M 3D print after PEG removal is shown in Figure 5.2 C)and it is found that the 3D structure with full fill density retained 7% of the PEG, out of the initial 30%. For the other two blends, the values are shown in Table 5.1.

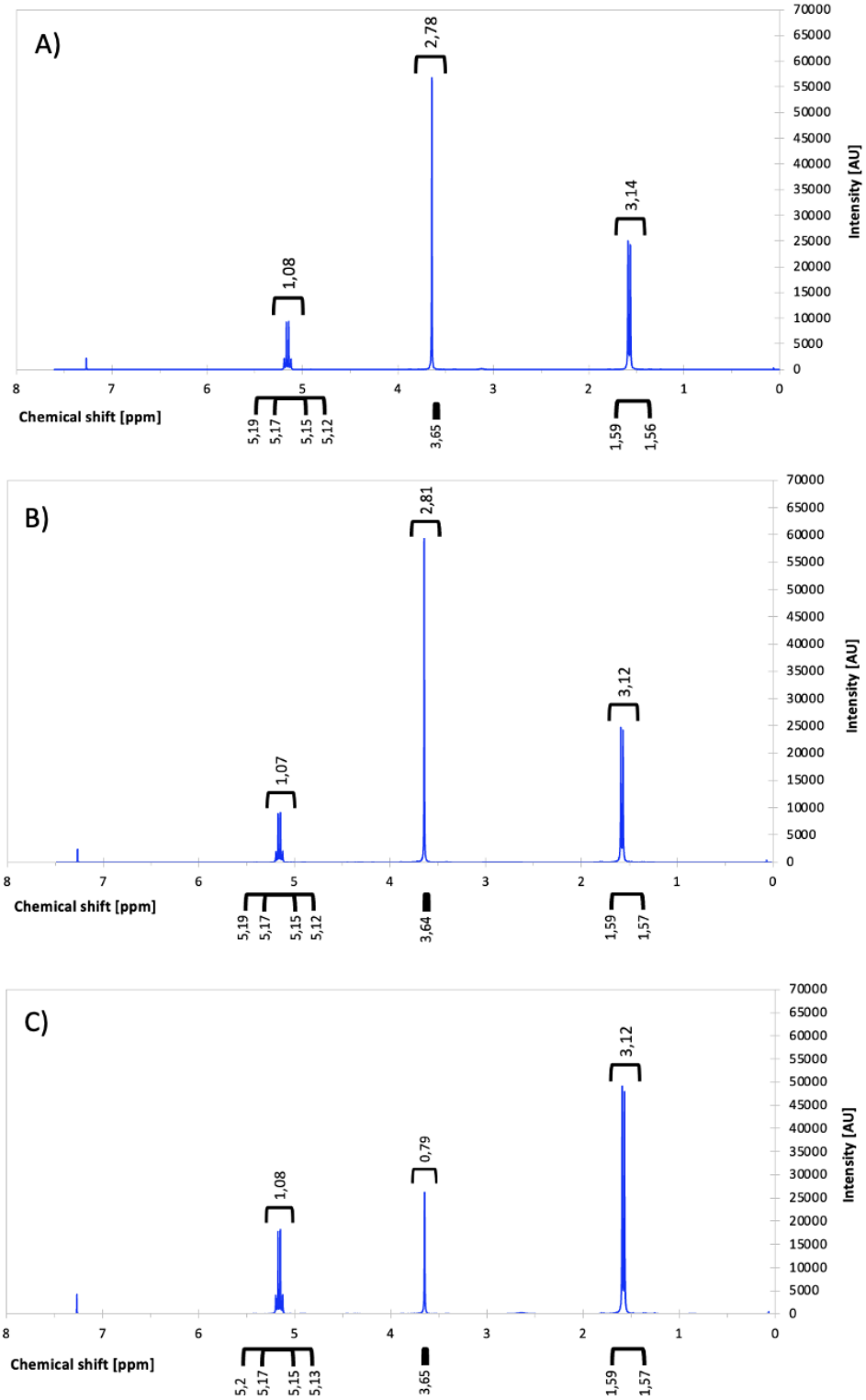

Figure 5.2: NMR spectra of A) the 70/30 PLA/PEO1M reference, B) the 70/30 PLA/PEO1M filament and C) the 70/30 PLA/PEO1M 3D print after PEG extraction

Table 5.1: Proportions of PEG in filaments, 3D prints after PEG removal and macroporous prints after PEG removal, for compositions comprising the three types of PEG (PEG3K, PEO100K and PEO1M)

	$\%_{PEG}$
PLA/PEG3K filament	28
PLA/PEO100K filament	28
PLA/PEO1M filament	28
3D print after removing PEG3K	7
3D print after removing PEO100K	10
3D print after removing PEO1M	7
Macroporous 3D print after removing PEG3K	7
Macroporous 3D print after removing PEO100K	7
Macroporous 3D print after removing PEO1M	10

In order to understand why PEG could not be completely removed from the mixtures, it is essential to analyze why water failed to reach and dissolve the PEG. Two distinct levels were identified where PEG is present: the interspherulitic and interlamellar regions.

The interspherulitic regions correspond to the space between two PLA spherulites, where PEG can localise. When samples are immersed in water, water can more easily penetrate these regions by sliding between the spherulites and dissolve the PEG present. As a result, these areas benefit from greater accessibility to water, allowing complete extraction of the PEG.
In contrast, the interlamellar regions lie between the lamellar layers of PLA, creating a structure in which PEG is trapped in the amorphous phase of PLA. Due to the hydrophobic nature of PLA, water has difficulty entering this region. As a result, PEG trapped in PLA at the interlamellar level is less accessible to water, which explains why its removal is not as efficient. This is summarized by Figure 5.3.

In summary, the presence of the hydrophobic PLA creates a physical barrier that hinders the accessibility of water to the PEG in the interlamellar regions, preventing PEG dissolution.

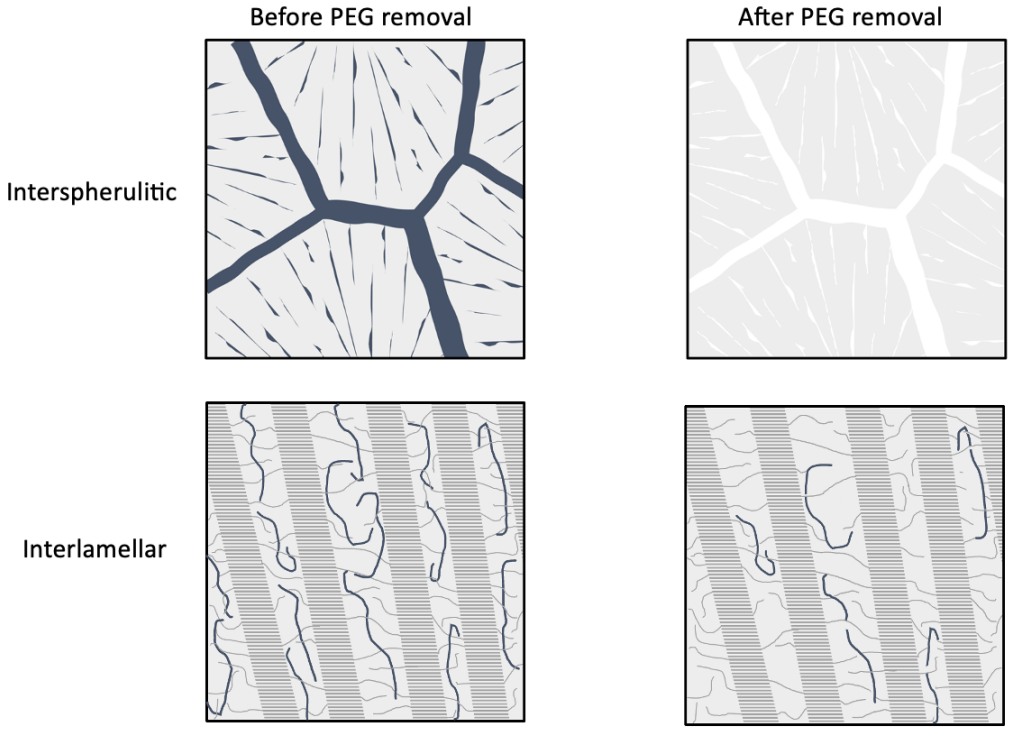

Figure 5.3: Distribution of PLA (in grey) and PEG (in blue) at the interspherulitic and interlamellar levels before and after PEG extraction

5.2 Evaluation of the thermal properties

Samples submitted for DSC analysis included the different stages of the process, including filaments (with the blends and PLA alone), 3D prints (with the blends and PLA alone) and 3D prints with PLA/PEG after PEG removal. The blends studied were composed of PLA/PEG3K, PLA/PEO100K and PLA/PEO1M. DSC was performed to obtain information on thermal properties (T_g, T_m and crystallinity).

The characteristic temperatures, i.e. glass temperature (T_g), cold crystallization temperature (T_{cc}) and melting temperature (T_m) of each mixture could be obtained by DSC. Using equation 4.1, it was possible to determine the degree of crystallinity (X_c) in each structure. The results are illustrated in the graphs 5.4, 5.5, 5.6 and 5.7 and the values are summarized in Table 5.2.

The degrees of crystallinity should be treated with caution as the area under each peak is not always easy to calculate as the peaks are not perfectly aligned at each end.

DSC results can be divided into several parameters that may have a direct effect on the physical properties of the material. The four main effects to be studied are: the effect of blending, the effect of PEG molecular weight, the effect of extrusion generated by the 3D printer and the effect of PEG removal after 3D printing.

Table 5.2: Summary of thermal property values for each type of structure studied (filaments, 3D prints before and after PEG extraction) for neat PLA and PLA/PEG blends with different PEG molar masses (3K, 100K and 1M)

	T_g [°C]	T_{cc} [°C]	T_m [°C]	ΔH_{cc} [J/g]	ΔH_m [J/g]	X_c [%]
Filament of pure PLA	68	113	184	3.66	6.66	3.2
Filament of PLA/PEG3K	41	96	173	1.82	7.46	8.6
Filament of PLA/PEO100K	44	96	176	2.34	6.96	7.1
Filament of PLA/PEO1M	45	96	178	1.19	5.99	7.3
3D printing of PLA/PEO3K	53	92	173	0.96	7.08	9.4
3D printing of PLA/PEO100K	55	95	176	0.77	6.98	9.5
3D printing of PLA/PEO1M	59	95	177	~ 0	5.94	8.8
3D printing of PLA after removing PEG3K	54	96	175	1.39	7.34	6.8
3D printing of PLA after removing PEO100K	66	97	174	1.05	8.17	8.5
3D printing of PLA after removing PEO1M	68	102	179	~ 0	7,82	9
3D printing of pure PLA	66	112	180	4.15	6.54	2.6

5.2.1 Effect of blending

Mixing effect considers how the addition of PEG to PLA affects the thermal properties of the material. To investigate this, the values of the different thermal characteristics of the PLA/PEG filaments were compared with those of a pure PLA filament used as a reference. This comparison is illustrated in Figure 5.4.

The DSC analysis revealed the appearance of an additional melting peak in all PLA/PEG mixtures compared to the pure PLA reference peak: the PEG melting peak. This observation is a consequence of phase separation between PLA and PEG at a certain percentage of PEG in the mixture, as previously mentioned in the section 2.2.2 ("Interest of PEG"), which claimed that from 30% PEG, phase separation could be observed between PLA and PEG. The blends show a T_g close to 45°C, a T_m of PEG around 60°C and a T_m of PLA at around 175°C. In addition, it was observed that the PEG melted without crystallizing during DSC analysis. This finding suggests that all the PEG has already crystallized prior to the DSC heating process, i.e. during extrusion to create 3D printing filaments. Despite the relatively rapid cooling rate during this extrusion, the PEG had sufficient time to crystallize. Finally, the DSC method applied in this study had a temperature range of -90°C to 200°C, in the expectation of detecting T_g of PEG, which is typically close to -45°C. However, no significant transition was observed at this temperature in the DSC curves because PEG is highly crystalline.

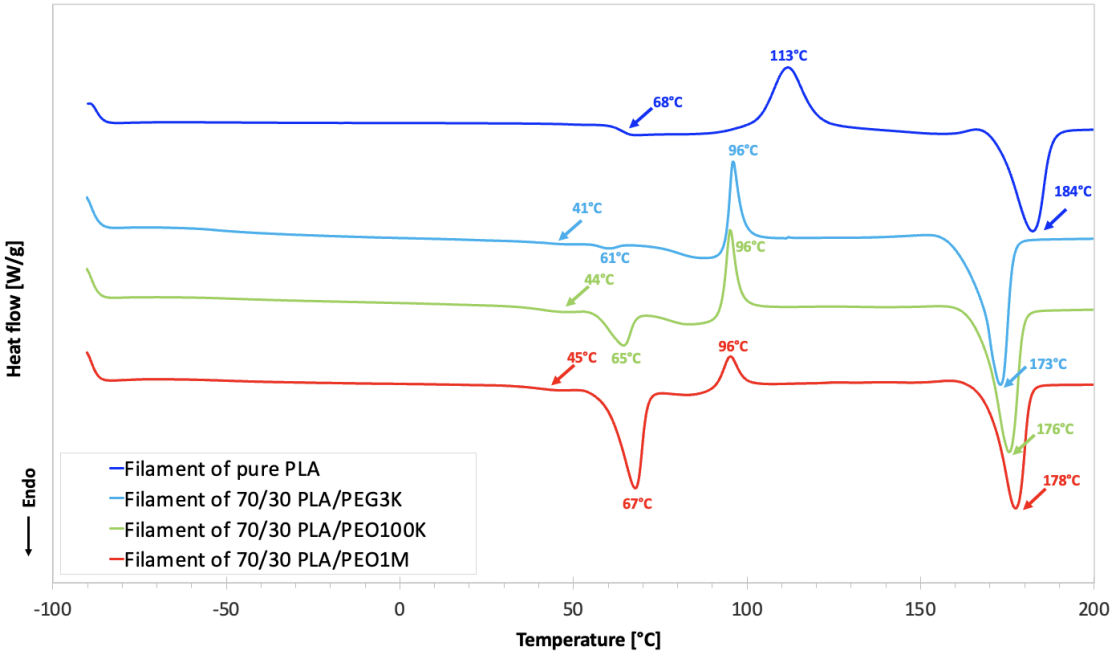

Figure 5.4: DSC curves from top to bottom for pure PLA filament, 70/30 PLA/PEO100K blend filament, 70/30 PLA/PEO100K blend 3D print, PLA/PEO1M blend 3D print after PEG removal and pure PLA 3D print

A second observation of the results is the decrease in the characteristic temperatures (T_g, T_{cc} and T_m) of the blends compared to the reference (pure PLA filament). This decrease is very marked for the T_g of PLA. For example, the T_g of the PLA/PEO100K filament is 44°C compared with 68°C for pure PLA. It turns out that PLA and PEG are miscible in the amorphous phase and thus Fox's law applies:

$$\frac{1}{T_g} = \sum \frac{w_i}{T_{gi}} \tag{5.2}$$

where w_i, in this case, do not represent the proportion of each component in the whole mixture but the proportion of each component in the amorphous phase. And as PEG has a much lower T_g than PLA, it is logical that the T_g of the amorphous phase blend is lower.

As far as crystallinity is concerned, blends are more crystalline than pure PLA filaments. This can be explained in two ways: the cooling rate and the nucleation effect of PEG. During filament creation, the single screw extrusion process involves heating the materials along the screw for a significant distance and then cooling them with two ventilators. This step is specifically designed to prevent premature crystallization of PLA and ensure that the resulting filaments remain flexible enough for later use in a 3D printer. By precisely controlling the temperature and cooling, it is possible to obtain quality filaments that offer good processability. The temperatures set in the machine were slightly higher for pure PLA than for the blends. For example, neat PLA goes from 180°C to room temperature and blends from 175°C to room temperature in a few seconds. The cooling rate for PLA is therefore slightly higher than for blends. A faster cooling rate leads to a less optimal crystal arrangement, which results in lower crystallinity.

However, due to the small difference in initial temperature between pure PLA and blends, the cooling rates are almost identical. Therefore, the cooling rate alone may not fully explain the observed difference in crystallinity.
Another explanation is that PEG acts as a nucleating agent for the crystallization of PLA. In several studies, it has been shown that PEG can act as a nucleating agent for PLA. When PEG is incorporated into a PLA/PEG mixture, there is a decrease in T_g, suggesting greater mobility of the polymer chains. The movement of the chains creates favourable conditions, where the PLA chains can organize and align themselves into a crystalline structure. As a result, PEG promotes the formation and growth of PLA crystals in the blend, resulting in an increase in overall crystallinity. Furthermore, the cold crystallization peak is much narrower for blends than for pure PLA, implying that the crystals formed in blends are of similar size, more homogeneous. This homogeneity contributes to the higher crystallinity observed in blends compared to pure PLA [60, 61].

As a result, the thermal properties of the blended material are well affected by the presence of PEG. Specifically, the addition of PEG results in a decrease in T_g of the blend, indicating increased chain mobility. In addition, the crystallinity of the blended material increases, reflecting a greater degree of molecular alignment in the presence of PEG.

5.2.2 Effect of PEG molecular weight

The effect of PEG molecular weight was studied using three different molar masses: PEO1M, PEO100K and PEG3K. A comparison was made based on the 3D prints obtained for each mixture, as shown in Figure 5.5.

The results show that the higher the molecular weight of PEG, the higher the characteristic temperatures, indicating that the molecular weight of PEG affects the thermal stability of PLA/PEG blends. This is consistent with what was said earlier in section 2.2.1 ("PEG"): PEG with a higher molecular weight has higher T_g and T_m.

In addition, the higher the molecular weight of PEG, the larger the melting peak of PEG. This relationship can be explained by the molecular structure. As the molecular weight of PEG increases, these polymer chains become longer and therefore more entangled. The higher molecular weight results in more intermolecular interactions and a higher degree of entanglement between chains. When PEG is heated, these intermolecular interactions must be disentangled to move from a solid to a molten state. Higher molecular weight PEG chains have a greater number of intermolecular interactions that need to be disentangled. To do this, more energy is required to induce PEG melting. Therefore, the melting area of PEG, which represents the energy required for melting, increases with PEG molecular weight. At the same time, it also suggests that low molecular weight PEG is more miscible with PLA.

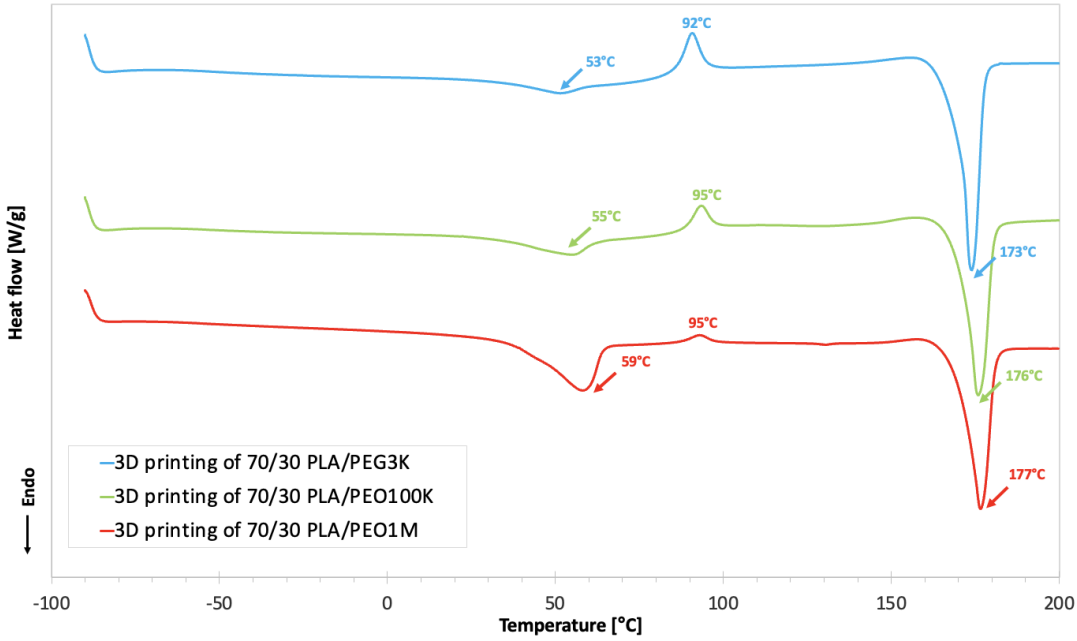

Figure 5.5: DSC curves from top to bottom for 70/30 PLA/PEG3K 3D print, 70/30 PLA/PEO100K 3D print and 70/30 PLA/PEO1M 3D print

By the same reasoning, crystallinity is inversely proportional to the molecular weight of PEG in the blends. This is because longer PEG chains are more intertwined and have more difficulty in arranging themselves to form a regular crystal structure. In addition, the formation of high-quality PLA crystals in the blend requires the ejection of PEG from the spherulites. For this, it is essential that the PEG has some mobility. However, as the molecular weight of PEG increases, the chains are longer and their mobility is therefore reduced. As a result, high molecular weight PEG has low mobility and is not easily ejected from PLA spherulites, leading to the formation of defects in PLA crystals. Similar results were obtained in the study of Feng-Jiao Li et al [62].

In summary, the molecular weight of PEG influences the thermal stability of the blends. High molecular weight PEGs have higher T_g and T_m, which implies that the T_g of the blend is also higher with higher molecular weight of PEG. Furthermore, the crystallinity of the blends is inversely proportional to the molecular weight of the PEG.

5.2.3 Effect of 3D printing

The effect of extrusion with the 3D printer is attributed to the heating that the filament underwent to create a 3D object in the extrusion head over a short distance. To understand this effect, a comparative analysis was carried out by examining the filaments before printing and studying the corresponding 3D prints, as shown in Figure 5.6.

The impact of heating the material during the extrusion process is relatively small on the different temperatures. The melting temperature (T_m) and the cold crystallization temperature (T_{cc}) decrease very slightly. Only the glass transition temperature increases

more significantly. This is due to the fact that the heating of the 3D printing allows an increase in crystallinity, which in fact implies an increase in T_g.

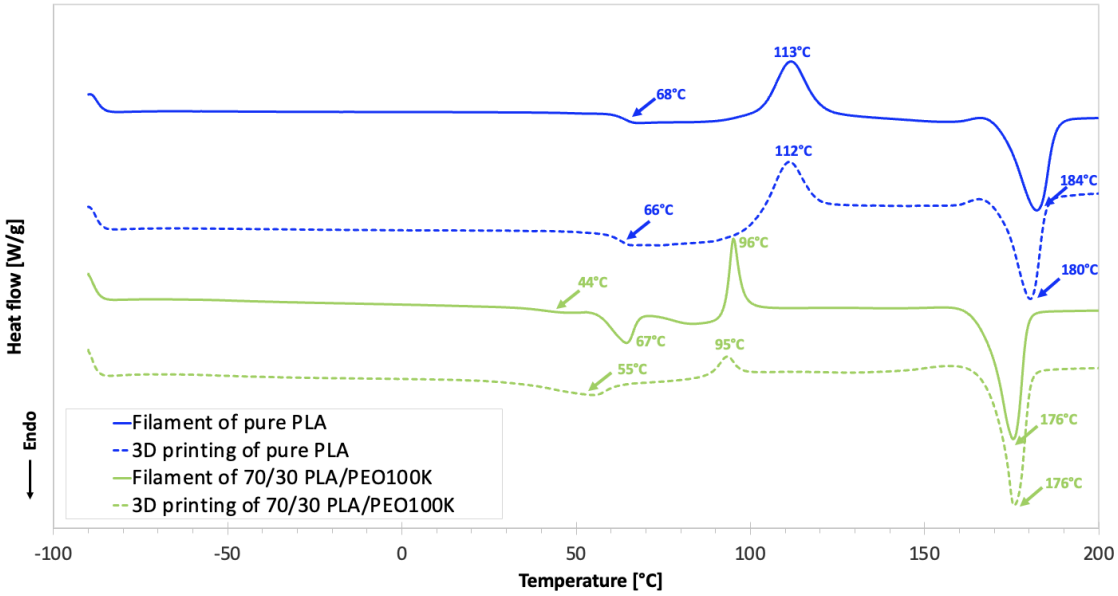

Figure 5.6: DSC curves from top to bottom for pure PLA filament, pure PLA 3D print, 70/30 PLA/PEO100K filament and 70/30 PLA/PEO100K 3D print

In terms of crystallinity, the object 3D printed with a blended filament has a higher crystallinity than the filament. This phenomenon is not observed for neat PLA, probably due to inaccuracies in the enthalpy calculations. The increase in crystallinity can be attributed to two mechanisms that occur during the 3D printing process and affect the cooling rate. Firstly, before the deposition of the first layer, the material is in a molten state and the chains are highly mobile and can arrange themselves in a more ordered structure before being cooled. When the first layer is deposited, it is cooled by the ambient air but maintained at the temperature set by the platform. As a result, the cooling rate after 3D printing is much slower than for the creation of the filaments which was accelerated by ventilators. In addition, when the second layer is deposited on top of the first layer, the heat from this layer heats up the first layer, which again promotes the mobility of the chains to adopt a crystal structure. Given this difference in cooling rate between 3D printing and filament creation, 3D printed materials have more time to form crystals, resulting in greater crystallinity [63].

In conclusion, the 3D printing process has the effect of increasing the crystallinity of the material used. The cooling rate and the heat transmitted to the previous layers promote the arrangement of PLA into a more crystalline structure. As a consequence, greater crystallinity implies an increase in T_g, which indicates that more energy will be required to change from the glassy to the rubbery state.

5.2.4 Effect of PEG removal

The effect of PEG removal is associated with the dissolution of the PEG present in the 3D prints in water. To evaluate this parameter, the physical properties of the 3D prints before and after PEG removal were compared in Figure 5.7. The DSC curves for the PLA after PEO1M removing is available in Appendix B.

A first observation is the disappearance of the PEG melting peak, which suggests that PEG could have been removed from the mixtures. Another interesting observation is the re-increase of the characteristic temperatures and more particularly of the T_g, which proves that some of the PEG present in the amorphous phases has been removed. However, it is important to note that the T_g obtained is still lower than that of pure PLA, which highlights the fact that some PEG is still present in the amorphous zone of PLA. The T_g of the mixture after removal of the PEO100K is 55°C, while the T_g of the pure PLA is 68°C. The residual presence of PEG in the amorphous zone can be explained by the difficulty for water to access this area as the PLA acted as a barrier against water.

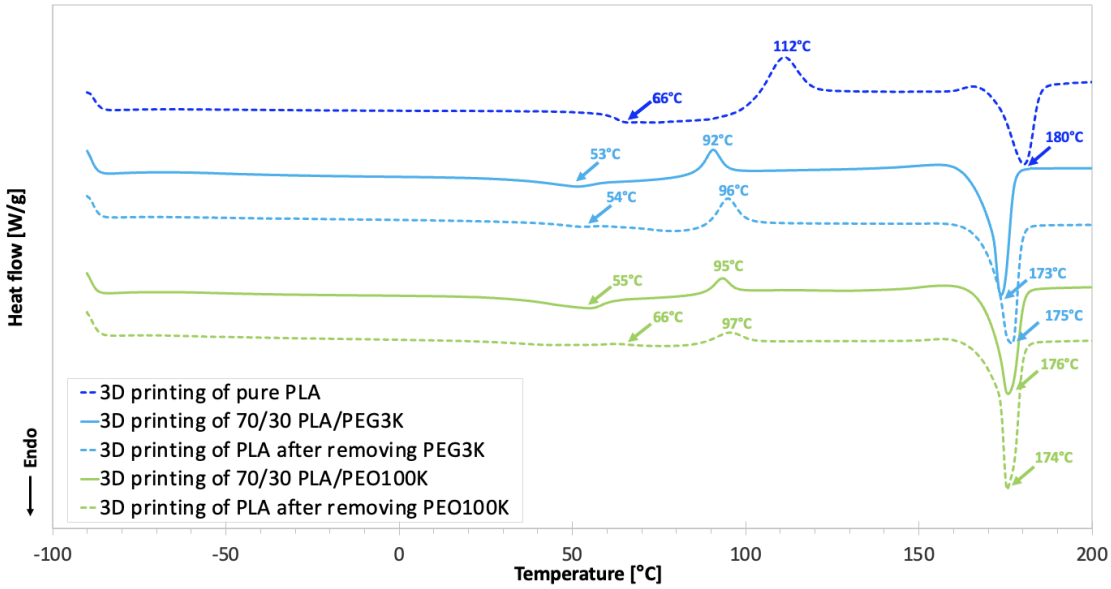

Figure 5.7: DSC curves from top to bottom for pure PLA 3D print, 70/30 PLA/PEG3K 3D print, PLA 3D print after PEG3K removal 70/30 PLA/PEO100K 3D print and PLA 3D print after PEO100K removal

The effect of PEG removal on the crystallinity of 3D prints where PEG has been extracted is difficult to assess because in each mixture the percentage of PEG remaining differs, which adds another factor in the analysis in addition to the imprecision in the enthalpy calculation. However, based on the PLA/PEO100K after PEG extraction, it can be assumed that the crystallinity increases slightly with PEG removal. Removing the PEG creates voids in the material that may be beneficial for the PLA crystals to crystallize further. This assumption is supported by the observation that the samples after PEG removal were significantly whiter, which is generally associated with an increase in

crystallinity.
Furthermore, the objects where PEG was removed are still much more crystalline than the pure PLA 3D print, as the blends retain the PLA crystals that were formed by the presence of PEG before.

In summary, the removal of PEG from the blends results in a convergence of temperatures towards those of pure PLA, while retaining the crystallinity previously induced by PEG, which acted as a nucleating agent for PLA.

5.3 Investigation of the porosity

In order to analyze the morphology after PEG extraction in each sample, these were cut with a razor blade and the slice was analyzed by SEM. Two types of structures were studied: those with an initial density of 100% before PEG extraction, known as solid structures, and those where a pore size ($\approx$ 850 µm) was imposed by design, referred as macroporous structures.
Two different solid structures, containing the mixture with PEO100K and PEO1M, were subjected to SEM analysis at two different thicknesses: 1 mm, designated as the thin structure, and 2 mm, called thick structure. This comparison will make it possible to assess the effect of thickness on porosity. When mixed with PEG3K, only the thin structure could be printed successfully.

5.3.1 PLA/PEG3K blend

From Figure 5.8 a), the pores generated by the removal of PEG within each layer can be easily distinguished from those induced by the 3D printer surrounded by a green circle. These pores created by the 3D printing process are a manufacturing defect where the material was not deposited correctly and the layers did not adhere as expected.

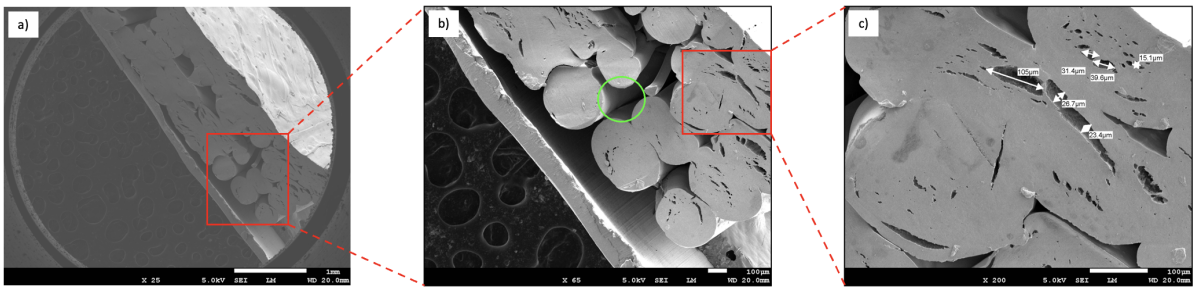

Figure 5.8: SEM images after PEG3K removal of a 1 mm thick PLA/PEG3K 3D print with a magnification of a) X25, b) X65 and c) X200

With regard to the pores induced by PEG removal, it can be seen in Figure 5.8 b) that the pores are not evenly distributed throughout the sample. Only the bottom of the

sample has pores within each filament layer.

If the part of the sample with pores is examined closely (see Figure 5.8 c)), it appears that all the pores are located in the centre of each layer and that no pores are present on the surface of each filament layer. Within each layer, there exists a region on the outer surface that is completely free of pores, while the inner region contains pores. In terms of shape and orientation, it can be observed that the pores all adopt the same type of geometry, i.e. an elongated shape along the length of the sample.

Finally, the pores are very few but quite large and variable in size ranging from less than 1 µm to more than 100 µm.

Thanks to the specific design of the model, it was possible to produce macropores with approximately 800 µm in size, demonstrating successful implementation of the design. It is represented in Figure 5.9 a).

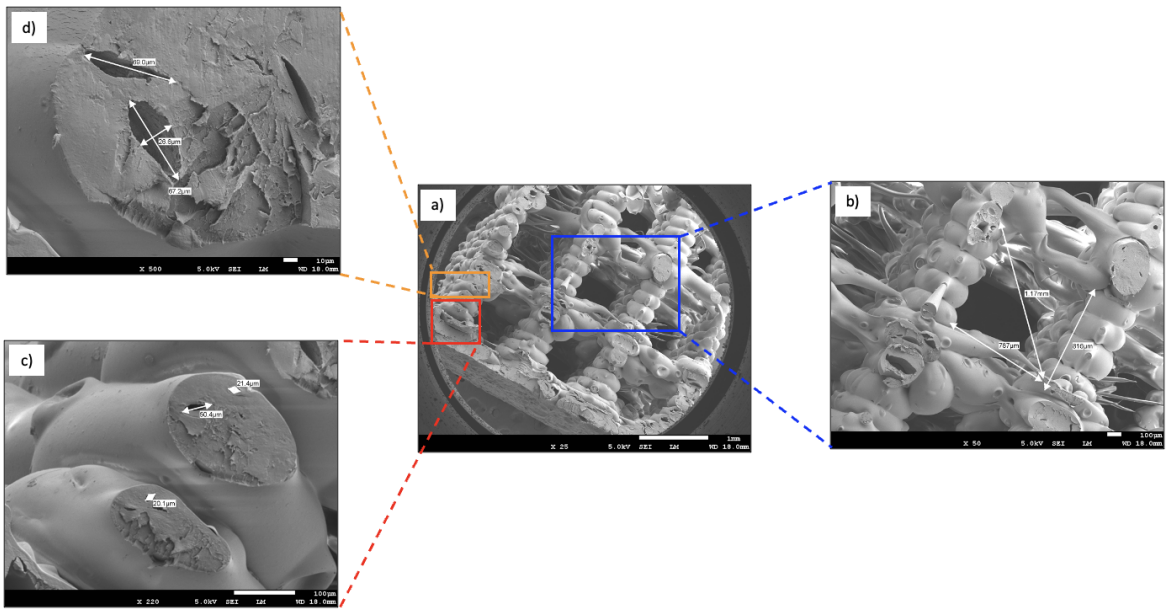

Figure 5.9: SEM images after PEG3K removal of a macroporous PLA/PEG3K 3D print with a magnification of a) X25, b) X50, c) X220 and d) X500

The observations described above on porosity are verified in the macroporous structure. The pores are inhomogeneously distributed throughout the sample. Pores are only observed in the lower part of the sample where the pores are located in the central part of the filaments. On the other hand, a new observation is the formation of round pores slightly raised on the surface of the layers, certainly due to a defect in the 3D printing.

5.3.2 PLA/PEO100K blend

The images of the thin structure show also the difference between the pores induced by 3D printing (circled in green) in Figure 5.10 d) and the pores obtained through PEG extraction in Figure 5.10 b).

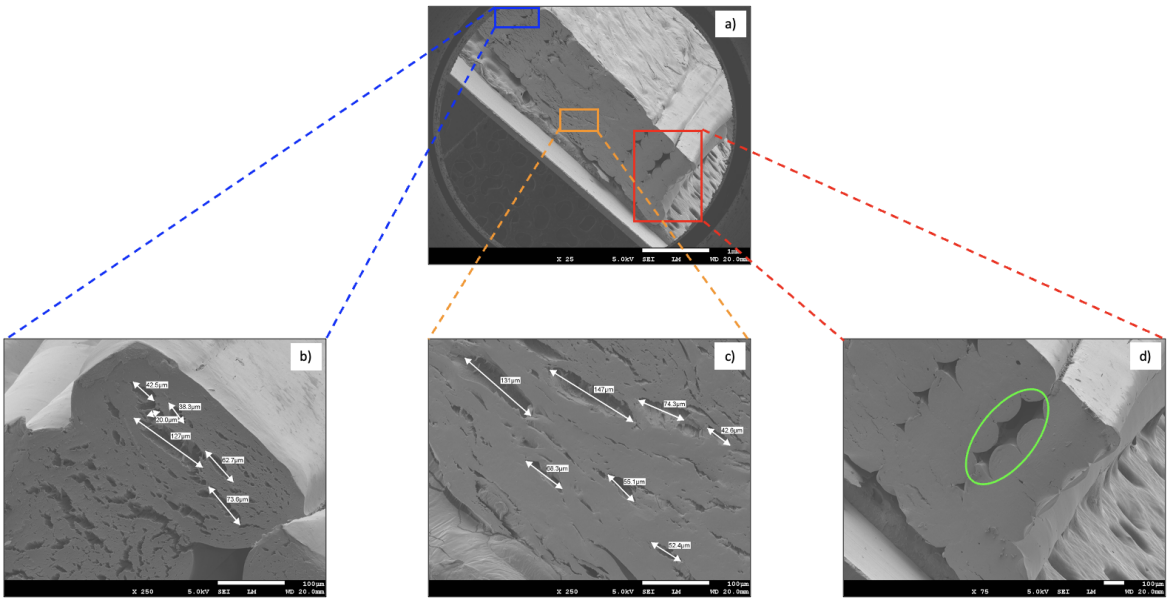

Figure 5.10: SEM images after PEO100K removal of a 1 mm thick PLA/PEO100K 3D print with a magnification of a) X25, b) X250, c) X250 and d) X75

Approximately one third of the sample is non-porous. This part is shown in Figure 5.10 d). This result again highlights the heterogeneous distribution of pores within the sample. For the remaining 2/3 of the sample, the pores are located in the centre of each filament, while a peripheral layer within each filament remains non-porous. The pores always follow a longitudinal orientation and adopt an elongated shape.

In terms of size and quantity, the pores are very abundant within each layer and range in size from a few micrometres to over 150 µm for the largest.

The thicker structure analyzed shows a completely different pattern to that of the previous structures. Previously, each layer was easily distinguishable, whereas in the upper part of Figure 5.11 a), it can be seen that several layers have been glued together, making them difficult to differentiate from each other. Moreover, this part does not have any pores. The filaments are "flattened", as if they had been crushed, which could explain why no pores are visible.

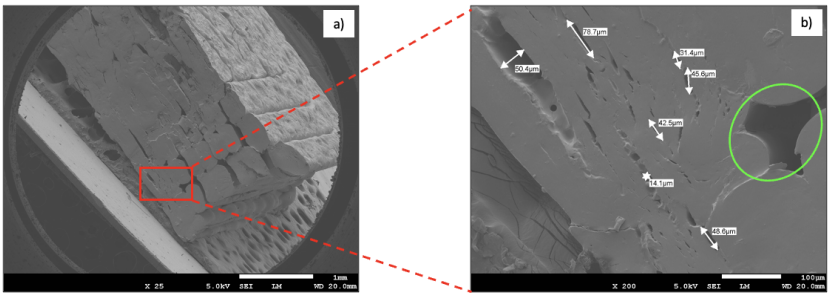

Figure 5.11: SEM images after PEO100K removal of a 2 mm thick PLA/PEO100K 3D print with a magnification of a) X25 and b) X200

Looking at the underside of the sample, the pores are elongated and significantly larger, with sizes ranging from about 15 to more than 200 µm. Due to the inability to distinguish the different layers in this area, it is hard to determine if the pores are in the centre of the filament. However, if the layer line adjacent to the area is taken into account, it is possible to represent the different layers in this area and it is very likely that the majority of pores are distributed in the centre of each layer. However, some pores are present between two layers of filaments.

The pores imposed in this macroporous 3D print were less well respected. In fact, the desired pore shape was square, whereas here the pores are rather round with an average radius of 650 µm, as illustrated in Figure 5.12. Again, the filaments have been flattened, which would be the cause of a less good reproduction of the design.

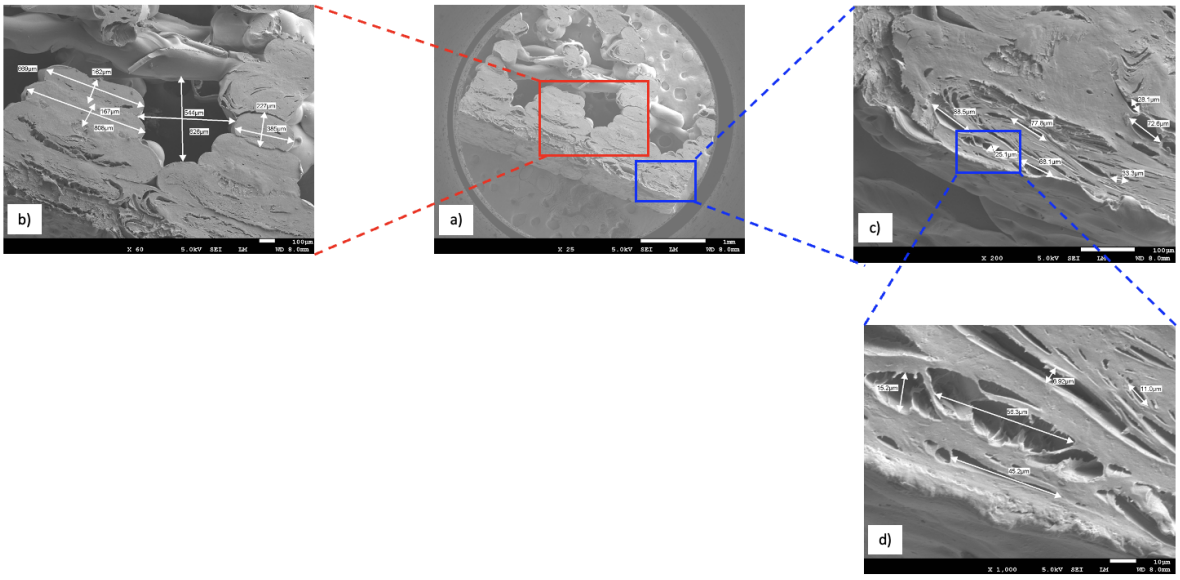

Figure 5.12: SEM images after PEO100K removal of a macroporous PLA/PEO100K 3D print with a magnification of a) X25, b) X60, c) X200 and d) X1000

Due to a handling issue, the sample broke and thus the top part of the sample can not be considered. However, the lower part exhibits similar features as described earlier, with a significant number of large, elongated pores present at the center of each layer. Additionally, the pores are relatively scarce but of significant size. Additionally, Figure 5.12 d) indicates a significant depth of the pores.

5.3.3 PLA/PEO1M blend

For the PLA/PEO1M blend, the distinction between pores due to printing inaccuracies (circled in green in Figure 5.13 d)) and pores due to the PEG removal method can be seen.

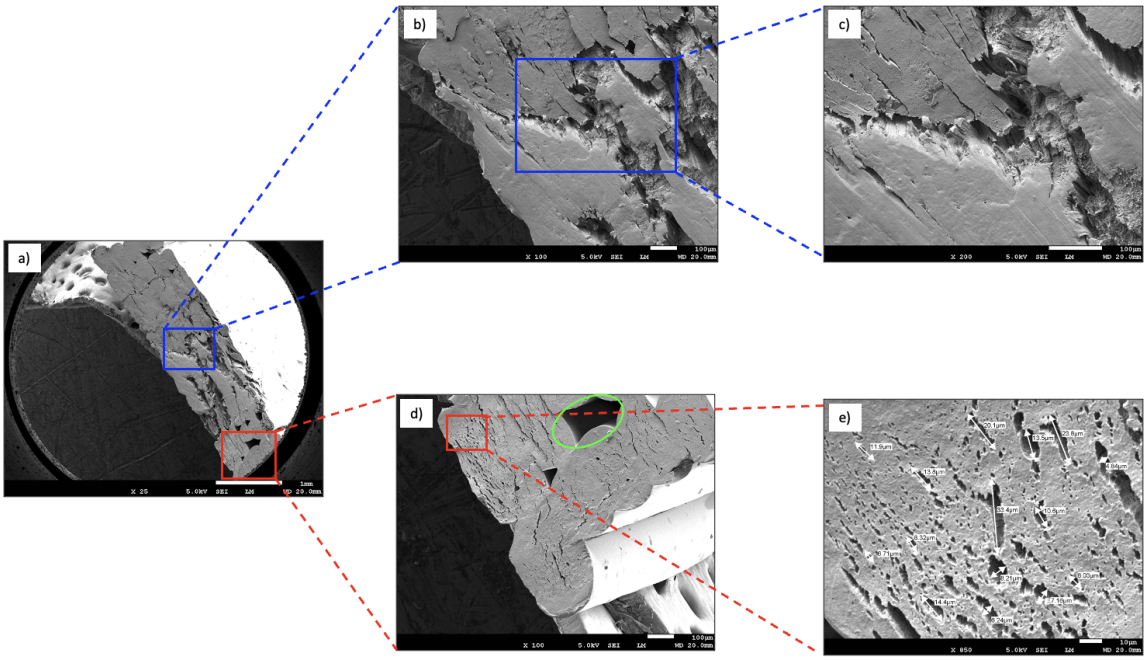

Figure 5.13: SEM images after PEO1M removal of a 1 mm thick PLA/PEO1M 3D print with a magnification of a) X25, b) X100, c) X200, d) X100 and e) X850

In the middle of the sample, a distinct crack can be observed in Figures 5.13 b) and c), likely resulting from the cutting process with a razor blade. But inside this crack, the sample is much more porous and the pores are deeper. The top side of the sample lacks pores, while the bottom side has pores, revealing the heterogeneous distribution of pores in this sample as well.

Focusing on the bottom part, it can be seen that the pores are in the central part of each layer, surrounded by a non-porous layer on the surface of the layer. The pores exhibit a stretched shape and are all oriented in the same direction, in the longitudinal direction. The pores are very numerous and rather homogeneous in size, ranging from a few to about 30 micrometers.

The thick 3D structure displays a similar phenomenon as the PEO100K structure, where the layers can not be distinguished from each another. This is shown in Figure 5.14 a).

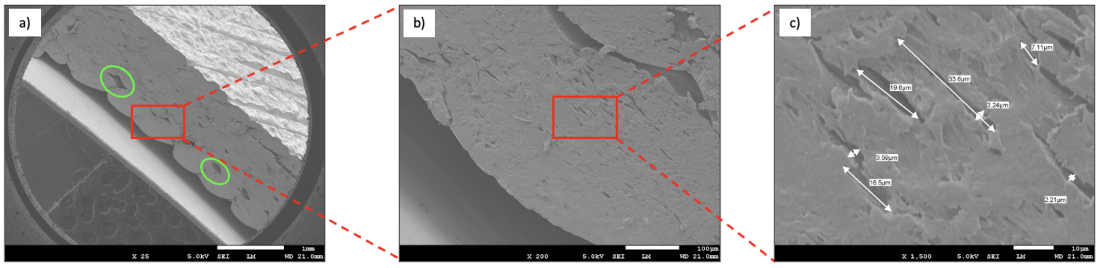

Figure 5.14: SEM images after PEO1M removal of a 2 mm thick PLA/PEO1M 3D print with a magnification of a) X25, b) X200 and c) X1500

On the other hand, in terms of porosity, it is identical to the one described above: the distinction between the porosity of the 3D printing and the extraction of PEG, the size of the pores, the pore shape and the distribution are identical.

For the PLA/PEO1M mixture, the imposed pores kept the desired square shape with an average size of 950 µm, as described in Figure 5.15.

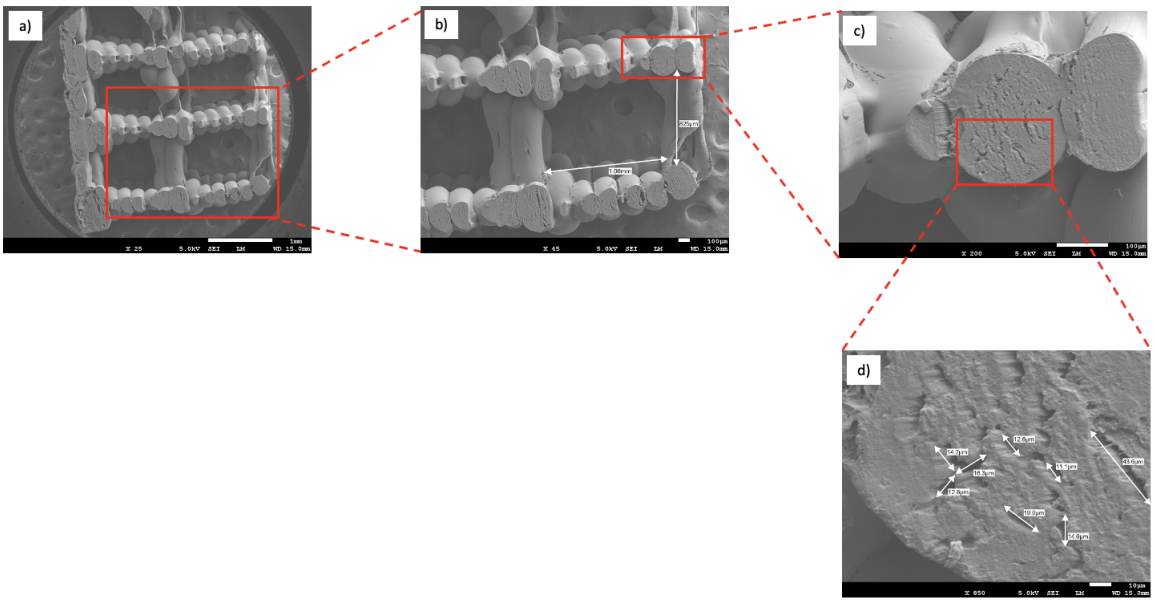

Figure 5.15: SEM images after PEO1M removal of a macroporous PLA/PEG1M 3D print with a magnification of a) X25, b) X45, c) X200 and d) X850

With regard to the porosity obtained by the PEG extraction, the same characteristics described above are reflected in this structure.

5.3.4 Synthesis of the results on porosity

Several aspects need to be examined, including the distribution of pores throughout the sample and within a layer, the shape of the pores, the effect of thickness, the effect of PEG molecular weight on porosity and double porosity.

Firstly, the non-uniform pore distribution observed in all samples indicates that a common factor has affected the overall porosity of the samples. This anomaly stems from the sample preparation process, where a razor blade was used to cut the samples in order to analyze the morphology within, resulting in the material being crushed. In addition, during the 3D printing process, the mixtures have a low viscosity, resulting in soft layers. This can lead to crushing of the layers, masking the presence of porosity.

Within one filament, it was noted that pores were only present in the central part, suggesting that the surface part had no pores and therefore no PEG. This means that PLA is present on the surface, while PEG is only located in the centre of the filament during the extrusion process for creating the PLA/PEG filaments. A possible explanation for this phenomenon is that during the heating of the material, the more viscous component was preferentially directed to the surface while the less viscous one was concentrated in the centre. PLA being more viscous than PEG, it is more present on the surface of the filament.
The ability to remove the central PEG from each layer indicates that water has been able to penetrate to that specific point in the structure and dissolve the PEG. If water has been able to infiltrate through the layers and reach the central region, this means that there is an interconnected path or network of voids in the material. These voids allow for the entry and diffusion of fluid, which allows the PEG located in the core region to be reached and dissolved. According to this hypothesis, it is possible that microscopic pores have formed on the surface of the material, as in the Figure 5.16, where very small pores are circled in red, which were not detected by the SEM images acquired at lower magnification. In order to confirm this hypothesis, it is necessary to perform images at a higher zoom level, which would allow a more accurate observation of the material surface and the detection of possible pores or microscopic defects.

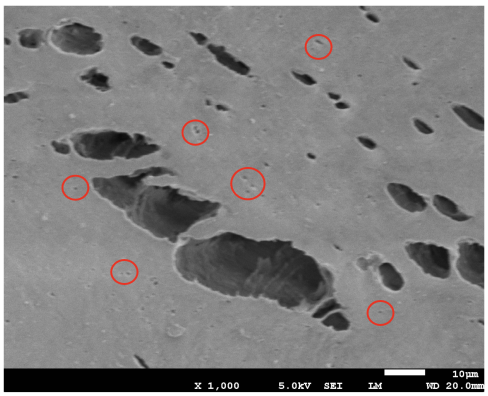

Figure 5.16: SEM images after PEG3K removal of PLA/PEG3K 3D print with a magnification of X1000

Another hypothesis is that PLA could swell in the presence of water. This would create pores or empty spaces within the structure of the material which would allow water to penetrate the PLA and reach the areas where the PEG is present. In a study carried out by B. Ndaz, it was verified that for 24 hours in water at 50°C, PLA swells by less than 1%, indicating fairly low swelling [64]. This hypothesis can therefore be rejected. Therefore, given the ability of water to infiltrate and reach the central region of each layer, it can be inferred that the material has open porosity, characterized by interconnected void spaces that allow for the transport and exchange of fluids within the 3D structure.

In addition to the distribution pattern, the shape and orientation of the pores are also similar in each sample. The pores have an elongated shape in the longitudinal direction, which is probably due to the printing process itself. This is because the extrusion head of the 3D printer deposits the material on the platform and then "pulls" on it to continue building the rest of the 3D object. At each layer of material, the filament is deposited and stretched over the previous layer. The 3D printing process is illustrated in Figure 5.17. The filament is therefore stretched throughout the 3D printing process and when the PEG is removed, its shape remains stretched in the direction of extrusion, resulting in elongated pores.

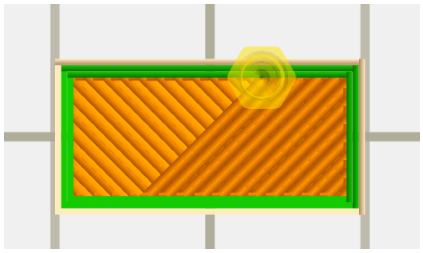

Figure 5.17: Schematic illustration of the process of depositing filament during 3D printing. The yellow circle represents the nozzle through which the filament is extruded

The results showed that when the 3D structure is thicker, the layers adhere better to each other. This can be explained by several phenomena. Firstly, when the structure is thicker, the volume of material present between the layers is larger. This larger volume allows more forces to be exerted on the previous layers that have not yet fully cooled, making it easier for them to collapse and adhere to the adjacent layers. In addition, the slower cooling rate associated with thicker structures allows the melting and solidification process to be prolonged, thereby strengthening the bond between layers. Finally, it is possible for polymer chains to diffuse between layers. When materials are partially melted, there may be molecular movement that facilitates the diffusion of polymer chains from one layer to another. This diffusion of chains between layers can contribute to better integration and adhesion between layers in the 3D structure. As a result, the micropores are slightly more evenly distributed in each layer and not just in the central part of the filaments. Some pores may therefore be present between 2 layers of filaments with a thicker structure. However, as the thicker structure causes the layers to collapse and adhere, it can isolate the pores rather than interconnect them.

Molar mass has an impact on pore size. Although 10% PEG remained in the PLA/PEO100K blend, the pores are the largest and quite numerous. The other two blends retained 7% PEG but the pore size was quite different. For PEG3K, the pores were mostly large but not numerous, whereas for 1M it was the opposite: smaller pores but much more numerous.

The study demonstrated that adding macropores with a size between 350 and 500 µm by imposing a specific 3D design with 70/30 PLA/PEG blends presented significant printing difficulties and that a larger pore size was required. In a previous study, it was shown that the printing parameters had to be adjusted so that the pores obtained with the PLA/PEG mixture were as regular as the pores obtained only with pure PLA [42]. However, it is clear that current printing parameters are not yet optimal. A recurring observation in many samples is that the filaments are crushed. The cause of this problem can be attributed to a too high temperature (T_{nozzle}), which disrupts the cooling process of the layer being printed. As a result, when the next layer is applied to a layer that is still insufficiently cooled, the latter fails to solidify properly and remains relatively soft. Under the effect of the weight of the new layer, the previous layer is then compressed, causing it to flatten and lose its circular shape.
Further research is therefore essential to determine the optimum printing parameters for achieving better structural stability and thus being able to induce regular and smaller macropores in PLA/PEG blends. Research should focus on optimizing nozzle temperature and printing speed.

5.4 Analysis of the viscoelastic properties

The results of the dynamic mechanical properties (storage modulus (E'), loss modulus (E") and Tan(δ)) obtained by DMA are illustrated in Figure 5.18. The samples that were subjected to this DMA were the 3D prints of different PLA/PEG blends before and after PEG removal and of pure PLA.

A first observation concerns the behaviour of the different samples with the frequency of oscillation. The lower the frequency, the wider the phase transition peaks, the more left-shifted the peak of the Tan(δ) and the lower moduli peaks, meaning that the glass transition occurs at a lower temperature and that the material is less rigid. This behaviour can be understood by thinking about the vioscoelastic nature of the material. When a material is deformed with a certain force, it takes some time to return to its original position. However, a high frequency means a low relaxation time, so if the material is deformed it will be stiffer because it does not have enough time to return to its initial state. And so a stiffer material needs more energy to go from a glassy to a rubber state, this will result in an increase in T_g.
Moreover, it appears that in many DMA tests, the frequency of 1 Hz is often used as a reference frequency because it is considered a good indicator of the overall behaviour of the material studied.

For the 70/30 PLA/PEG blends (represented on Figures 5.18 A), D), G)), the Tan(δ) and modulus curves almost merge for the PLA/PEO100K and PLA/PEO1M blends, suggesting that these two blends have fairly similar viscoelastic properties, although it can be seen that the PLA/PEO100K blend is slightly stiffer with a storage modulus at room temperature of 1.15 GPa at 100 Hz compared to 883 MPa for PLA/PEO1M (see Figure 5.18 A)), which is quite surprising as normally the reverse would be observed. It is important to note that the DMA analysis used in this study is not sufficiently precise to accurately determine the Young's modulus. Firstly, it should be noted that storage modulus is different from Young's modulus. Storage modulus measures the elastic response of a material, whereas Young's modulus is a specific measure of stiffness in a given direction. Furthermore, the value of the storage modulus is highly dependent on the geometry of the sample, which may not be optimal in the context of 3D printing. Consequently, the difference in stiffness between the materials studied is not the most important aspect, and the storage moduli remain very close to each other. However, for the PLA/PEG3K blend, the curves show a storage modulus of 129 MPa at 100 Hz (see Figure 5.18 A)) and lower T_g, indicating that this blend is much less stiff. For example, at 1 Hz, the T_g of PLA/PEO1M is 67°C, that of PLA/PEG3K is 62°C.
Comparing all the curves with those for pure PLA (see Figures 5.18 C), F), I)), it can be seen that in general the T_g remains lower for the blended materials, and this is also true for the moduli. The storage modulus of pure PLA at 25°C and 100 Hz is 2,2 GPa and the T_g of pure PLA is 70°C. These results suggest that the addition of PEG to PLA reduces the T_g and storage modulus, and that the T_g and modulus values are more affected the lower the molecular weight of the PEG. This is in agreement with the findings of previous studies described in section 2.2.2 which stated that PEG is a plasticizer of PLA. In addition, the graphs show that the transition peaks of the blends are wider than those of neat PLA, indicating the occurrence of phase separation. This is due to the proximity of the T_g of PLA and the melting temperature of PEG, which causes these two events to merge into one broad peak. As a last point, the intensity of the Tan(δ) peak for neat PLA is much higher than for the blends. It turns out that a lower intensity of this peak is a sign of greater crystallinity. If a material is highly crystalline, this means that it contains less amorphous phases and more crystalline phases, leading to a decrease in the amplitude of the glass transition peak. This explains why blends are more crystalline than PLA alone.

The results for the blends where PEG has been removed are shown in Figures 5.18 B), E), H)). The T_g of each blend converges to almost the T_g of pure PLA (80°C at 100Hz). In addition, the values of the storage modulus (E') and the loss modulus (E") increase in comparison with Figures 5.18 A) and D). For PLA/PEO1M, PLA/PEO100K and PLA/PEG3K blends after PEG extraction, the moduli are 1.9 GPa, 1.9 GPa and 1.55 GPa respectively at 25°C and 1 Hz, as shown in Figure 5.18 B), compared to 2.15 GPa for pure PLA (see Figure 5.18 C)). In each of the mixtures, a narrowing of the transition peak can be observed, indicating a reduced influence of PEG melting. These three observations confirm the elimination of PEG. However, there are still slight disparities between the blends, with the T_g and modulus values being lower for the blends with PEG3K removed than for PEG1M. It should be noted that there is still PEG in each of the blends, which explains why the values are different within the blends and between the blends and neat PLA. It is relevant to note that there are variations in crystallinity within the blends.

The intensity of the Tan(δ) peak in PLA/PEG3K is significantly higher than in the other two blends. Low intensity of this peak, high T_g and broadening of the transition peaks are all indicators of higher crystallinity. As a result, PLA after extraction from PEO1M has the highest crystallinity, followed by PEO100K and PEG3K. This observation can be attributed to variations in the amount of residual PEG in each blend. Finally, these peaks remained less intense than the Tan(δ) peak of PLA, suggesting that neat PLA is even less crystalline.

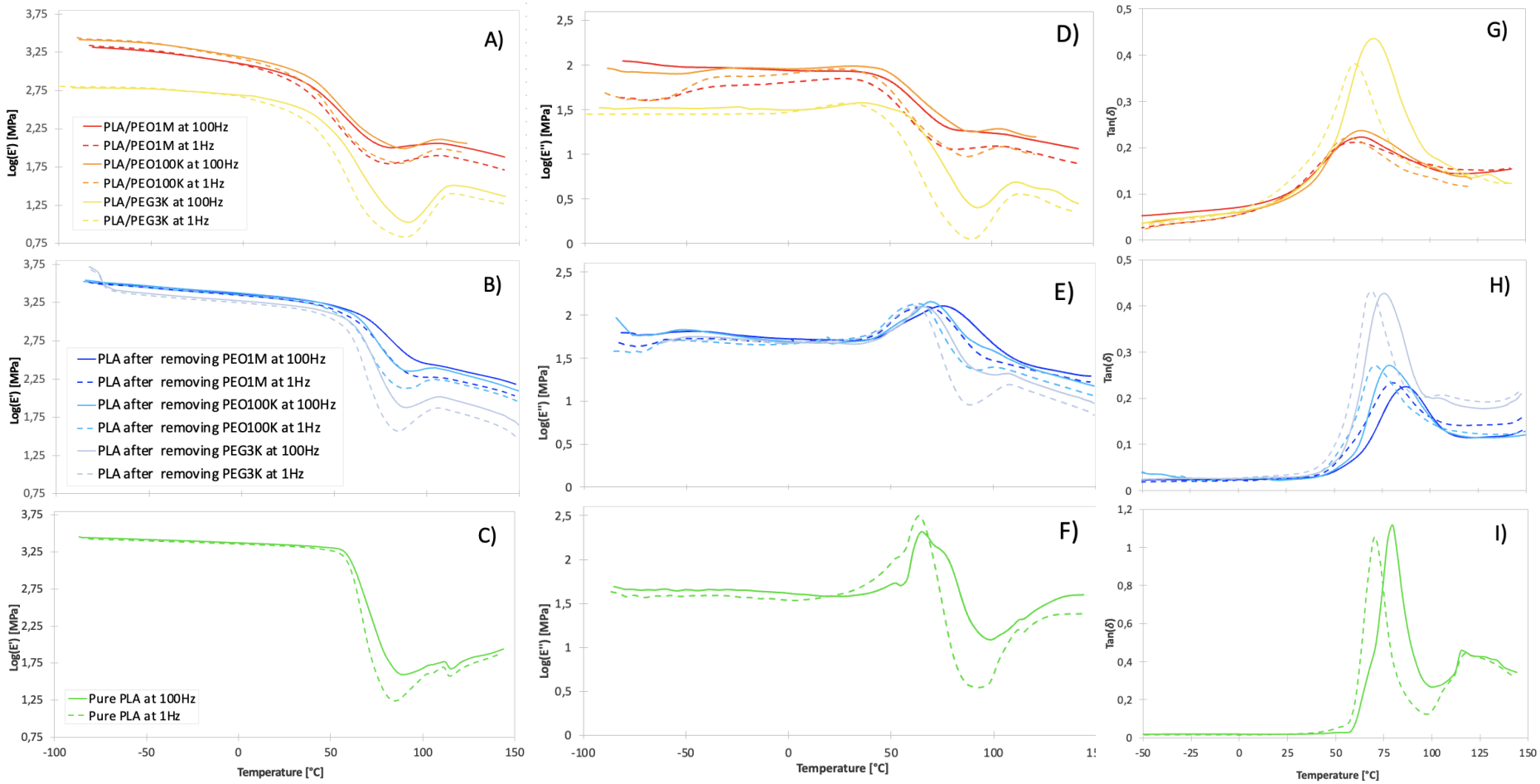

Figure 5.18: The dynamic mechanical properties of different PLA/PEG blends (in red tones), PLA after PEG removal (in blue tones) and pure PLA (in green) using the DMA test at 1 Hz and 100 Hz: storage modulus (E) (A, B, C), loss modulus (E") (D, E, F) and Tan δ (G, H, I)

5.5 Characterization of the mechanical properties

Tensile tests were performed on several samples, including pure PLA, PLA/PEO1M, PLA/PEO100K, PLA with PEO1M removed, and PLA with PEO100K removed and the results are presented in Figure 5.19. However, it was not possible to 3D print the tensile specimens containing PLA/PEG3K blend due to the limited availability of filament and the challenging nature of printing large structures with this blend.

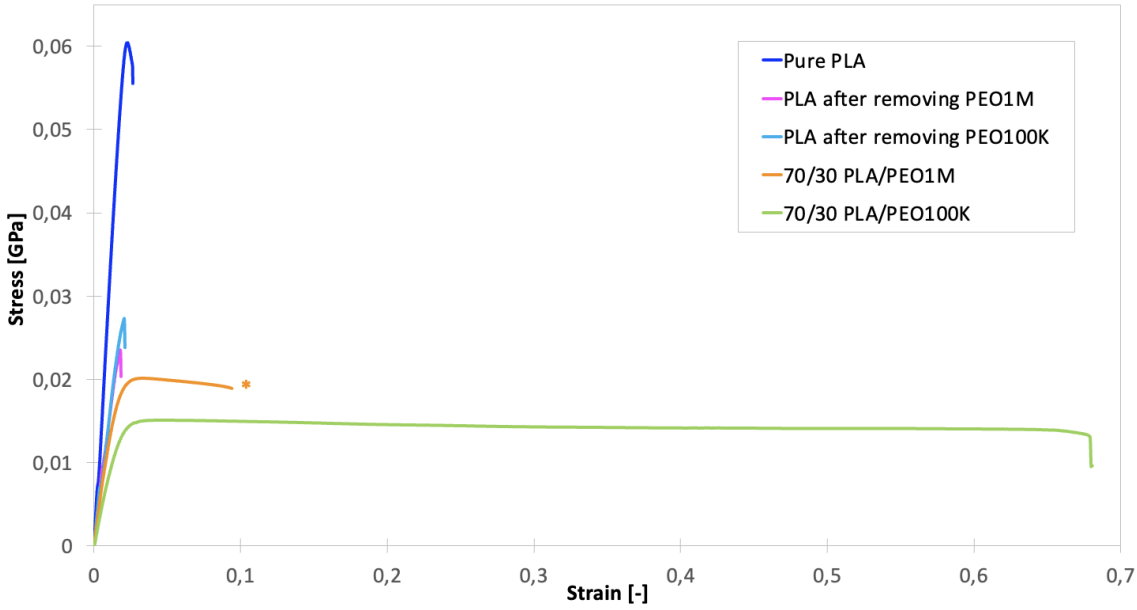

Figure 5.19: Tensile tests on various structures with different compositions, including pure PLA, a 70/30 PLA/PEO1M blend, a 70/30 PLA/PEO100K blend, PLA after removal of PEO1M and PLA after removal of PEO100K

Each material category was tested three times and the final result was obtained by averaging the three tests. This seems to be a good choice as the triplicates were quite similar, except for the PLA/PEO1M blend where the breaking point was quite random. In the tensile test, these samples broke in a surprising way: a hole was created in the centre of the sample but the whole sample was still held together by the contour, as shown in Figure 5.20. This was due to poor adhesion of the layers during 3D printing. As soon as this hole was formed, the sample was considered broken. Therefore, it was not possible to give a fixed value for elongation at break, but rather a range of values.

The stress-strain curve of the PLA/PEO1M and PLA/PEO100K samples showed a characteristic pattern, while the curves of the other samples showed a defect in the linear region. This imperfection can be attributed to minor displacement of the sample between the jaws or to equipment malfunction. The Young's modulus was therefore determined on the basis of the slope of the line to this imperfection. Although it is not visible on Figure 5.19 due to its scale, it is demonstrated in Appendix C.

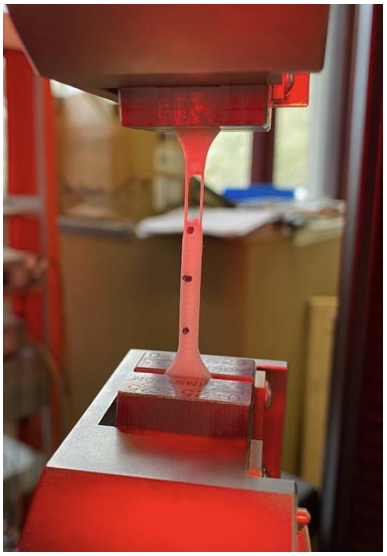

Figure 5.20: Fracture of the PLA/PEO1M blend during the tensile test

With all these considerations, the mechanical properties namely Young's modulus (E), yield strength (σ_y) and elongation at break for each sample could be quantified and are shown in this Table 5.3.

Table 5.3: Mechanical properties (E, σ_y and elongation at break) for 70/30 PLA/PEO1M blend before and after PEG extraction, 70/30 PLA/PEO100K blend before and after PEG extraction and neat PLA

	E [GPa]	$\boldsymbol{\sigma_y}$ [MPa]	**Elongation at break** [%]
70/30 PLA/PEO1M	1.42	17.7	9-35 *
70/30 PLA/PEO100K	0.87	13.9	67
PLA after removing PEO1M	1.72	20.7	1.8
PLA after removing PEO100K	1.85	24.8	2
Pure PLA	3.37	52.6	2.6

The results of the mechanical tests confirm the previous findings in the section 2.2.2 ("Interest of PEG"), which indicated that the addition of PEG to a PLA blend reduces the stiffness of the material [42]. In fact, the presence of PEG leads to a reduction in the stiffness and an increase in the flexibility of the material, manifested by a lower Young's modulus (E) and a higher elongation at break. This is illustrated by the following values: for pure PLA, E and elongation at break are 3.37 GPa and 2.6%, while for PLA/PEO1M, E is 1.42 GPa with an elongation of 9 to 35%.
Theoretically, as stated in the section 2.2.1 ("PEG"), the molar mass of PEG influences the mechanical properties: the higher the molar mass of PEG, the stiffer the material. This observation is also verified for the PLA/PEO1M and PLA/PEO100K blends. For example, E is 1.42 GPa with a elongation at break between 9 and 35% compared to 0.87 GPa and 67% for PLA/PEO100K.

For 3D prints where PEG has been dissolved in water, the mechanical properties are closer to those of pure PLA. In other words, the Young's modulus increases and the elongation at break decreases compared to 3D prints made of PLA/PEG blend. This observation is consistent given that PEG, which contributed to lowering the Young's modulus and increasing the elongation at break, was removed from the blend. However, it is important to note that the Young's modulus and elongation at break of 3D prints with PEG removed is still significantly lower than that of pure PLA. The reason for this difference is that the material lost more than 20% of its weight after the PEG was removed, creating pores in the structure. The presence of these pores leads to a redistribution of the charge and a reduction in the density of the material, which reduces its ability to withstand mechanical stress. The pores create discontinuities in the solid structure, weakening the bonds between the molecules and reducing the rigidity of the material. The presence of pores also allows cracks to propagate more easily, reducing the material's resistance to fracture. A porous structure is therefore less rigid and has lower mechanical strength than a material without pores.

Comparing the PLA/PEO100K and PLA/PEO1M blends after PEG extraction, 10% and 7% of PEG remained in each blend respectively. In terms of mechanical properties, the PLA/PEO100K blend after PEG extraction was slightly stiffer. This finding may be surprising and suggests that the difference in stiffness can not be attributed solely to the molecular weight of PEG. Other factors such as crystallinity or porosity may be involved. A greater presence of crystalline regions in a material may contribute to increased stiffness. The crystalline regions provide a more ordered and rigid structure, thus improving the mechanical properties of the material. If the PLA/PEO100K blend has a higher degree of crystallinity than the PLA/PEO1M blend, this would explain its higher stiffness.
On the other hand, differences in porosity between the blends can also affect their mechanical properties, including stiffness. If the PLA/PEO1M blend has a higher level of porosity, with more voids in its structure, this may result in reduced stiffness. Porosity affects the ability of the material to transfer stress and can contribute to a reduction in rigidity and strength.
It is therefore more plausible that porosity and/or crystallinity are the cause of the difference in stiffness between PLA/PEO100K and PLA/PEO1M blends after PEG extraction.

5.6 General discussion

Once the thermal, porosity and mechanical properties have been analyzed individually, a complete profile of characteristics can be established for each major stage of the manufacturing process. To this end, the characteristics observed at each stage of the manufacturing process of macroporous and/or microporous structures, including filament manufacture, 3D printing before and after PEG removal, using a 70/30 PLA/PEG blend, will be summarized. As a result of this discussion, the differences in properties resulting from the use of a PLA/PEG blend compared to the use of a 100% PLA material will be identified. In addition, it will be verified whether the properties obtained by the structures after PEG removal comply with the requirements necessary for biological applications in tissue engineering.

To produce filaments, it was necessary to use two separate extrusion stages with long screws for the 70/30 PLA/PEG blends, while a single extrusion stage was sufficient for the PLA-only filament. DSC revealed that PLA and PEG were miscible in the amorphous phase of PLA, resulting in a decrease in T_g of PLA. However, they were immiscible in the rest of the sample.
When comparing these blends with pure PLA, it was found that the blends were much more crystalline. It was therefore concluded that PEG acts as a nucleating agent for PLA. PLA typically crystallizes at around 110°C, but with the addition of PEG, crystallization conditions occur at lower temperatures. When the cooling rate is the same for the materials, a lower crystallization temperature allows the polymer chains to move and organize themselves longer into a more complete crystalline structure. In addition, PEG acts as a plasticizer for PLA, increasing the mobility of PLA chains and encouraging their movement to form crystalline structures. Thus, the addition of PEG gives PLA more time to crystallize and greater mobility to the chains, which increases crystallinity.
In addition, the molar mass of the PEG also has an influence on crystallinity. To form good quality crystals, the PLA must expel the PEG from its spherulites, which is only possible if the PEG is mobile. It turns out that the mobility of the PEG is all the greater when the molar mass of the PEG is low.

The filaments obtained were used to print 3D structures. Due to the slower cooling speed during 3D printing (from the printhead nozzle to the platform with $\Delta T° = -160°C$), compared with the cooling speed at the output of the screw extruders (accelerated by ventilators) used to manufacture the filaments, the 3D structures slightly increased their degree of crystallinity. As a result, PLA had more time to crystallize, resulting in a higher degree of crystallinity. This has significant advantages. In fact, it is preferable for the filament not to be fully crystallized and rigid, as this would lead to difficulties when winding it around the spool and would require a longer melting time during 3D printing. On the other hand, after the 3D printing process, a slight increase in the crystallization of the material is beneficial, as it helps to reinforce its structural stability. Despite this increase in crystallinity in all the 3D printed structures, PLA/PEG-based structures remained much more crystalline than PLA alone, which was also confirmed by DMA. DSC and DMA also show that phase separation is still present within 3D prints. The mechanical properties of these structures were analyzed by DMA and tensile testing. It was observed that the

blends were much more crystalline but less rigid than pure PLA. The same phenomenon was observed within the blends; the greater the molecular weight of the PEG, the greater the degree of crystallinity, the lower its Young's modulus. Logically, a more crystalline material is more rigid, but here, the opposite trend is observed. This is explained by the presence of PEG, which is a PLA plasticizer and therefore makes the material more flexible and this effect is more pronounced with low molecular weight PEG. This can also be seen in another way with phase separation. The phase separation observed in blends leads to a non-uniform distribution of phases in the material, which can alter the overall mechanical properties. PEG-rich regions can form distinct domains in the PLA matrix, which can lead to an irregular distribution of crystalline and amorphous phases. These amorphous phases create points of weakness in the material, reducing the mechanical properties of the material as a whole. When tensile forces are applied to the sample, the polymer chains present in the amorphous phases tend to elongate, which can lead to separation between these chains and eventually to sample rupture. The addition of PEG, which acts as a plasticizer for the amorphous phase of PLA, enhances this effect and can potentially reduce the modulus of the sample. The mechanical properties are therefore reduced because the structures made from the blends have defects in their structure and the degree of crystallinity would not be representative of the real mechanical properties of the structure. This reasoning also explains why blends with PEG3K are much more crystalline but less rigid than blends with PEG1M. As the molecular weight of PEG increases, the chains become longer and less mobile. This reduced mobility reduces PEG's plasticizing effect and increases the material's rigidity, as the chains stretch less and are therefore harder to break.

When the PEG present in 3D prints is dissolved in water, some structures gained in crystallinity, while others showed a decrease in their degree of crystallinity, as indicated by DSC analysis. But this change, although negligible, is difficult to assess because the amount of residual PEG in each sample is different and calculations of the different enthalpies are not at all accurate. The results obtained from the DMA and DSC analyses call into question the hypothesis that an increase in the molecular weight of PEG leads to a decrease in the degree of crystallinity. However, it is important to note that the residual amount of PEG varies in each blend, which influences crystallinity and explains why this hypothesis no longer seems applicable in this specific type of structure. To discredit this hypothesis, each of the blends should have had an identical proportion of residual PEG, which is practically impossible to achieve. Despite this, it should be emphasised that this hypothesis remains valid and has been confirmed in subsequent studies [60, 61]. Another possible explanation is that the removal of a component from the mixture leads to a rearrangement of the PLA chains. This rearrangement effect could vary depending on the molar mass of the PEG. When PEG is removed, the interactions between the polymer chains can be altered, which can lead to a spatial rearrangement of the chains and influence the crystal structure of the material. It is likely that the molar mass of the PEG plays a role in this rearrangement effect, as longer chains can have a greater influence on the overall structure of the material when rearranged. This may also explain the variations observed in the crystallinity of different PLA/PEG structures after PEG removal. The removal of PEG from the mixtures is confirmed by the increase in T_g of PLA. PEG was present in the amorphous phases of PLA, where they formed a miscible mixture. The increase in T_g suggests that the component that reduced this value, PEG, is less present.

However, the T_g is still lower than that of pure PLA, indicating that the PEG has only been partially removed. NMR analyses were used to calculate the composition of the blends after PEG extraction and the structures still contained between 7 and 10% PEG. After PEG extraction, the PLA/PEG structures, which now have micropores, show an improvement in their mechanical properties compared with the structures before PEG removal, as shown by the results of DMA analyses and tensile tests. The reduction in PEG content, which had a plasticizing effect on the mechanical properties of the structures, led to an increase in these mechanical properties. Compared with pure PLA, however, the modulus of elasticity of blends remains lower. This is because even though some of the PEG has been removed from the blends, there is still a certain amount that influences the mechanical properties. In addition, the removal of part of the structures has created pores, which also have an impact on the mechanical properties. The creation of pores leads to a reduction in the density of the material, which in turn leads to a reduction in mechanical strength. As a result, a porous structure is less rigid and less resistant than one without pores.

By removing the PEG from the structures made from the PLA/PEG mixture, microporosity was created, as observed by SEM. When the PEG is dissolved and removed, it leaves voids within the structures. However, contrary to the expectation of an even distribution of pores in the structure, the SEM images revealed a non-homogeneous distribution of pores. This non-uniformity can be attributed to the sample preparation used, where samples were cut for observation. The cutting process resulted in the pores being crushed, creating an absence of pores in one part of the sample and a presence of pores in the other part. However, in some samples that showed a crack, a better visualisation of the porosity is observed in the cracks that have not been subjected to the razor blade cut, proving that what is observed after the samples have been cut was not representative of reality. In order to confirm this hypothesis, it would be necessary to repeat the observation of these samples in the SEM by preparing the sample in a different way in order to analyze the inside of the sample, such as cryogenising the sample followed by cold fracturing.
In each section where pores were observed, it was noted that the pores were distributed in a particular pattern. The pores were consistently present in the central part of each filament layer, suggesting that the PEG was predominantly located in the centre of the filament, surrounded by PLA. Therefore, this also indicates that water could have reached this region and had to take a path through the voids to get there, confirming that the pores are interconnected and that the porosity is of the open type.
Other observations were made concerning the shape of the pores. This elongated shape is probably due to the 3D printing process, where the filament is stretched after deposition. In addition, the size and percentage of pores vary according to the molecular weight of the PEG. For PEG3K, the pores are relatively large (1-100 µm) but few in number. For PEO100K, the pores are more variable, ranging from 15 to 200 µm, and present in greater quantity. Finally, PEO1M has smaller pores (5-30 µm) and very many. These results must be interpreted with caution, as the method used still has limitations and significant biases in the observations.

Some of the structures analyzed exhibited double porosity, comprising both microporosity resulting from PEG removal by dissolution in water, and macroporosity imposed by the 3D printing design. Crucially, the microporosity achieved through PEG removal differs from the intentional porosity created when 3D printing porous structures. In the case of intentional porosity, the pores are generally larger and deliberately designed. In contrast, the microporosity resulting from PEG removal is more subtle and can be considered an intrinsic characteristic of the structure obtained after PEG extraction.
As far as macroporosity is concerned, it was not possible to reduce the pore size below 650 µm, whereas the target size was between 300 and 500 µm. This is attributed to inappropriate printing parameters that were observed in the SEM images. The filament layers clearly lost their circular shape and became oval. This deformation is due to too high a temperature of the printing nozzle and an excessive printing speed, preventing the layer from cooling sufficiently before the next layer is deposited. As a result, the layer becomes soft and deforms, creating an oval shape. It is important to note that these printing defects are not always perceptible during the 3D printing process, but they become clearly visible during SEM observation. It is therefore essential to continue optimizing the printing parameters in order to achieve the desired macroporosity in the structures and to obtain greater structural stability in the 3D prints.

At this stage, it is possible to show the variations in properties between 3D prints made from pure PLA and PLA mixed with PEG, subsequently dissolved in water. The summary values for each property and for each blend are shown in Table 5.4. It should be noted that tensile tests were not carried out with PEG3K. However, given that the storage modulus values obtained by DMA were almost similar for PEO1M and PEO100K (1.9 GPa for the two mixtures in DMA compared with 1.72 GPa and 1.85 GPa respectively for the tensile tests), an approximation of the Young's modulus value for PEG3K can be made using its storage modulus value obtained by DMA. Care should be taken when approximating Young's modulus in this way. This approach gives a rough estimate of its value, but it is not totally accurate. It is important to note that this approximation is only used for indicative purposes and to get a general idea of the Young's modulus of the PLA/PEG3K material after PEG removal.

Clearly, the main advantage lies in the ability to generate microporosity in PLA/PEG blends by dissolving the PEG in water, without the use of any solvent, which is impossible to achieve in a material composed solely of PLA. However, it is entirely possible to create macropores using both pure PLA filament and PLA/PEG-based filaments. The lower T_g of the blends compared with pure PLA indicate that PEG is still present in the structures and has not been completely removed. This is not a problem at all, given that PEG is also a biocompatible biopolymer and will not alter the biocompatibility of the implant. Finally, the mechanical properties are also lower due to the porosity created, but are still acceptable (around 2 GPa).

Table 5.4: Comparison of the important properties between the three different PLA blends after PEG extraction with neat PLA

Characteristics	**PLA after removing PEG3K**	**PLA after removing PEO100K**	**PLA after removing PEO1M**	**Neat PLA**
Macroporosity	√	√	√	√
Microporosity	√	√	√	X
T_g **of PLA** [°C]	54	66	68	66
T_m **of PLA** [°C]	175	174	179	180
X_c [%]	6.08	8.5	9	2.6
E [GPa]	$\sim$ 1.55	1.85	1.72	3.37
σ_y [MPa]	-	24.8	20.7	52.6
Elongation at break [%]	-	2	1.8	2.6

In order to answer the research question of whether the properties of PLA/PEG 3D prints after PEG extraction are acceptable for tissue engineering, it is necessary to compare the properties obtained for PLA/PEG blends after PEG extraction with those required for biological applications. This is summarized in Table 5.5.

Table 5.5: Comparison of key characteristics between the three different PLA blends (PLA/PEG3K, PLA/PEO100K and PLA/PEO1M) after PEG extraction with values for biological applications

Characteristics	**PLA after removing PEG3K**	**PLA after removing PEO100K**	**PLA after removing PEO1M**	**Values for biological applications**
Macroporosity [µm]	800	650	950	300-500
Microporosity [µm]	1–100	15-200	5-30	50-200
E [GPa]	$\sim$ 1.55	1.85	1.72	0.0001-71 [65]
σ_y [MPa]	-	24.8	20.7	21-130 [66]
Elongation at break [%]	-	2	1.8	0.6-2.5 [66]

As far as macroporosity is concerned, none of the blends fall within the range defined by biological applications. The blend that comes closest is PLA after PEG100K extraction (650 µm vs. 300-500 µm). With regard to microporosity, the PEG1M blend has significantly smaller pores than desired. The other two blends more or less meet the pore requirements for biological applications, although they also have some pores that fall below the specified range. However, the PEG100K blend encompasses the pore size range within its own values.

In terms of mechanical properties, biological applications range from microstructures (0.0001 GPa) to bone replacement (71 GPa). All three blends fall within this broad range, but it is worth noting that PLA after PEO100K removal is the stiffest, followed closely by PLA after PEO1M removal, with a larger gap for PLA after PEG3K removal. Unfortunately, the other mechanical properties could not be calculated for PLAPEG3K due to the difficulty of printing large structures with this blend and thus printing the required structure for the tensile test. For the other two blends, the values are well within the requirements for biological applications, although PLA/PEG100K has also a better yield strength and elongation at break.

Based on these results, it can be stated that PLA after PEO100K removal meets the requirements of biological applications in terms of mechanical properties and porosity. PLA after PEO1M extraction satisfies the mechanical properties but not the pore size, while PLA after PEG3K extraction has lower mechanical properties but a more suitable porosity for tissue engineering.

A 3D printed scaffold made from a 70/30 mixture of PLA/PEO100K after generating microporosity by dissolving PEG in water seems most suitable for use in biomedical applications for tissue engineering and more specifically in bone regeneration applications. Bone implants must be able to withstand mechanical loads during the healing process and promote bone growth. A scaffold with a high mechanical strength of almost 2 GPa can provide this adequate structural support. In addition, the pore size between 50 and 200 µm and their interconnectivity allow bone cells (osteocytes 5-20 µm, osteblast 20-50 µm and osteoclast 10-300 µm) to infiltrate throughout the scaffold and establish intercellular connections and promote the formation of a vascular network [67, 68, 69]. This controlled porosity facilitates the circulation of nutrients, oxygen and growth factors, while allowing the removal of metabolic waste products. It also allows for an even distribution of cells throughout the scaffold, thus enhancing the formation of new bone tissue. In conclusion, the use of a 3D printed scaffold made from a 70/30 PLA/PEO100K blend that induces microporosity by dissolving PEG in water is promising for biomedical applications in tissue engineering, particularly in the field of bone regeneration. However, it should be noted that there are still limitations, such as optimizing 3D printing parameters and obtaining optimum micropore and macropore sizes. These aspects require particular attention if this scaffold is to be used effectively in practical applications.

Chapter 6

Conclusion and perspectives

The main aim of this research was to develop a process for creating porosity by mixing PLA and PEG, followed by dissolving the PEG in water. PEG, which is soluble in water, played a key role as a porogen, enabling the formation of micropores through its removal by water. This removal of PEG created open spaces within the structure. A second porosity was added to the structures by imposing a porous design on the 3D printer. The structures benefited from both microporosity thanks to the mixture of PLA and PEG, and macroporosity thanks to the design of the 3D printer. By creating a double porous structure, it could be used in the future as a scaffold for tissue engineering, given the importance of porosity in this type of application.

To achieve this objective, a first step was to determine the optimal proportion of PLA and PEG in the mixture. Based on the results of a previous study, it was found that the 70/30 composition of PLA/PEG had previously been identified as the most suitable for films [59]. On this basis, this research focused solely on this composition of 70% PLA and 30% PEG. However, the optimum molar mass of PEG is a key parameter to be determined as part of the research. Three different PEG molar masses were studied, namely PEG3K, PEO100K and PEO1M, in order to assess their influence on porosity properties and other important characteristics such as mechanical and thermal properties.

A second important step in this research was the 3D printing of the different mixtures, made possible by the creation of filaments through extrusion. 3D printing offers a number of advantages, including the ability to create patient-specific structures, which is particularly important in the context of tissue engineering. Each patient may have specific needs in terms of shape and size. Thanks to the versatility offered by 3D printing, it is possible to design customised structures for each patient.
As well as being able to create custom structures, 3D printing also makes it possible to generate macroporosity in scaffolds. Macroporosity corresponds to pore sizes of between 300 and 500 µm. Unfortunately, it was not possible to achieve this pore size in the prints made with the three different mixes. Due to the difficulties encountered when printing structures with pores of this specific size, it was necessary to increase the pore size in order to obtain a successful print. SEM images showed that the minimum size that could be printed for each of the blends was around 800 µm for PLA/PEG3K, 650 µm for PLA/PEO100K and 950 µm for PLA/PEO1M.

With regard to the extraction of PEG to generate micropores, NMR confirmed that not all of the PEG could be removed. However, the removal of most of the PEG (more than two thirds) still allowed the formation of micropores in each type of structure. However, the distribution of micropores observed is not uniform, probably due to the razor blade cutting of the samples for SEM analysis. The target pore sizes were 50 to 200 µm. Pore sizes and quantities were found to vary with the molecular weight of the PEG, with smaller pore sizes (5-30 µm) for PEO1M. Despite these limitations, the target microporosity, with pore sizes between 50 and 200 µm, was achieved for PLA/PEG3K (1-100 µm) and PLA/PEO100K (15-200 µm) blends.

One of the main questions raised when porosity was introduced into structures was its impact on mechanical properties However, it was found that the 3D prints retained satisfactory mechanical properties. Mechanical and DMA tests revealed that these porous structures exhibited a certain level of rigidity and mechanical strength, making them potentially suitable for biomedical applications. In addition, the incorporation of PEG led to structures that were significantly more crystalline than those composed solely of PLA, suggesting that PEG acts as a nucleating agent for PLA. However, it is important to note that the mechanical properties of the porous structures remained inferior to those of pure PLA.

Theoretically, the PLA/PEO100K blend, after extraction of the PEG, demonstrated the best properties in terms of porosity and mechanical properties, and appears to best meet the requirements of biological applications. It could therefore be used as a scaffold in tissue engineering applications to promote bone tissue regeneration. However, it is essential to verify whether this remains feasible in practice. The promising results obtained in this preliminary study pave the way for potential applications in the medical field. However, in-depth studies, including in vitro and in vivo trials, are needed to confirm the efficacy and safety of these implants in real-life conditions.

However, despite the promising results, there are still a number of areas for improvement before envisaging in vivo and in vitro tests.
Firstly, the printing parameters used were not optimal. SEM images revealed deformation of the layers due to the weight of the top layers. Insufficient solidification of the previous layer under the weight of the next led to inaccuracies in the 3D printing and limited the possibility of printing smaller macropores. To overcome this problem, it would be necessary to reduce the temperature of the 3D printer nozzle and adopt a slower printing speed.
With regard to microporosity, using a razor blade to cut the samples potentially altered their structure, masking some of the porosity. An alternative would be to cryogenically freeze the samples and fracture them cold to observe the internal porosity. In addition, the porosity was assumed to be open, given the presence of pores in the centre of each filament. This suggests that the water used a network of pores to reach this area. In order to precisely identify the routes taken by the water, it would be necessary to check the surface porosity of the sample. Another approach to assessing open porosity is to use a dye or contrast agent applied to the surface of the sample. If the sample has open porosity, the liquid will be absorbed and penetrate the pores, which will be visible to the naked eye or

using an appropriate imaging technique, such as micro-computed tomography (micro-CT). Finally, the preferential location of the micropores in the centre of the filaments, suggesting a preferential distribution of PEG in this area while PLA is on the surface, raises questions. This asymmetric distribution could be attributed to a difference in viscosity between the two components during the manufacturing process. To confirm this hypothesis, dedicated viscosity analyses would be required.

Although the 3D printing and porosity analysis processes were difficult and limited, the results obtained indicate that the aim of the study was successfully achieved. Mixing PLA and PEG, followed by extraction of the PEG, induces the formation of microporous structures in the 3D prints. However, it should be mentioned that the macroporosity of the structures did not reach the desired target values.

In summary, this study has confirmed the feasibility of creating porous structures using PLA and PEG blends, opening up new prospects for tissue engineering and other biologic applications. However, further efforts are needed to improve the precision of 3D printing and to analyze porosity more optimally. These advances will enable the full potential of these porous structures to be exploited in the biomedical field.

Bibliography

[1] *Maladies cardiovasculaires - Ministère de la Santé et de la Prévention*. URL: https://solidarites-sante.gouv.fr/soins-et-maladies/maladies/maladies-cardiovasculaires/article/maladies-cardiovasculaires (visited on 11/27/2022).

[2] Fondation de France. *Recherche sur le cancer*. URL: https://www.fondationdefrance.org/fr/maladies-cardiovasculaires (visited on 11/27/2022).

[3] *Peripheral Nerve Injuries Epidemiology Forecast Report 2017-2030 - Focus on United States, Germany, France, Italy, Spain, United Kingdom, and Japan - ResearchAndMarkets.com*. 2021. URL: https://www.businesswire.com/news/home/20210108005424/en/Peripheral-Nerve-Injuries-Epidemiology-Forecast-Report-2017-2030---Focus-on-United-States-Germany-France-Italy-Spain-United-Kingdom-and-Japan---ResearchAndMarkets.com (visited on 11/27/2022).

[4] *Le don d'organes et de tissus humains, une problématique mondiale*. URL: https://www.france-adot.org/don-international/ (visited on 11/27/2022).

[5] Ks Katti et al. "4 - Materials for joint replacement". In: *Joint Replacement Technology*. Ed. by Peter A. Revell. Woodhead Publishing, 2008, pp. 81–104. DOI: 10.1533/9781845694807.1.81.

[6] Charles A. Vacanti. "The history of tissue engineering". In: *Journal of Cellular and Molecular Medicine* 10 (2006), pp. 569–576. DOI: 10.1111/j.1582-4934.2006.tb00421.x.

[7] Zia Ullah Arif et al. "Recent advances in 3D-printed polylactide and polycaprolactone-based biomaterials for tissue engineering applications". In: *International Journal of Biological Macromolecules* 218 (2022), pp. 930–968. DOI: 10.1016/j.ijbiomac.2022.07.140.

[8] Jeroen Rouwkema et al. "Vascularization in tissue engineering". In: *Trends in Biotechnology* 26 (2008), pp. 434–441. DOI: 10.1016/j.tibtech.2008.04.009.

[9] Tiziano Serra et al. "Relevance of PEG in PLA-based blends for tissue engineering 3D-printed scaffolds". In: *Materials Science and Engineering: C* 38 (2014), pp. 55–62. DOI: 10.1016/j.msec.2014.01.003.

[10] Jiang-Ze Wang et al. "A review of emerging bone tissue engineering via PEG conjugated biodegradable amphiphilic copolymers". In: *Materials Science and Engineering: C* 97 (2019), pp. 1021–1035. DOI: 10.1016/j.msec.2019.01.057.

[11] K. Deshmukh et al. “3 - Biopolymer Composites With High Dielectric Performance: Interface Engineering”. In: *Biopolymer Composites in Electronics*. Ed. by K. K. Sadasivuni et al. Elsevier, 2017, pp. 27–128. DOI: 10.1016/B978-0-12-809261-3.00003-6.

[12] M. Savioli Lopes et al. “Poly (Lactic Acid) Production for Tissue Engineering Applications”. In: *Procedia Engineering*. CHISA 2012 42 (2012), pp. 1402–1413. DOI: 10.1016/j.proeng.2012.07.534.

[13] Pran Kishore Deb et al. “Chapter 6 - Pharmaceutical and Biomedical Applications of Polymers”. In: *Basic Fundamentals of Drug Delivery*. Ed. by Rakesh K. Tekade. Advances in Pharmaceutical Product Development and Research. Academic Press, 2019, pp. 203–267. DOI: 10.1016/B978-0-12-817909-3.00006-6.

[14] Shiro Kobayashi et al. “Enzymatic Polymerization”. In: *Chemical Reviews* 101 (2001), pp. 3793–3818. DOI: 10.1021/cr9901211.

[15] Hossein Ramezani Dana et al. “Synthesis, properties, and applications of polylactic acid-based polymers”. In: *Polymer Engineering & Science* 63 (2023), pp. 22–43. DOI: 10.1002/pen.26193.

[16] Elisa Capuana et al. “Poly-l-Lactic Acid (PLLA)-Based Biomaterials for Regenerative Medicine: A Review on Processing and Applications”. In: *Polymers* 14 (2022), p. 1153. DOI: 10.3390/polym14061153.

[17] Miroslav Pohanka. “D-Lactic Acid as a Metabolite: Toxicology, Diagnosis, and Detection”. In: *BioMed Research International* 2020 (2020), p. 3419034. DOI: 10.1155/2020/3419034.

[18] Carsten Dingler et al. “Semiconducting Polymer Spherulites—From Fundamentals to Polymer Electronics”. In: *Macromolecular Rapid Communications* 40 (2019), p. 1800601. DOI: 10.1002/marc.201800601.

[19] L. -T. Lim et al. “Processing technologies for poly(lactic acid)”. In: *Progress in Polymer Science* 33 (2008), pp. 820–852. DOI: 10.1016/j.progpolymsci.2008.05.004.

[20] Jin Zhang et al. “Highly crystallized poly (lactic acid) under high pressure”. In: *AIP Advances* 2 (2012), p. 042159. DOI: 10.1063/1.4769351.

[21] Shady Farah et al. “Physical and mechanical properties of PLA, and their functions in widespread applications — A comprehensive review”. In: *Advanced Drug Delivery Reviews* 107 (2016), pp. 367–392. DOI: 10.1016/j.addr.2016.06.012.

[22] *How does molecular weight effect glass transition temperature? | Socratic*. URL: https://socratic.org/questions/how-does-molecular-weight-effect-glass-transition-temperature (visited on 03/14/2023).

[23] Mehrshad Mehrpouya et al. “4D printing of shape memory polylactic acid (PLA)”. In: *Polymer* 230 (2021), p. 124080. DOI: 10.1016/j.polymer.2021.124080.

[24] Biolin Scientific. *Effect of wettability in biomedical applications*. URL: https://content.biolinscientific.com/effect-of-wettability-in-biomedical-applications (visited on 03/13/2023).

[25] *Plasma Treatment - Learn the basics and much more here | Tantec*. URL: https://tantec.com/the-basics-of-plasma-treatment/ (visited on 04/12/2023).

[26] Decai Li et al. "Preparation of plasticized poly (lactic acid) and its influence on the properties of composite materials". In: *PLOS ONE* 13 (2018). DOI: 10.1371/journal.pone.0193520.

[27] *Plastiques résistants à basse température | Ensinger*. URL: https://www.ensingerplastics.com/fr-fr/produits-semi-finis/choix-des-materiaux-plastiques/basse-temperature (visited on 03/08/2023).

[28] Jose Gamez-Perez. "Fracture behavior of quenched poly(lactic acid)". In: *eXPRESS Polymer Letters* 5 (2010), pp. 82–91. DOI: 10.3144/expresspolymlett.2011.9.

[29] Yuval Ramot et al. "Biocompatibility and safety of PLA and its copolymers". In: *Advanced Drug Delivery Reviews*. PLA biodegradable polymers 107 (2016), pp. 153–162. DOI: 10.1016/j.addr.2016.03.012.

[30] Hongbo Zhang et al. "Control of Scaffold Degradation in Tissue Engineering: A Review". In: *Tissue Engineering Part B: Reviews* 20 (2014), pp. 492–502. DOI: 10.1089/ten.teb.2013.0452.

[31] Oliver Riester et al. "Challenges in Bone Tissue Regeneration: Stem Cell Therapy, Biofunctionality and Antimicrobial Properties of Novel Materials and Its Evolution". In: *International Journal of Molecular Sciences* 22 (2021). DOI: 10.3390/ijms22010192.

[32] Tianyang Qiu et al. "Research into biodegradable polymeric stents: a review of experimental and modelling work". In: *Vessel Plus* 2 (2018), p. 12. DOI: 10.20517/2574-1209.2018.13.

[33] Yihong Gong et al. "In vitro and in vivo degradability and cytocompatibility of poly(l-lactic acid) scaffold fabricated by a gelatin particle leaching method". In: *Acta Biomaterialia* 3 (2007), pp. 531–540. DOI: 10.1016/j.actbio.2006.12.008.

[34] Aleš Gregor et al. "Designing of PLA scaffolds for bone tissue replacement fabricated by ordinary commercial 3D printer". In: *Journal of Biological Engineering* 11 (2017), p. 31. DOI: 10.1186/s13036-017-0074-3.

[35] Xibao Chen et al. "3D printed porous PLA/nHA composite scaffolds with enhanced osteogenesis and osteoconductivity in vivo for bone regeneration". In: *Biomedical Materials (Bristol, England)* 14 (2019), p. 065003. DOI: 10.1088/1748-605X/ab388d.

[36] Robert Paberit et al. "Cycling Stability of Poly(ethylene glycol) of Six Molecular Weights: Influence of Thermal Conditions for Energy Applications". In: *ACS Applied Energy Materials* 3 (2020), pp. 10578–10589. DOI: 10.1021/acsaem.0c01621.

[37] Takashi Uemura et al. "Unveiling thermal transitions of polymers in subnanometre pores". In: *Nature Communications* 1 (2010), p. 83. DOI: 10.1038/ncomms1091.

[38] Ah-Young Jee et al. "Determination of the elastic modulus of poly(ethylene oxide) using a photoisomerizing dye". In: *Chemical Physics* 422 (2013), pp. 246–250. DOI: 10.1016/j.chemphys.2012.12.028.

[39] Ruilong Li et al. "Effect of molecular weight of polyethylene glycol on crystallization behaviors, thermal properties and tensile performance of polylactic acid stereocomplexes". In: *RSC Advances* 10 (2020), pp. 42120–42127. DOI: 10.1039/D0RA08699A.

[40] *Plasticizers: Types, Uses, Classification, Selection & Regulation*. URL: https://polymer-additives.specialchem.com/selection-guide/plasticizers (visited on 04/06/2023).

[41] Yijun Guo et al. "The effect of plasticizer on the shape memory properties of poly(lactide acid)/poly(ethylene glycol) blends". In: *Journal of Materials Research* 33 (2018), pp. 4101–4112. DOI: 10.1557/jmr.2018.359.

[42] Saiedeh Salehi et al. "The effect of polyethylene glycol on printability, physical and mechanical properties and osteogenic potential of 3D-printed poly (l-lactic acid)/polyethylene glycol scaffold for bone tissue engineering". In: *International Journal of Biological Macromolecules* 221 (2022), pp. 1325–1334. DOI: 10.1016/j.ijbiomac.2022.09.027.

[43] Birru Bhaskar et al. "Composite porous scaffold of PEG/PLA support improved bone matrix deposition *in vitro* compared to PLA-only scaffolds: COMPOSITE POROUS SCAFFOLD OF PEG/PLA". In: *Journal of Biomedical Materials Research Part A* 106 (2018), pp. 1334–1340. DOI: 10.1002/jbm.a.36336.

[44] Tiaan Heunis et al. "Release of Bacteriocins from Nanofibers Prepared with Combinations of Poly(D,L-lactide) (PDLLA) and Poly(Ethylene Oxide) (PEO)". In: *International Journal of Molecular Sciences* 12 (2011), pp. 2158–2173. DOI: 10.3390/ijms12042158.

[45] Xigeng Miao et al. "Graded/Gradient Porous Biomaterials". In: *Materials* 3 (2010), pp. 26–47. DOI: 10.3390/ma3010026.

[46] Naghmeh Abbasi et al. "Porous scaffolds for bone regeneration". In: *Journal of Science: Advanced Materials and Devices* 5 (2020), pp. 1–9. DOI: 10.1016/j.jsamd.2020.01.007.

[47] Puja yadav et al. "A review on pore and porosity in tissue engineering". In: *Materials Today: Proceedings*. International Conference on Materials, Processing & Characterization 44 (2021), pp. 2623–2628. DOI: 10.1016/j.matpr.2020.12.661.

[48] Osmar Alejandro Chanes-Cuevas et al. "Macro-, micro- and mesoporous materials for tissue engineering applications". In: *AIMS Materials Science* 5 (2018), pp. 1124–1140. DOI: 10.3934/matersci.2018.6.1124.

[49] Qiu Li Loh et al. "Three-Dimensional Scaffolds for Tissue Engineering Applications: Role of Porosity and Pore Size". In: *Tissue Engineering. Part B, Reviews* 19 (2013), pp. 485–502. DOI: 10.1089/ten.teb.2012.0437.

[50] Islam M. Adel et al. "Conventional and Recent Trends of Scaffolds Fabrication: A Superior Mode for Tissue Engineering". In: *Pharmaceutics* 14 (2022), p. 306. DOI: 10.3390/pharmaceutics14020306.

[51] Tarun Garg et al. "Scaffold: a novel carrier for cell and drug delivery". In: *Critical Reviews in Therapeutic Drug Carrier Systems* 29 (2012), pp. 1–63. DOI: 10.1615/critrevtherdrugcarriersyst.v29.i1.10.

[52] Angelika Zaszczyńska et al. "Advances in 3D Printing for Tissue Engineering". In: *Materials* 14 (2021), p. 3149. DOI: 10.3390/ma14123149.

[53] *Découvrez la technologie d'impression 3D*. URL: https://myago3d.fr/technologie/ (visited on 03/28/2023).

[54] E. Castro-Aguirre et al. "Poly(lactic acid)—Mass production, processing, industrial applications, and end of life". In: *Advanced Drug Delivery Reviews* 107 (2016), pp. 333–366. DOI: https://doi.org/10.1016/j.addr.2016.03.010.

[55] *Rapid Prototyping - Selective Laser Sintering (SLS)*. URL: https://www.custompartnet.com/wu/selective-laser-sintering (visited on 03/28/2023).

[56] N. J. Castro et al. "12 - Biomimetic nanocomposite hydrogels for cartilage regeneration". In: *Nanocomposites for Musculoskeletal Tissue Regeneration*. Ed. by Huinan Liu. Oxford: Woodhead Publishing, 2016, pp. 259–281. DOI: 10.1016/B978-1-78242-452-9.00012-1.

[57] Irene Buj et al. "3D Printing of Porous Scaffolds with Controlled Porosity and Pore Size Values". In: *Materials* 11 (2018), p. 1532. DOI: 10.3390/ma11091532.

[58] T. Serra et al. "High-resolution PLA-based composite scaffolds via 3-D printing technology". In: *Acta Biomaterialia* 9 (2013), pp. 5521–5530. DOI: 10.1016/j.actbio.2012.10.041.

[59] Marie Goffin. "Development of porous biodegradable polymer materials for biological applications". PhD thesis. 2022.

[60] Khalid Lamnawar. "Crystallization of Poly (Lactic Acid), PLA: Effect of Nucleating Agents and Structure-Properties Relationships". In: *Journal of Composites and Biodegradable Polymers* 6 (2018), pp. 34–46. DOI: 10.12974/2311-8717.2018.06.5.

[61] Samira Karimi et al. "PEG-Grafted Graphene/PLLA Nanocomposites: Effect of PEG Chain Length on Crystallization Kinetics of PLLA". In: *ACS Omega* 7 (2022), pp. 31197–31204. DOI: 10.1021/acsomega.2c03397.

[62] Feng-Jiao Li et al. "Effect of polyethylene glycol on the crystallization and impact properties of polylactide-based blends". In: *Polymers for Advanced Technologies* 26 (2015), pp. 465–475. DOI: 10.1002/pat.3475.

[63] Xia Gao et al. "The role of poly (ethylene glycol) on crystallization, interlayer bond and mechanical performance of polylactide parts fabricated by fused filament fabrication". In: *Additive Manufacturing* 35 (2020), p. 101414. DOI: 10.1016/j.addma.2020.101414.

[64] B. Ndazi. "Characterization of hydrolytic degradation of polylactic acid/rice hulls composites in water at different temperatures". In: *eXPRESS Polymer Letters* 5 (2011), pp. 119–131. DOI: 10.3144/expresspolymlett.2011.13.

[65] Michael Liebschner et al. "Mechanical Aspects of Tissue Engineering". In: *Seminars in Plastic Surgery* 19 (2005). DOI: 10.1055/s-2005-919717.

[66] Elise F. Morgan et al. "Bone Mechanical Properties in Healthy and Diseased States". In: *Annual Review of Biomedical Engineering* 20 (2018), pp. 119–143. DOI: 10.1146/annurev-bioeng-062117-121139.

[67] René F. M. van Oers et al. "Osteocyte Shape and Mechanical Loading". In: *Current Osteoporosis Reports* 13 (2015), pp. 61–66. DOI: 10.1007/s11914-015-0256-1.

[68] Zhi-Ye Qiu et al. “Chapter 1 - Natural Bone Tissue and Its Biomimetic”. In: *Mineralized Collagen Bone Graft Substitutes*. Ed. by Xiu-Mei Wang, Zhi-Ye Qiu, and Helen Cui. Woodhead Publishing Series in Biomaterials. Woodhead Publishing, 2019, pp. 1–22. DOI: 10.1016/B978-0-08-102717-2.00001-1.

[69] Kerstin Tiedemann et al. “Regulation of Osteoclast Growth and Fusion by mTOR/raptor and mTOR/rictor/Akt”. In: *Frontiers in Cell and Developmental Biology* 5 (2017). DOI: 10.3389/fcell.2017.00054.

Appendices

A ISO-527-2-5A

The structure established by the ISO-527-2-5A is shown here:

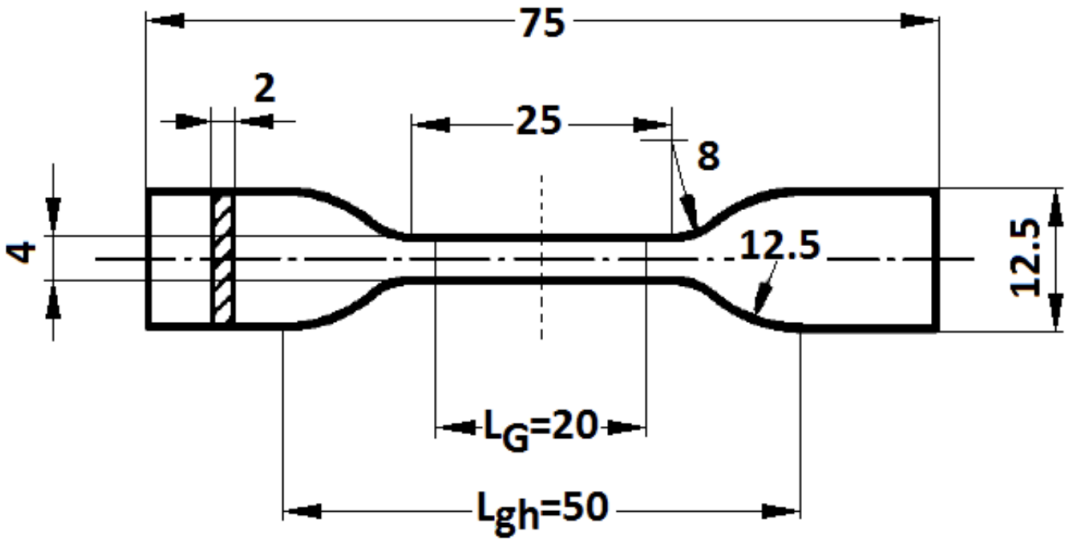

Figure 1: Dimensions in mm of the ISO 527-2-5A specimen

B DSC curves of PLA/PEO1M before and after PEG removal

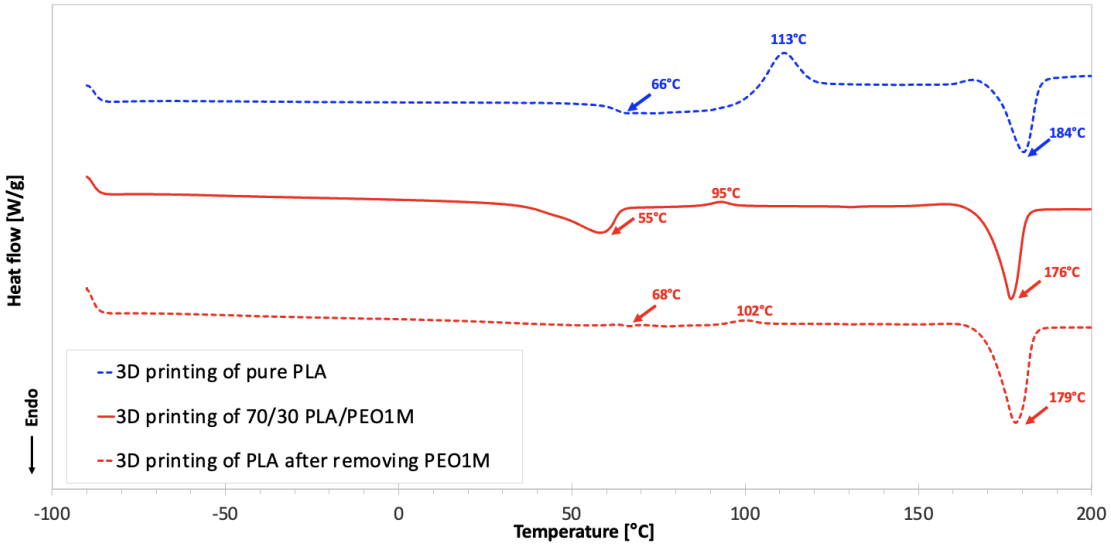

Figure 2: DSC curves from top to bottom for pure PLA 3D print, 70/30 PLA/PEO1M 3D print and PLA 3D print after PEO1M removal

C Individual tensile test results

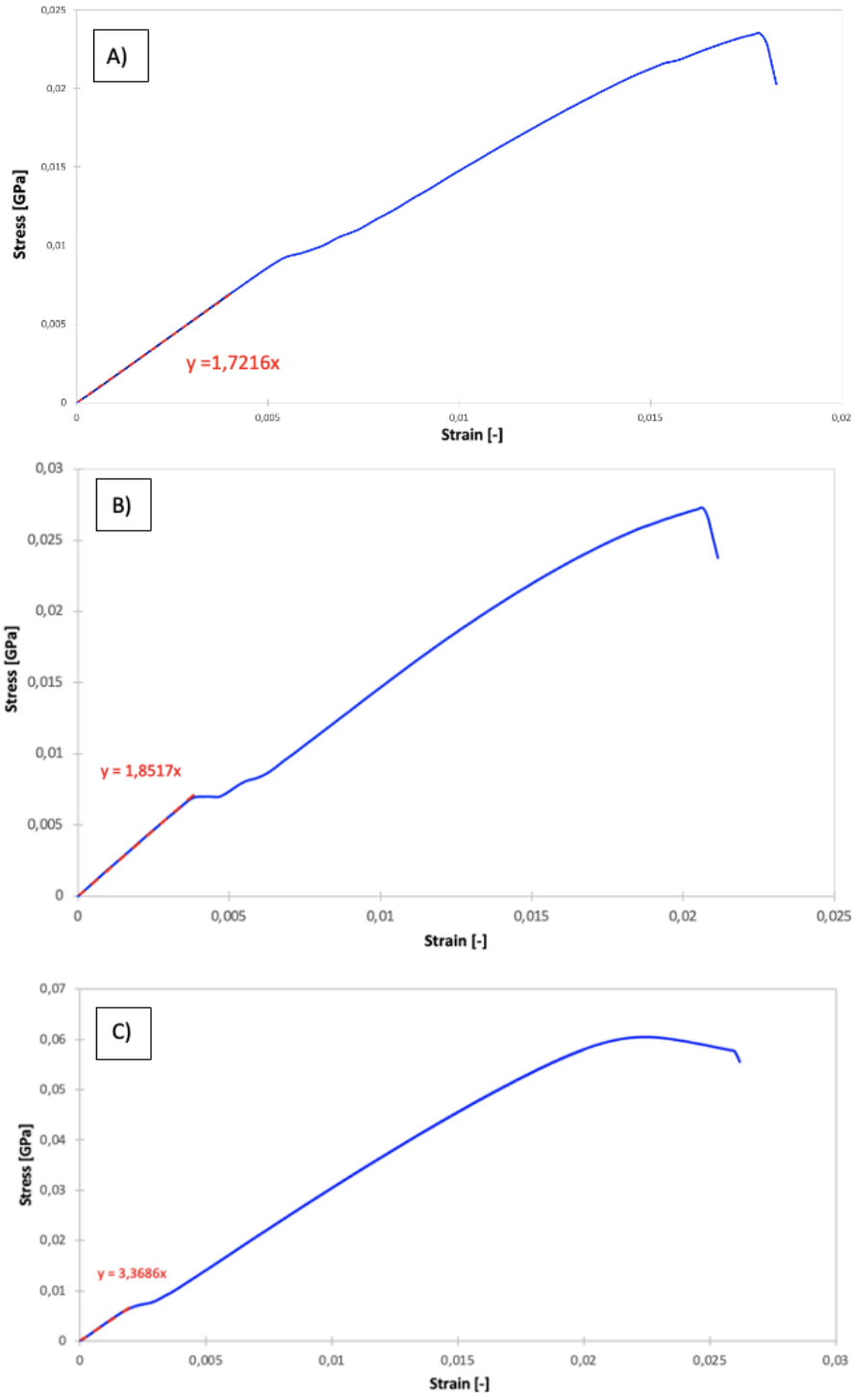

Figure 3: Tensile test results of A) PLA/PEO1M after PEG extraction, B) PLA/PEO100K after PEG extraction and C) pure PLA. The red dotted line represents the slope used to determine the Young's modulus.

UNIVERSITÉ CATHOLIQUE DE LOUVAIN
École polytechnique de Louvain
Rue Archimède, 1 bte L6.11.01, 1348 Louvain-la-Neuve, Belgique | **www.uclouvain.be/epl**